

ADA031273

12

FG

See  
1473

D D C  
RECEIVED  
OCT 28 1976  
RECEIVED  
A

Best Available Copy

Approved for public release;  
distribution unlimited.

UNCLASSIFIED

Advanced concepts are being used by IIT Research Institute to solve research, development, and design problems for industry and government through contract research. Our services encompass virtually all of the physical and biological sciences. Principle areas are: chemistry, computer sciences, electronics, engineering mechanics, life sciences, mechanics of materials, medical engineering, metals, and management and social sciences research.

The interdisciplinary approach at IITRI brings the latest technology to bear upon the problem-solving process.

Principal office:  
10 West 35th Street  
Chicago, Illinois 60616

**Best Available Copy**

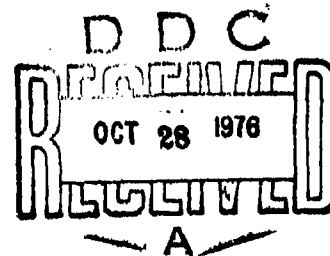
Approved for release by NSA on 05-08-2014 pursuant to E.O. 13526

Engineering Mechanics Division  
IIT Research Institute  
10 West 35th Street  
Chicago, Illinois 60616

AFOSR - TR - 76 - 1068  
IITRI Interim Report No. J6352  
Contract No. F44620-75-C-0059

INITIATION MECHANISMS OF SOLID ROCKET  
PROPELLANT DETONATION

Air Force Office of Scientific Research  
Bolling, AFB, D.C.



Prepared by  
A. N. Taketa  
A. H. Wiedermann

15 August 1976

FOREWORD

This interim report has the ultimate objective of identifying and alleviating the causes of solid propellant rocket motor detonations, and covers the period from Jan. 1, 1975 through June 30, 1976. The study was sponsored by the Air Force Office of Scientific Research (AFOSR), Directorate of Aerospace Sciences, United States Air Force under contract number F44620-75-C-0059. The program was monitored initially by Capt. L.R. Lawrence and presently by Major T. Meir of AFOSR.

IIT Research Institute (IITRI) personnel who contributed to this research are H.S. Napadensky, A.N. Takata and A.H. Wiedermann.

Respectfully submitted,  
IIT Research Institute

*A. N. Takata*

A. N. Takata  
Senior Research Engineer

*A. H. Wiedermann*

A. H. Wiedermann  
Science Advisor

Approved,

*H. S. Napadensky*

H. S. Napadensky  
Engineering Advisor  
Manager, Fire and  
Safety Research

APPROVED BY	
BY	White Stamp <input checked="" type="checkbox"/>
DD	Buff Stamp <input type="checkbox"/>
MANUFACTURE	
JUSTIFICATION	
BY	
DISTRIBUTION/AVAILABILITY CODE	
NO.	MAIL, NO. or SPECIAL
A	

## ABSTRACT

This study is directed at the problem of identifying the processes involved in causing deflagrating propellants to detonate, and use the results to devise means for minimizing rocket motor detonations consistent with optimal motor performance and reliability. Of primary concern to this study are rapid pressure rises within cracks, flaws or debonds within propellant grains that could initiate detonation.

This report covers the formulation of a computerized model with which to study the consequence of sudden exposure of cracks to gas at higher pressures and temperatures than those initially existing within the crack. Simple one-dimensional formulations were developed to predict the transient gas flows and propellant regression rates within cracks of variable shapes with the downstream end of the crack open or closed. Provisions were also made for predicting the consequence of reflected stress waves upon the crack thicknesses.

The most important finding of this study is that stress waves reflected from stiff motor cases can cause cracks to contract at sufficient rates to produce appreciable pressure rises. Unfortunately the maximum pressures and pressure rises could not be quantified due to computational difficulties in the gas dynamic calculations created by highly variable crack thicknesses produced during the final stages of crack contraction. Questions regarding possible impact of burning crack surfaces remain to be resolved.

## TABLE OF CONTENTS

	<u>Page</u>
1. INTRODUCTION	1
2. MODEL DEVELOPMENT	5
2.1 Gas Dynamics	8
2.1.1 Gas Dynamic Model	8
2.1.2 Gas Dynamic Results	9
2.2 Mechanical Response of Cracks (Lateral)	14
2.2.1 Mechanical Response Model	14
2.2.2 Mechanical Response Results	18
2.3 Dynamic Burn Model	20
2.3.1 Problem Definition	20
2.3.2 Rates of Heat Transfer to Propellant	23
2.3.3 Burn Model	25
2.3.4 Model Results for Arbitrary Thermal Fluxes	34
3. DYNAMIC MODEL OF CRACK BURNING	38
3.1 Computer Code	38
3.2 Results from Dynamic Model	41
4. SUMMARY, CONCLUSIONS AND FUTURE NEEDS	46
4.1 Summary and Conclusions	46
4.2 Future Needs	47
REFERENCES	
APPENDIX A - Means for Predicting Regression Velocities	
APPENDIX B - Gas Dynamic Model	
APPENDIX C - Mechanical Response Models	
APPENDIX D - Technique for Predicting Propellant Temperatures	

## LIST OF FIGURES

<u>Figure</u>		<u>Page</u>
1	Composition B Fragments Found in Chamber Following Sudden Pressure Drop	3
2	Description of Crack Conditions Considered	7
3	Wave Diagram for Initial Disturbance	11
4	Pressure and Velocity Distribution - Entry Phase	13
5	Pressure Histories - Reference Solution	15
6	Particle Velocity History - Reference Solution Cell 2	16
7	Temperature Histories - Reference Solution	17
8	Stress Wave System in Propellant During Initial Transient	19
9	Influence of Remote Boundaries on Mechanical Response	21
10	Typical Crack Thickness Histories	22
11	Temperatures Computed by Approximate and Exact Solutions for a Velocity of 1 cm/sec	29
12	Temperatures Computed by Approximate and Exact Solutions for a Velocity of 3 cm/sec	30
13	Temperatures Computed by Approximate and Exact Solutions for a Velocity of 5 cm/sec	31
14	Calculated Effect of Abrupt Rise of Heat Flux Upon Regression Velocity of HMX	35
15	Calculated Effect of Abrupt Rise of Heat Flux Upon Regression Velocity of Propellant with $E/R = 15,000^\circ K$	36
16	Principal Features of Dynamic Model	39
17	Spread of Burning; Crack Deformation; and Gas Pressures and Velocities	44

## 1. INTRODUCTION

During recent years high-energy propellants have been developed containing HMX in order to improve the performance of rocket motors. During the course of this development two explosions have occurred. The first was the Hercules plant in Bacchus, Utah in May 1974, the second was at the Naval Weapons Center in China Lake, California. Experimental evidence (1,2,3) indicates that a first necessary condition for detonation is a rapid pressure rise. For this reason, this report is concerned with identifying the conditions by which burning within cracks, flaws or debonds will result in pronounced pressure rises.

Deflagration to detonation (DDT) can occur as a result of a number of stimuli such as heat and impact (1,4-6). Such stimuli can cause a burning reaction that rapidly accelerates under suitable conditions causing shock/stress wave formation and subsequent detonation. The existing detonation theories describe the initiation of propellants and explosives by strong shock waves reasonably well. However, detonation can occur as a result of low-amplitude shocks that are well below those predicted by hydrodynamic theories of detonation. Equally important as high-order detonations is the class of chemical decompositions referred to as subdetonation reactions. While such reactions are not as destructive as high-order detonations, they can destroy rocket motors.

In view of the complex nature of this problem, a combined theoretical/experimental investigation is called for. Analytical studies reveal parameters whose role or significance is frequently lost or not measurable in experiments; while experiments serve to validate the accuracy of analytical models and to resolve any untractable features of the problem.

Recognizing the importance of putting the problem into perspective, we have focused our attention upon the development of simple analytical models with which to gain a better appreciation of the importance of various parameters in causing the initiation of high-energy propellants. Through such studies a clearer picture will be gained by which to identify the kinds of analysis

and experiments needed to compliment and guide model development, and to speed the resolution of this complex problem.

Important aspects of the problem requiring consideration are transient heating and burning of the propellant, gas dynamics, crack propagation, and positive and negative deformations of cracks that retard or speed burning. For this purpose computer routines have been developed using a number of simplifying assumptions and datum estimates -- none of which is believed will compromise identification of the essential features of the problem. Particular attention was given to structuring the computerized model so it can be readily upgraded -- serving as it does as a research tool.

The most important findings of this study are twofold. The first is the consequence of sensible heat deposited in the propellant during the relatively long times prior to appreciable pressure rises. Such heat will speed burning over and above quasi-steady state values if and when thermal fluxes increase due to rising gas pressures, velocities and/or temperatures.

Of equal or greater importance is closure of cracks by stress waves reflected from motor cases or generated by other cracks. Under suitable conditions, i.e. stiff case and sudden exposure of cracks to high pressure gas, cracks will contract causing pronounced pressure rises.

One other possibility, which has not been explored in this study, is the fragmentation of the propellant by multiple cracking resulting in burning fragments being propelled against one another. In this regard high explosives can be fragmented during high-pressure burning. Evidence of this is shown in Fig. 1 from Ref. 8.

Fragments shown in Fig. 1 were recovered from a closed bomb containing a burning cylinder of Composition B following separation of the closed bomb. Failure was caused by abnormal increases of pressure, which in other similar tests lead to detonation (1). In this test, burning was extinguished by the sudden

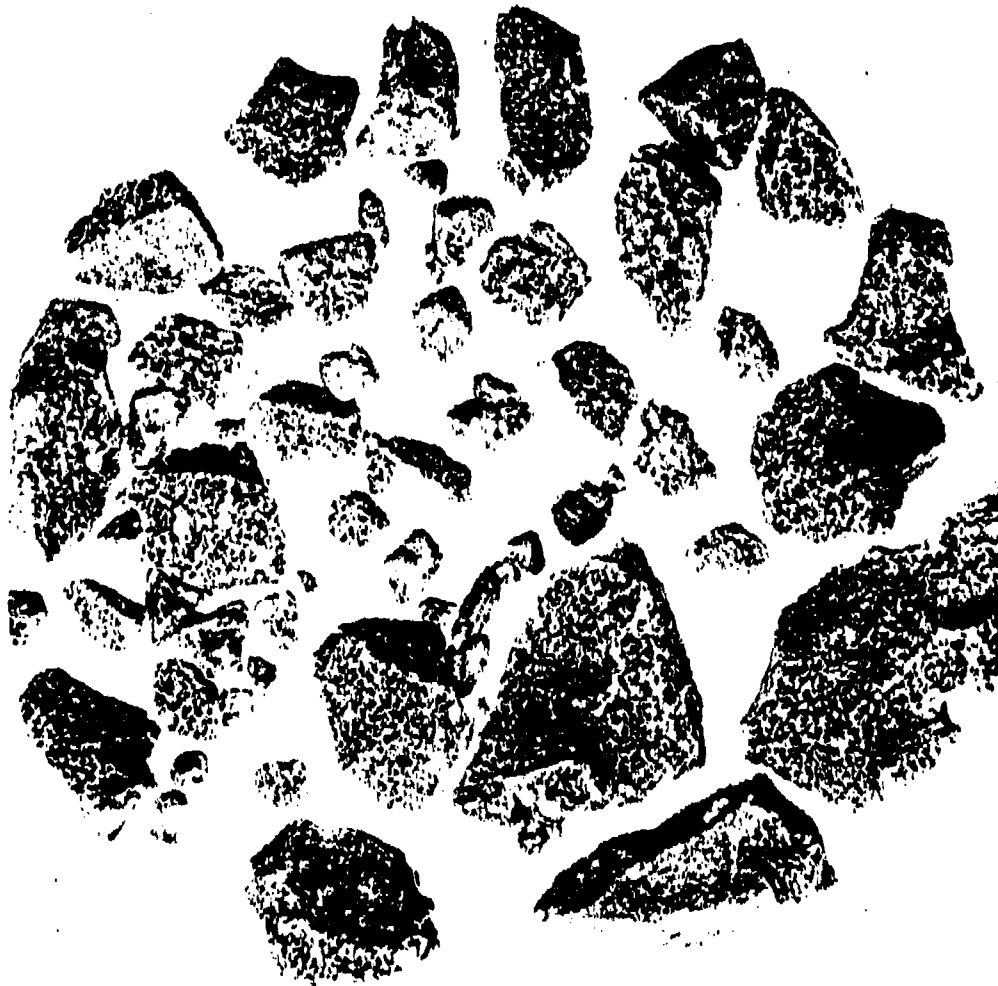


Figure 1 COMPOSITION B FRAGMENTS FOUND IN CHAMBER  
FOLLOWING SUDDEN PRESSURE DROP

drop in pressure. It was concluded that all surfaces of all Composition B fragments were in the process of burning as evidenced by a "frozen" foam layer over all surfaces. In other similar tests (1) it was observed that ionization probes located at various depths within the explosive fired in a random fashion with respect to depth. Random firing occurred during the period of abnormal pressure rises starting at about 1000 psi, and frequently was followed by detonation. One possible explanation of the random firing is multiple cracking such as indicated by Fig. 1.

In the remainder of this report we shall discuss analyses used in developing the model and results produced thereby. At the conclusion we shall indicate which of the many areas of uncertainties are in greatest need of study.

## 2. MODEL DEVELOPMENT

Before commencing model development, the literature was reviewed for information and data to assist in describing various aspects of the DDT process, and to guide the conduct of the program. In this regard, considerable information was found describing specific aspects of the problem. This includes

- Experimental ignition of propellants and explosives by shocks, radiation, hot wires and hot gases (9-11)
- Experiments describing the spread of burning or flame over surfaces or into pores or cracks (12-14)
- Combustion, ignition and detonation theories and/or experiments (15-30)
- Studies of crack initiation and propagation (1,31,32)

Unfortunately no comprehensive treatment of the problem of crack deformation and burning was found with which to put the problem into perspective. This is not at all surprising in view of the many complex interdependent phenomena involved.

Based upon this finding a dynamic model was developed using a number of simplifications to gain a better appreciation of the problem. In this model provisions were made for

- Single crack within monopropellant of variable dimensions, shape and end conditions
- Sudden flow of hot high-pressure gases (with friction) into crack
- Crack or flaw propagation (at present introduced artificially)
- Crack deformations -- positive and negative -- induced by pressure environment and case response to stress waves

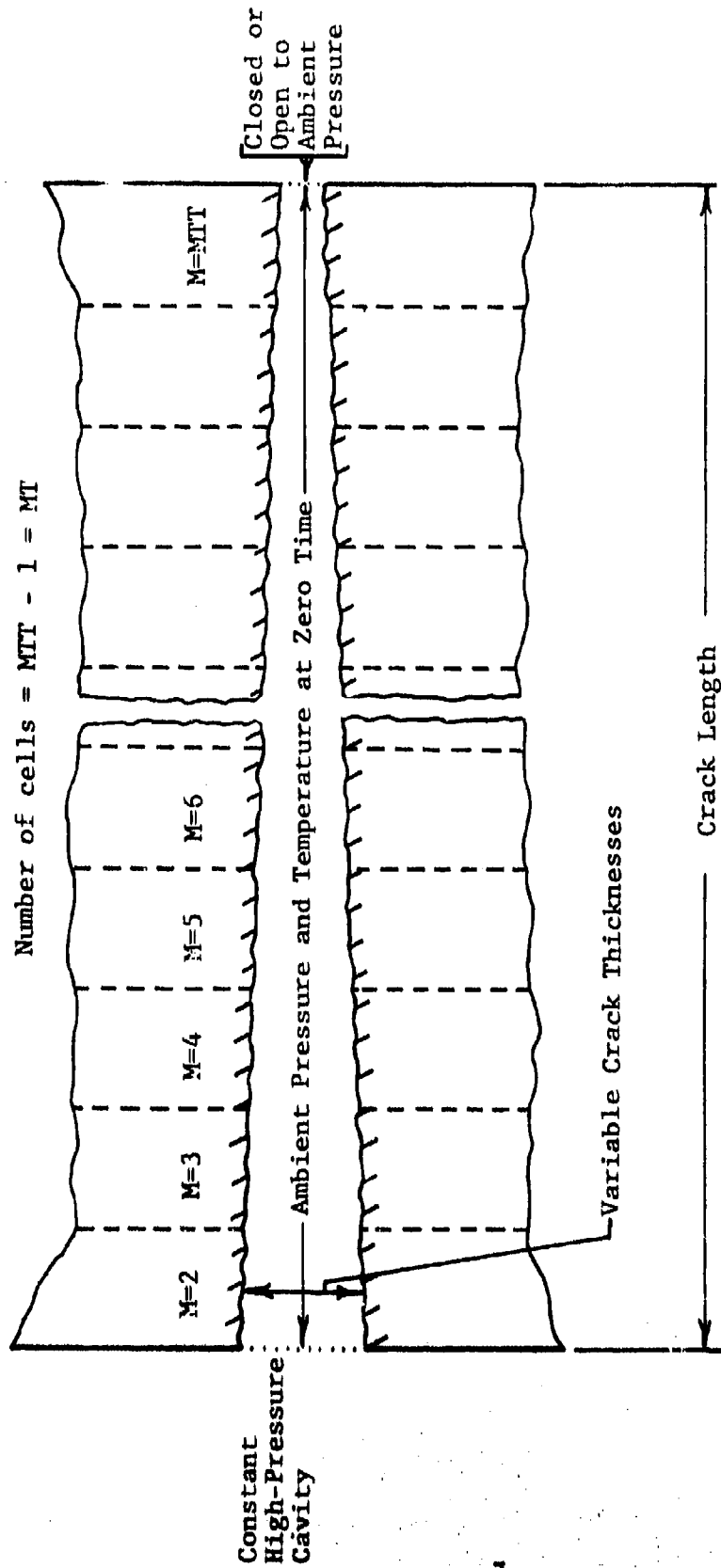
- Convective (turbulent) and internal heating of propellant
- Propellant regression rates due to one of two idealized situations namely
  - gas evolution assuming molten propellant remains in place
  - immediate discharge of molten propellant into gas stream

At present, gas flow is treated as one-dimensional with friction, assuming that the gas behaves as a perfect gas and that reactions occur instantaneously. Propellant temperatures are calculated on a transient basis and used to predict regression rates at various crack locations for either one of the two idealized cases cited above. The consequences of transient pressures upon crack deformation is modeled assuming the propellant behaves as a simple linear isotropic visco-elastic material. Yield or failure of surrounding propellant is not considered, and the dependence of property data upon temperature and pressure is neglected. Moreover, no provisions have been made for heat feedback from the burning propellant other than through the effect of burning upon the bulk pressures, temperatures and velocities of the gases.

Figure 2 illustrates provisions made regarding the crack and flow conditions. The crack was subdivided into uniformly long elements. The width of the crack is considered sufficient to accommodate a one-dimensional treatment of the gas flow. Means were provided for variable crack thicknesses from element to element. In addition provisions were provided for altering the

- Initial pressure and temperature within the crack
- End conditions of crack -- open or closed
- Gas pressure and temperature in cavity at the upstream end of the crack
- Length of crack as a function of time (crack propagation)

In the remainder of this section we shall discuss how each of the principal phenomena has been modeled and pertinent results obtained thereby. Topics covered are gas dynamics, mechanical response of cracks and transient regression velocities of propellant.



Assumption: Crack width and length large compared to thickness

Figure 2 DESCRIPTION OF CRACK CONDITIONS CONSIDERED

## 2.1 Gas Dynamics

### 2.1.1 Gas Dynamic Model

One essential aspect of the problem is the transfer of gaseous products and heat along the length of the crack. To achieve high convective heating and strong stress-waves, we have chosen to consider the problem of suddenly exposing a crack to a high pressure gas cavity.

Even though the gas dynamic model includes a variety of important flow features, it represents a preliminary version subject to modification. These modifications will be identified and incorporated in the course of treating various aspects of the problem.

The gas dynamic model is based upon an Eulerian representation of the flow region and is limited to a one-dimensional treatment. The selection of the Eulerian representation permits a simple identification with locations along the crack and allows for mixing of freshly burnt reaction gas. It is also convenient for large movements experienced by some of the gas.

The one-dimensional treatment is appropriate because the width and length of cracks are usually large compared to their thickness. Thus the most significant flow gradients and movements will occur along the length of the crack. Since flow gradients will exist across the thickness of the crack, the values of the variables used in the one-dimensional treatment represent average cross-sectional values.

The model treats a crack of some specified thickness variation at zero time. The gas in the crack at zero time is considered to have the same composition as the reaction products, and to exist in a rest state (no flow) at some specified pressure and temperature. The crack is then suddenly connected to a cavity filled with gaseous reaction products at high temperature and pressure. The cavity state is treated as a constant with respect to time due to the relatively short duration of the events occurring within the crack.

The downstream end of the crack can either be closed or connected to another cavity held at a specified low pressure. The low-pressure cavity could be a large debonded region. For open-ended cracks, the crack length is held constant. If the closed crack condition is selected, the crack may be allowed to grow in length in some arbitrary fashion. At present the growth feature is not based upon any physically plausible crack propagation mechanism. The incorporation of such a criterion together with crack branching represents one of the ultimate goals for improving the model.

### 2.1.2 Gas Dynamic Results

A computer program was developed to implement the gas dynamic model. This computer program exists

- (1) in the form of a main program with which to examine some aspects of the gas dynamic phenomena and to serve as a vehicle for further development, and
- (2) in the form of a subroutine of the overall Dynamic Model of Crack Burning.

These codes were programmed in FORTRAN IV user-oriented source language and have been successfully executed on a UNIVAC 1108, a large scientific computer.

This section presents the computed results of a reference problem to acquaint the reader with the adequacy of the model and with a typical response of the gas dynamic system in the absence of a reacting propellant. The reference problem was selected for the validation of the code and the subsequent evaluation of various effects. The problem configuration is that of a constant thickness crack, which is 10 cm long with the downstream end closed. This crack is connected at the upstream end to a cavity filled with air at a pressure of 60 bars and a temperature of 2000°C. Air is also in the crack or flow channel, but is at a pressure of 1 Bar and a temperature of 20°C. The thickness of the crack will not be a factor until certain physical effects such as friction are introduced. The initial validation examines

the inertial effects of the flow. The influence of the various other effects, such as friction, area variation, etc. have been examined, but are not discussed herein.

At time equal to zero a shock wave will be generated at the cavity end of the flow channel and propagate downstream compressing the gas which was originally in the crack to a pressure of 20.4 Bars. The cavity gas will expand to a sonic state at the inlet region of the crack and then undergo a further (nonsteady) expansion within the crack until the pressure drops to 20.4 Bars. Thus a centered rarefaction wave system will also be generated at the inlet and propagate downstream. The corresponding wave diagram is presented in Figure 3. An interface moving along with the fluid separates the two masses of gas. Region A is the undisturbed region; Region B is the compressed gas state region; Region C is the fully expanded cavity gas region; and Region D is the nonsteady expansion region. Regions A, B, and C are uniform state regions.

The shock wave is travelling at a velocity of 139.8 cm/ms and accelerates the rest gas to a velocity of 109.9 cm/ms. The fully expanded cavity gas is also accelerated to this velocity. These two uniform regions are at the same pressure and flow velocity conditions; however, their entropy is different. The temperature of the compressed gas is 1007°C corresponding to a sound velocity of 69.6 cm/ms. The cavity gas sound velocity is 92.7 cm/ms in the cavity, 84.6 cm/ms at the sonic inlet state and 79.6 cm/ms in the fully expanded state (Region C). The gas pressure at the sonic inlet state is 31.7 Bars. This initial flow field is self-similar in nature for a short period of time in that all the variables are constant along rays passing through the origin. This period of time terminates when the initial shock wave reflects from the closed end of the flow channel and creates a uniform high pressure rest region, Region E. The reflected shock wave propagates back upstream and interacts with the interface.

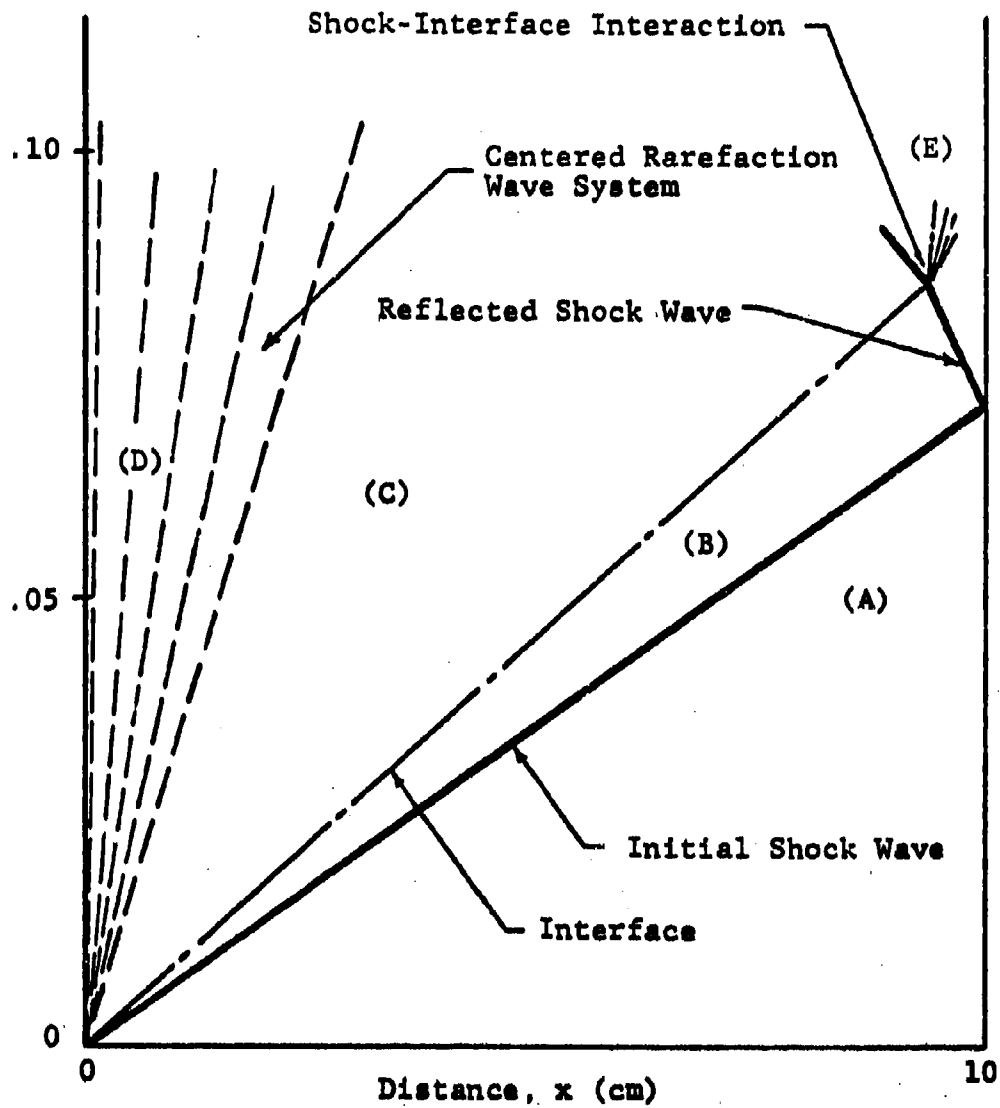


Figure 3 WAVE DIAGRAM FOR INITIAL DISTURBANCE

This shock-interface interaction generates additional disturbances and a more complex flow environment is established.

The initial self-similar flow field can be used to evaluate the fidelity of the computer flows during the entry phase. The lengthwise or distance resolution will depend upon the number of cells,  $MT$ , used to define the flow channel. In general 20 cells have been used to define the 10 cm long crack, although in some preliminary calculations only 10 cells have been used. Thus, for the former case the cells are 0.5 cm long. For a given crack length the number of calculation units required to obtain a solution for a given period of time will be proportional to  $MT^2$  since  $MT$  effects both the distance and time increments.

The pressure and velocity distribution within the crack are presented in Figure 4. The dotted line represents the theoretical solution at the corresponding time. These results are for Time Step 20 and corresponds to a time of 0.044 ms. Approximately 12 of the 20 cells have been engulfed by the shock wave at this time, hence this comparison represents a rather severe test of the fidelity of the calculations. Notice that the shock discontinuity (located at a distance of 6.2 cm) is smeared over some small distance. Similar results of the pressure distribution in the vicinity of the shock front are shown in the inset for the case where 40 cells have been used to define the crack. These latter results are better at the shock front and support the known fact that shock waves will be smeared out over three to four cells when this type of numerical method is used. There is also some overshoot in the vicinity of the shock front. The degree of overshoot varies with the flow variables. The front (downstream edge) of the centered rarefaction wave is located at a distance of 1.3 cm. The computed results for this flow feature are more diffuse than the theoretical solution, however this should be expected since only several cells are used to define this wave system detail at this early time.

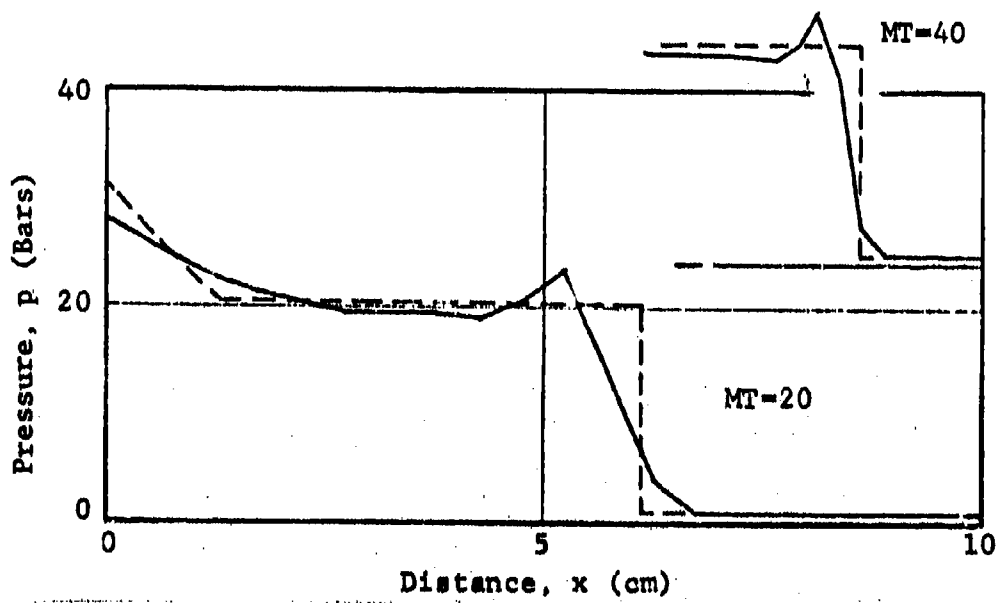
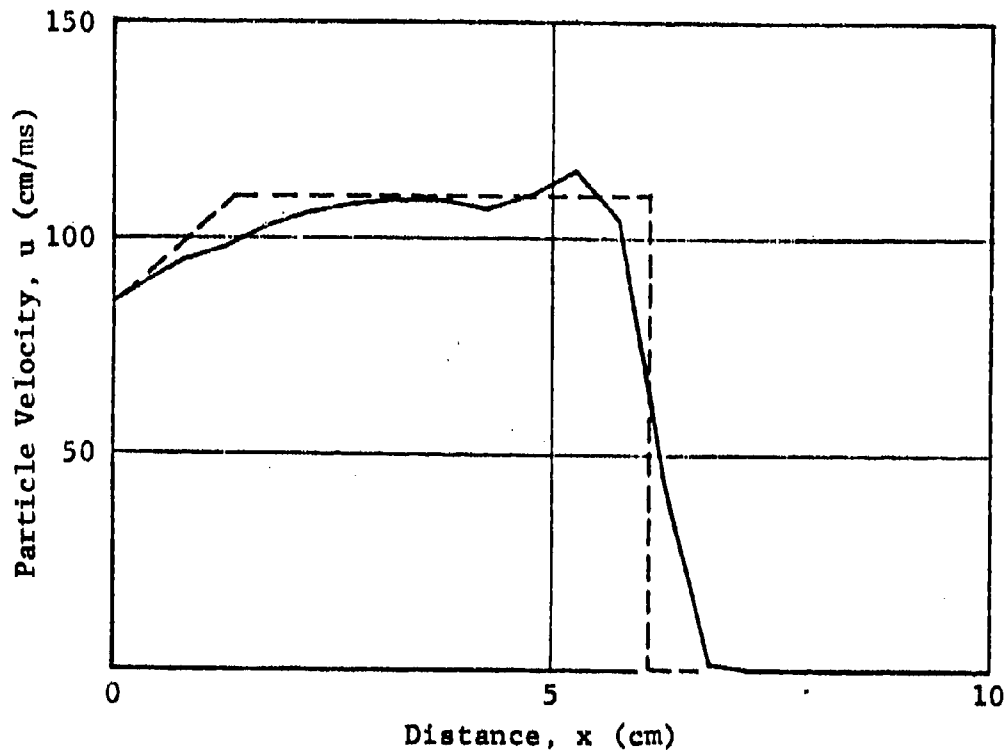


Figure 4 PRESSURE AND VELOCITY DISTRIBUTION - ENTRY PHASE

The pressure and particle velocity are correspondingly equal in Regions B and C; however, the other variables such as temperature, density, etc. are discontinuous at the interface. The interface at this time is located at 4.8 cm. The numerical results reproduce these discontinuities with about the same fidelity as they reproduced the shock discontinuity.

The reflected shock wave propagates back up toward the high pressure cavity end of the crack and interacts with both the interface and the centered rarefaction wave. The gross effect of this reflection process is to decelerate the gas to essentially a rest state and to increase the pressure to approximately 105 Bars. This strong disturbance will interact with the upstream end of the crack and create a more diffuse rarefaction wave system which will then propagate downstream initiating another cycle of the transient flow. This second cycle, however represents a pressure drop as compared to the pressure rise (shock wave) of the first cycle. The primary disturbance will continue to reverberate within the crack producing alternate cycles of compression waves and rarefaction waves of decreasing magnitude until a quiescent or rest state is achieved which is in pressure equilibrium with the high pressure cavity. Temperature and density gradients will exist within the crack due to the nonuniform entropy production, however these variations will be rather small. The time history of the pressure, particle velocity and temperature at the two ends of the crack are presented in Figures 5, 6, and 7 respectively. The particle velocity at the closed end is identically zero and is therefore not shown.

## 2.2 Mechanical Response of Cracks (Lateral)

### 2.2.1 Mechanical Response Model

The flow of high pressure gases into cracks within and adjacent to the propellant mass and any subsequent burning of these propellant surfaces will create a time varying pressure environment with the cracks. The surrounding propellant mass, which was originally in mechanical equilibrium with a low pressure distribution with the crack will respond to these new mechanical loads.

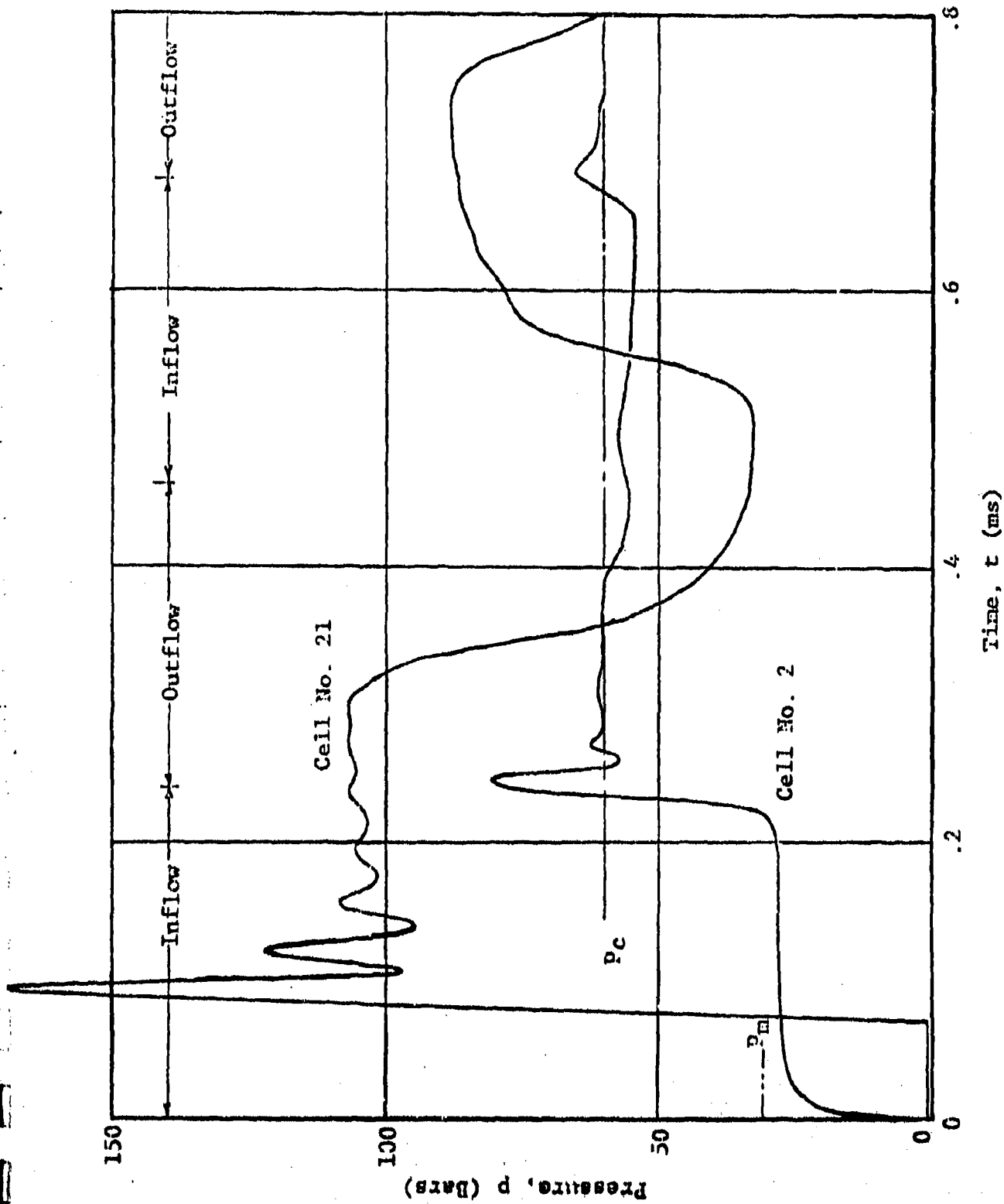


Figure 5 PRESSURE HISTORIES - REFERENCE SOLUTION

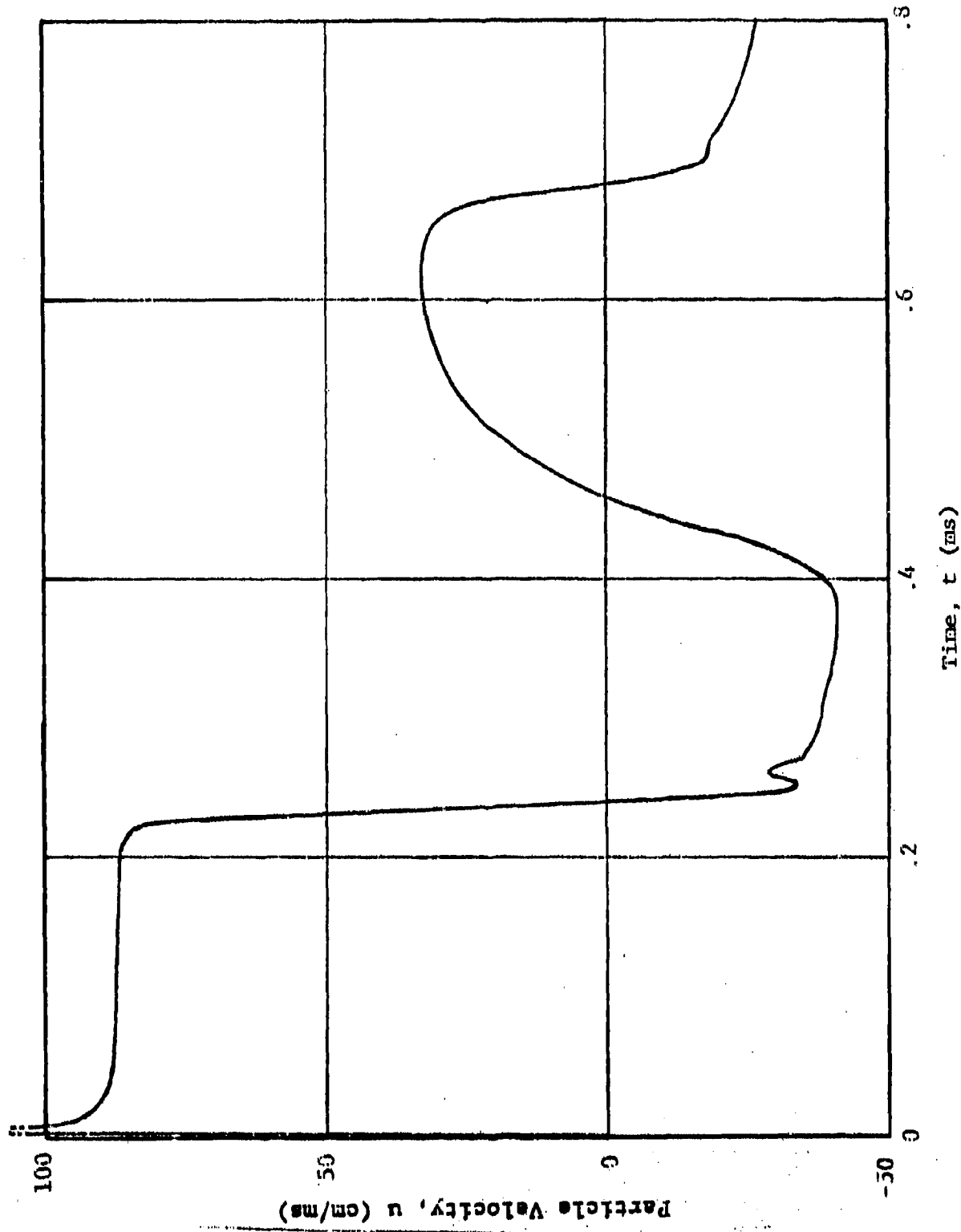


Figure 6 PARTICLE VELOCITY HISTORY - REFERENCE SOLUTION  
CELL 2

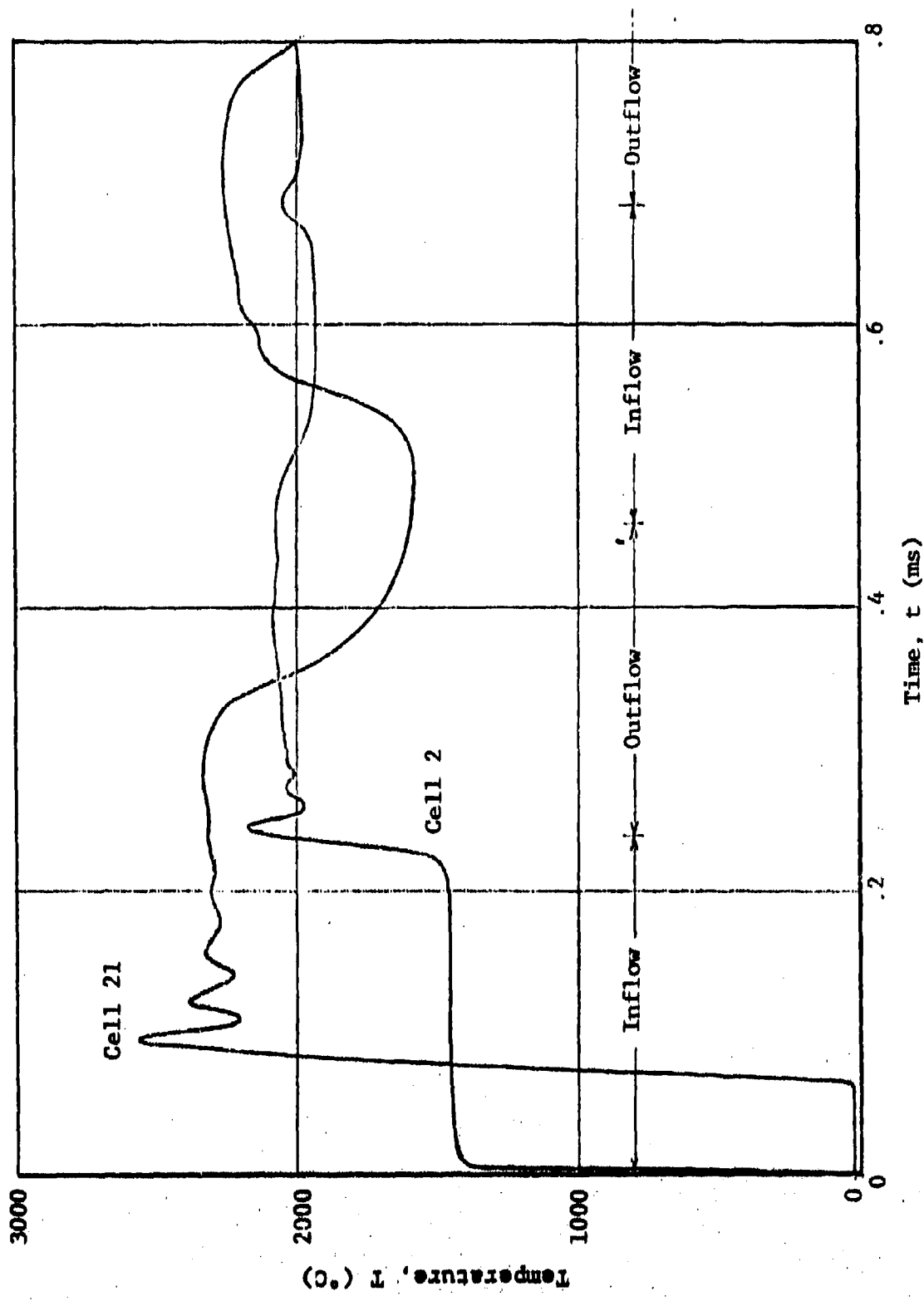


Figure 7 TEMPERATURE HISTORIES - REFERENCE SOLUTION

Two mechanical response models have been developed and are used in conjunction with the gas dynamic mode. One response model treats the early phases of the mechanical response when stress waves radiate away from the crack and the crack is in a growth phase. The second model treats, in a simple fashion, the interaction of these radiating waves with the confining shell structure and their subsequent interaction with the crack. Under these conditions the crack growth may be arrested and lead to partial or complete crack collapse.

### 2.2.2 Mechanical Response Results

The mechanical response of the propellant mass to the pressure environment within the crack is very complex due to the multiplicity of stress wave types present and the variety and complexity of the overall geometry of the system, i.e., the crack, the propellant mass, and the case configuration and location. The stress wave system in the propellant mass during the initial transient is illustrated in Figure 8. The primary motion of the propellant will be in a direction normal to the crack and will be roughly one of plane strain. For this reason a simple local plane strain representation for the transient stress field was adopted as a model of the mechanical response of the propellant mass in the absence of remote boundary effects such as the case response. In this manner the crack thickness growth feature could be coupled directly into the gas dynamic model and the coupled response determined. This initial response model is valid until the stress waves which radiate away from the crack interact with the remote boundaries of the propellant mass and its confining system, and propagate back to the crack locations. This process is very complex and varied.

A simple shell response model was selected as an initial version of the remote boundary effect. The model treats the shell as a simple single degree-of-freedom lumped mass which is position restrained and which responds to the mean radiative stress field. The response generates a reflected stress wave system which arrives back at the crack after some specified

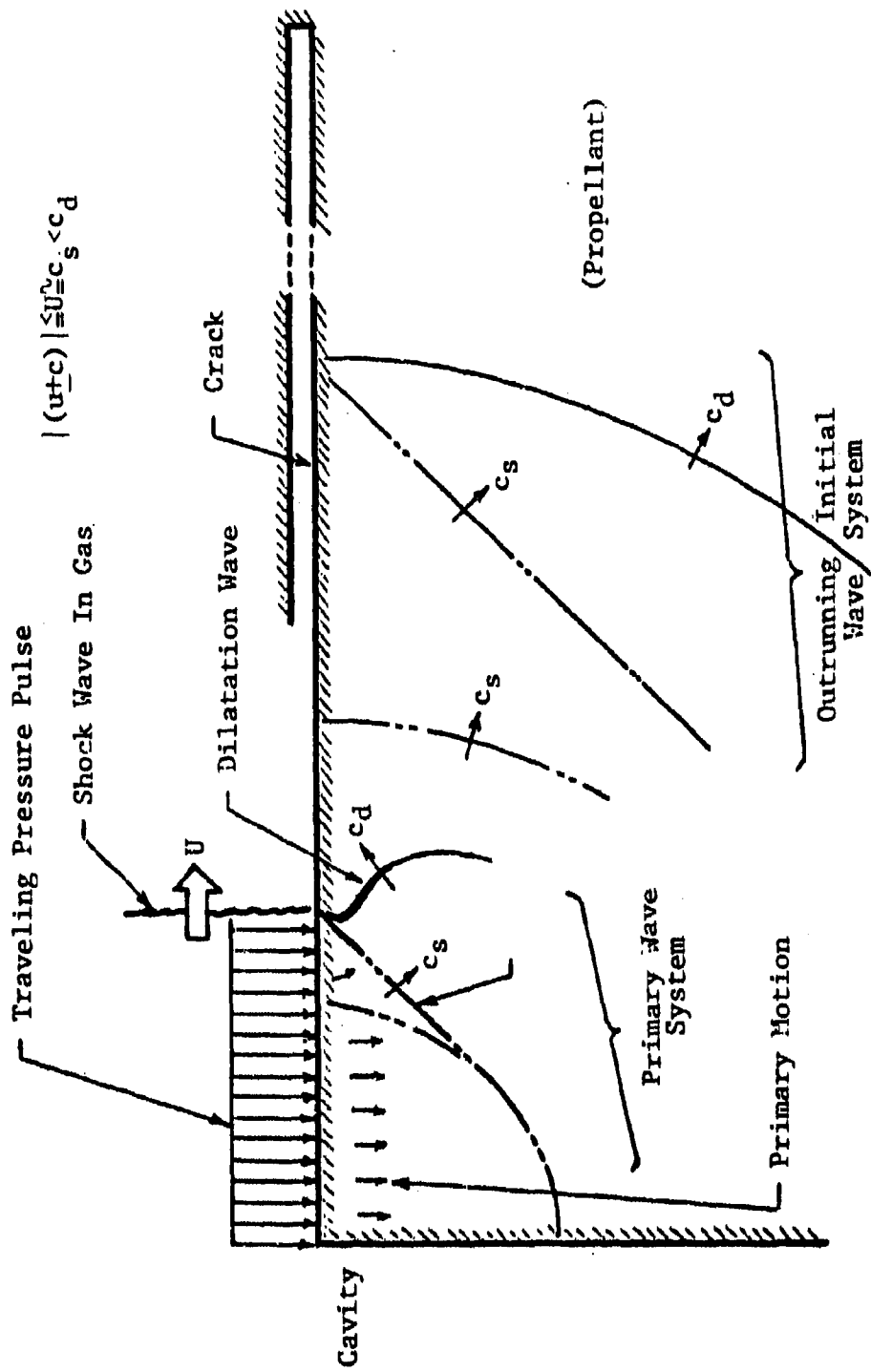


Figure 3 STRESS WAVE SYSTEM IN PROPELLANT DURING INITIAL TRANSIENT

delay period corresponding to the mean distance to the remote boundary. This model is illustrated in Figure 9. Two typical crack thickness histories are shown in Figure 10 for a cell near the midpoint of the crack for (1) a cased propellant mass and (2) one where the remote boundary is very far away (i.e., a very large propellant mass) from the crack.

### 2.3 Dynamic Burn Model

#### 2.3.1 Problem Definition

Before discussing the dynamic model it is desirable to examine two features of the problem having to do with crack surfaces. The first concerns the amount of exposed surface area, and the second the limitations of a one-dimensional treatment.

#### Exposed Surface Area

Crack surfaces are, of course, highly irregular and will present greater areas than that of a planar surface. To appreciate the extent by which crack areas exceed planar areas, we shall consider the two crack surfaces to contain a number of spherical particles of various radii  $r$ . The particles shall have half or less of their area exposed. In that the exposed area is proportional to the height  $x$  of the particle above base plane associated with the crack, the exposed particle area is given by  $2\pi r x$  for either crack surface. On the other hand the cross-sectional area of particles of radius  $r$  in the base plane is given by  $\pi(2rx-x^2)$ . Since all  $x$  values from 0 to  $r$  are equally likely, the average areas associated with each particle can be found by integrating each of the above expressions with respect to  $x$  and dividing by  $r$ . The ratio of the average areas of the exposed area to that of the cross-sections is given by

$$\frac{\pi r^2}{2\pi r^2/3} = 1.5 \quad (1)$$

Since the above result is independent of particle radius, the exposed surface is about 1.5 times greater than that of a planar surface. Provisions have been made in the code for accommodating such a correction.

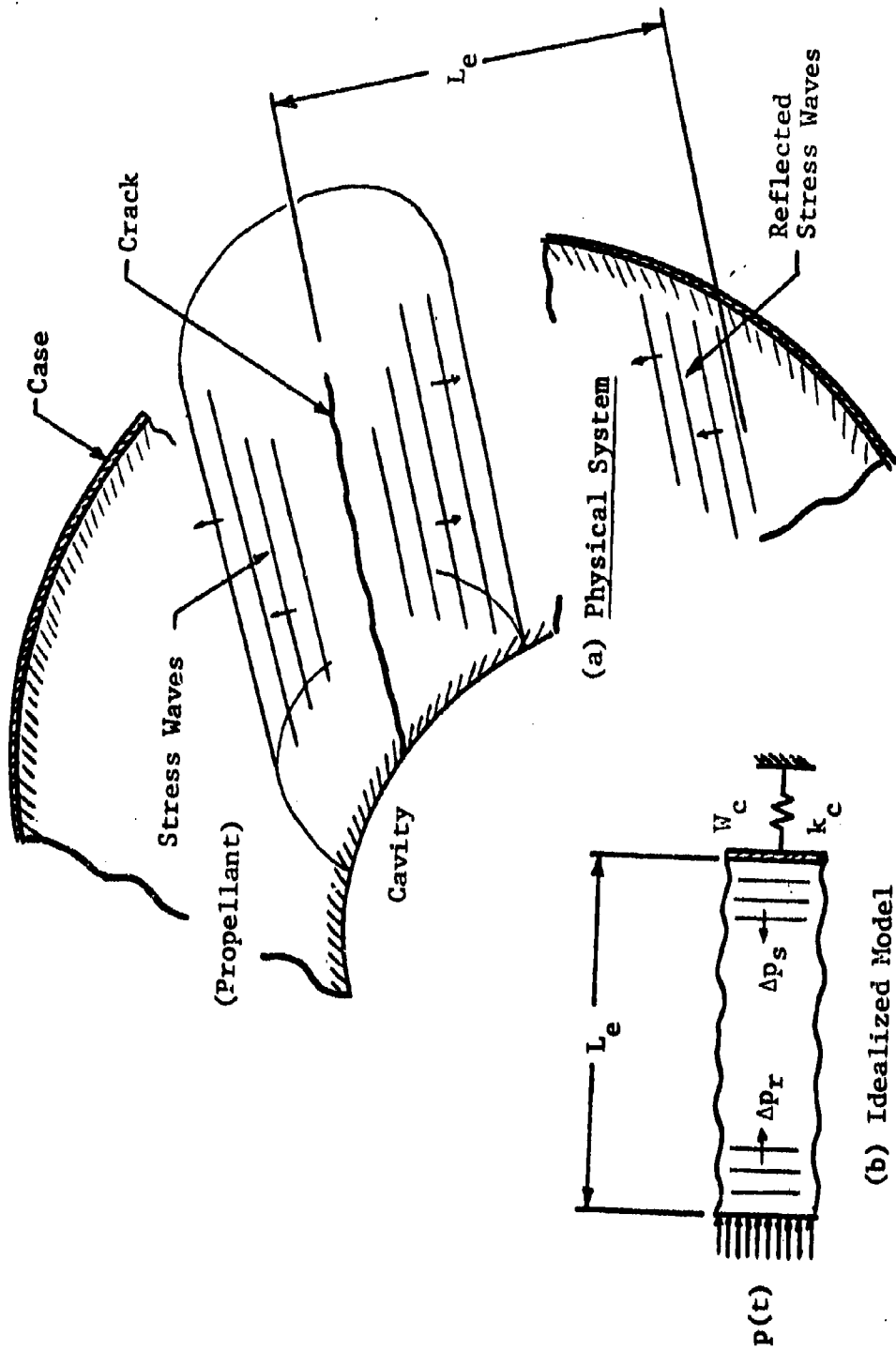


Figure 9 INFLUENCE OF REMOTE BOUNDARIES ON MECHANICAL RESPONSE

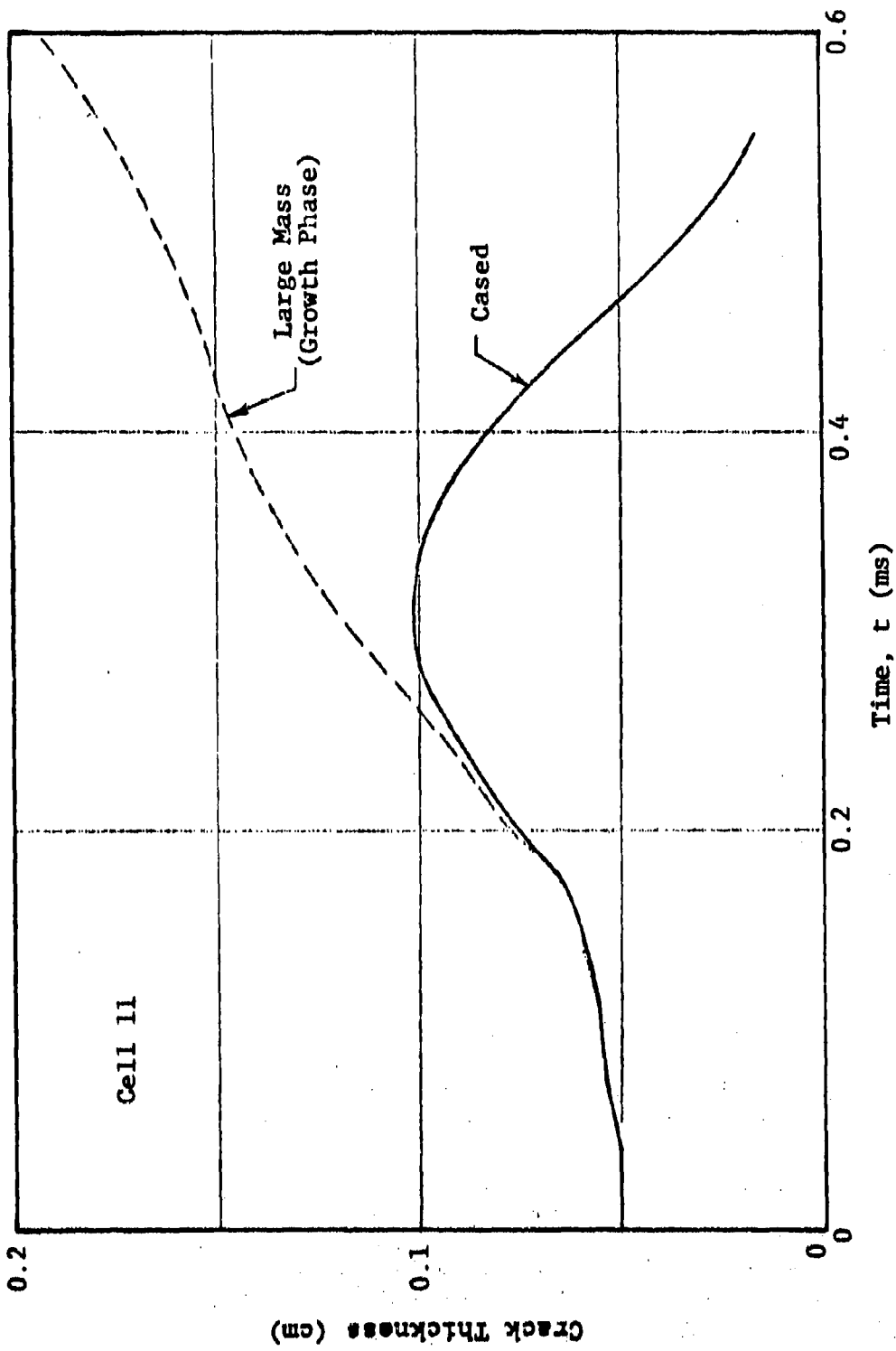


Figure 10 TYPICAL CRACK THICKNESS HISTORIES

### Limitations of One-Dimensional Heat Transfer Analysis

The presence of surface irregularities raises a question as to the accuracy of treating heat-transfer into the propellant as one-dimensional. Of particular concern is whether or not the irregularities are commensurate with the depths to which appreciable heat is transferred into the propellant and the depths of material evolved during critical periods of burning.

Depths of appreciable heat penetration will be greatest just prior to ignition and can be crudely estimated using the expression  $\sqrt{\alpha t}$ , where  $\alpha$  represents the thermal diffusivity of the propellant and  $t$  represents the period over which the heat is being transferred. Since  $\alpha$  is in the vicinity of  $0.002 \text{ cm}^2/\text{sec}$  for non-metallic ingredients, and the heating periods can be as small as  $0.25 \text{ msec}$  (see Section 3), it is concluded that the depths of appreciable heat penetration are of the order of  $7\mu$  or more for the class of problems treated in this study. Depths of propellant evolved during burning are of similar magnitude.

Unfortunately the depths of appreciable heat penetration are not always small compared to particle dimensions. Only with large particles of the order of  $100\mu$  or greater will one-dimensional analysis represent an adequate approximation. With particles of the order of  $10\mu$  or less, one-dimensional analysis will appreciably underpredict the velocities. However, until the significance of such errors on detonation is established, it is premature to embark upon a two-dimensional analysis.

#### 2.3.2 Rates of Heat Transfer to Propellant

In this study we have considered the convective heating of crack surfaces caused by the flow of hot high-velocity high-pressure gas. Also allowance was made for internal heating assuming it remains constant per unit mass of propellant evolved.

Because of uncertainties in the thermal gradients within the gas, heat feedback from burning propellant was not considered other than through the effect of burning upon the bulk temperatures, pressures and velocities of the gases.

Heat fluxes  $q$  are evaluated as follows:

$$q = h(T_g(t) - T(t)) + Q_p \rho V \quad (2)$$

where

$h$  = convective heat-transfer coefficient  
(see Eq. 3)

$T_g(t), T(t)$  = gas and propellant temperatures at time  $t$

$Q_p$  = net internal heating (reactions plus phase changes) per unit mass of evolved propellant

$V, \rho$  = propellant velocity and density

In that the thickness of the layer in which internal heating occurs is very small (1) compared to the depth of heat penetration, the net internal heating is assumed to occur at the propellant's surface.

#### Net Internal Heating

Indirect determinations (1) of the magnitude of the net internal heating suggest it can be appreciable for some secondary high explosive materials during steady burning. The above study suggests values as high as 130 cal/gm for HMX during low-pressure burning. Values estimated by other investigators for other propellants are of similar magnitude (11,28,31). Rates of pressure rise have important implications in this regard through their effect upon the residence times of reacting gases.

#### Convective Heat-Transfer

Convective heat-transfer coefficients are known for established flow conditions over given surfaces. Cracks, of course, present highly irregular surfaces to the gas flow. The result is large uncertainties in the flow conditions which in turn affect the heat-transfer coefficient  $h$ . These uncertainties would be greatest during the final stages of crack collapse wherein

the problem becomes most complex and is best dealt with by experimental means.

As a starting point, we shall neglect local variations of the heat-transfer coefficient, and use the conventional formulation for the heat transfer coefficient  $h$  for turbulent flow given by McAdams (34) and presented below.

$$h = \bar{C} \frac{K_g}{C_w} \left( \frac{C_w U \rho_g C_{gp}}{K_g} \right)^{0.8} \quad (3)$$

where  $K_g$  = thermal conductivity of gas  
 $C_w$  = crack thickness  
 $U$  = gas velocity  
 $\rho_g$  = gas density  
 $C_{gp}$  = specific heat of gas at constant pressure  
 $\bar{C}$  = dimensionless constant generally taken as 0.025

The constant  $\bar{C}$  is inputted into the code to allow for future sensitivity studies to establish the importance of flux uncertainties.

### 2.3.3 Burn Model

An important consideration in modeling burning is that one must account for highly transient temperatures within the propellant involving orders of magnitude differences of time for ignition and accelerated burning. To expedite the calculations, it was necessary to develop a novel technique for predicting the transient temperatures and burning rates. This involved modifying an existing solution of the temperatures produced in a semi-infinite body by a constant flux to account for a moving boundary subject to transient fluxes. Rates at which gases evolve from the propellant were made by applying a first-order Arrhenius relationship to the propellant temperatures as a function of depth. The result is an efficient means for approximating the transient burning rates.

Two versions of this routine were compiled -- one for examining the consequences of arbitrarily chosen time-dependent fluxes upon the burning rates, and one for determining regression velocities at various locations within a crack.

#### Means for Predicting Transient Propellant Temperatures

Predictions of transient regression rates require a knowledge of the transient temperatures produced within the propellant. Because of rapid changes in the heating, quasi-steady state analysis will not suffice. For this purpose we have developed an approximate solution of the problem involving one-dimensional heat transfer into the propellant with a regressing surface. Means for predicting velocities of the regressing surface are discussed in Appendix D. In this section we shall briefly discuss means for predicting the transient temperature rises and refer the reader to Appendix D for further details.

The most common method used to treat thermal problems involving regressing surfaces employs finite-difference techniques. Unfortunately such techniques require an unacceptably large number of spacial and temporal elements to follow highly dynamic burning rates. Moreover no closed-form solution of the problem exists.

Hence it was decided to develop an alternative method for predicting the propellant temperatures. This method is predicated upon constant thermal properties, and starts with the solution of the problem of a semi-infinite slab exposed to a constant heat flux. Modifications are then made to treat the problem of a regressing surface exposed to time-dependent fluxes. In doing so the coordinate system is fixed, and the regressing surface moves with respect to the fixed coordinates. Incremental time intervals are used during each of which the incident fluxes are considered constant.

Essential to this method is the use of Duhamel's principle to determine the conductive fluxes produced by each incident flux

at particular depths and times within the semi-infinite body. These depths represent given depths of the boundary during each of the time intervals. Negative fluxes are introduced to eliminate conductive fluxes negated by the loss of material. By doing so, one arrives at a number of constant fluxes at the given depths with which to approximate the heating of the underlying propellant over time. These constant fluxes are maintained only over the time interval associated with the particular mean depth.

The result is a number of simple independent heat-conduction problems for each of the constant fluxes. Solutions of these problems are acquired using Duhamel's principle to account for differences in the depths and times at which the various fluxes are applied. Summing the various temperature contributions one arrives at an approximation of the temperature rise of the boundary at appropriate times caused by heat conduction. Here it is only necessary to compute surface temperatures to predict regression rates, even though the method could have just as easily predicted indepth temperatures.

#### Validation of Means for Predicting Propellant Temperatures

To check the above procedure for predicting transient temperatures, we have applied it to a problem involving a moving boundary having an analytical solution. This problem is presented below:

$$\frac{\partial^2 T}{\partial x^2} - \frac{V}{\alpha} \frac{\partial T}{\partial x} - \frac{1}{\alpha} \frac{\partial T}{\partial t} = 0, \quad x > 0, \quad t > 0 \quad (4)$$

$$T = T_0, \quad x > 0, \quad t = 0 \quad (5)$$

$$\frac{\partial T}{\partial x} = hT, \quad x = 0 \quad (6)$$

$$V = V_0, \quad t > 0 \quad (7)$$

where  $T$  = temperature at time  $t$  at depth  $x$   
beneath moving boundary at  $x = 0$

$\alpha$  = thermal diffusivity

$h$  = heat transfer coefficient divided  
by thermal conductivity

$V_0$  = velocity of moving boundary at  $x = 0$

The above equations describe the consequence of conduction within a semi-infinite body at a uniform initial temperature with a moving boundary that loses heat convectively to a zero temperature environment. The body is considered to move at a velocity  $V_0$  with respect to a fixed coordinate system in such a way that the moving boundary is always located at  $x = 0$ . Solution of the above problem is presented on page 389 of Ref. 35 as

$$T = T_0 - 0.5 T_0 \left( \operatorname{erfc} \frac{x - V_0 t}{2\sqrt{\alpha t}} - \frac{\alpha h}{\alpha h - V_0} \exp V_0 x / \alpha \operatorname{erfc} \frac{x + V_0 t}{2\sqrt{\alpha t}} \right) + \frac{V_0 (2\alpha h - V_0)}{2(\alpha h - V_0)} \exp (\bar{h}x - \bar{h}t(V_0 - \alpha h)) \operatorname{erfc} \frac{x + (2\alpha h - V_0)t}{2\sqrt{\alpha t}} \quad (8)$$

Constants used were:

$$\alpha = .0018 \text{ cm}^2/\text{sec}$$

$$\bar{h} = 277/\text{cm}$$

$$T_0 = 100^\circ\text{C}$$

$$V_0 = 1, 3 \text{ and } 5 \text{ cm/sec}$$

A comparison of the temperatures predicted by the two methods is presented in Figs. 11, 12 and 13 for the velocities cited above. It may be observed that the temperatures predicted by the approximate solution of Appendix D are in good agreement with those predicted by the exact solution presented by Eq. 8 for all three of the velocities considered. Thirty time intervals were used for each of the approximate solutions -- each of which was intentionally kept large to severely test the approximate method.

The reason for the discrepancies being larger at the moving boundary is due to the fact that errors in the stepwise approximations of the incident fluxes having their greatest impact upon the surface temperatures. Errors in the changes of surface temperature range from 1.4 to 4.0 percent with the highest values occurring

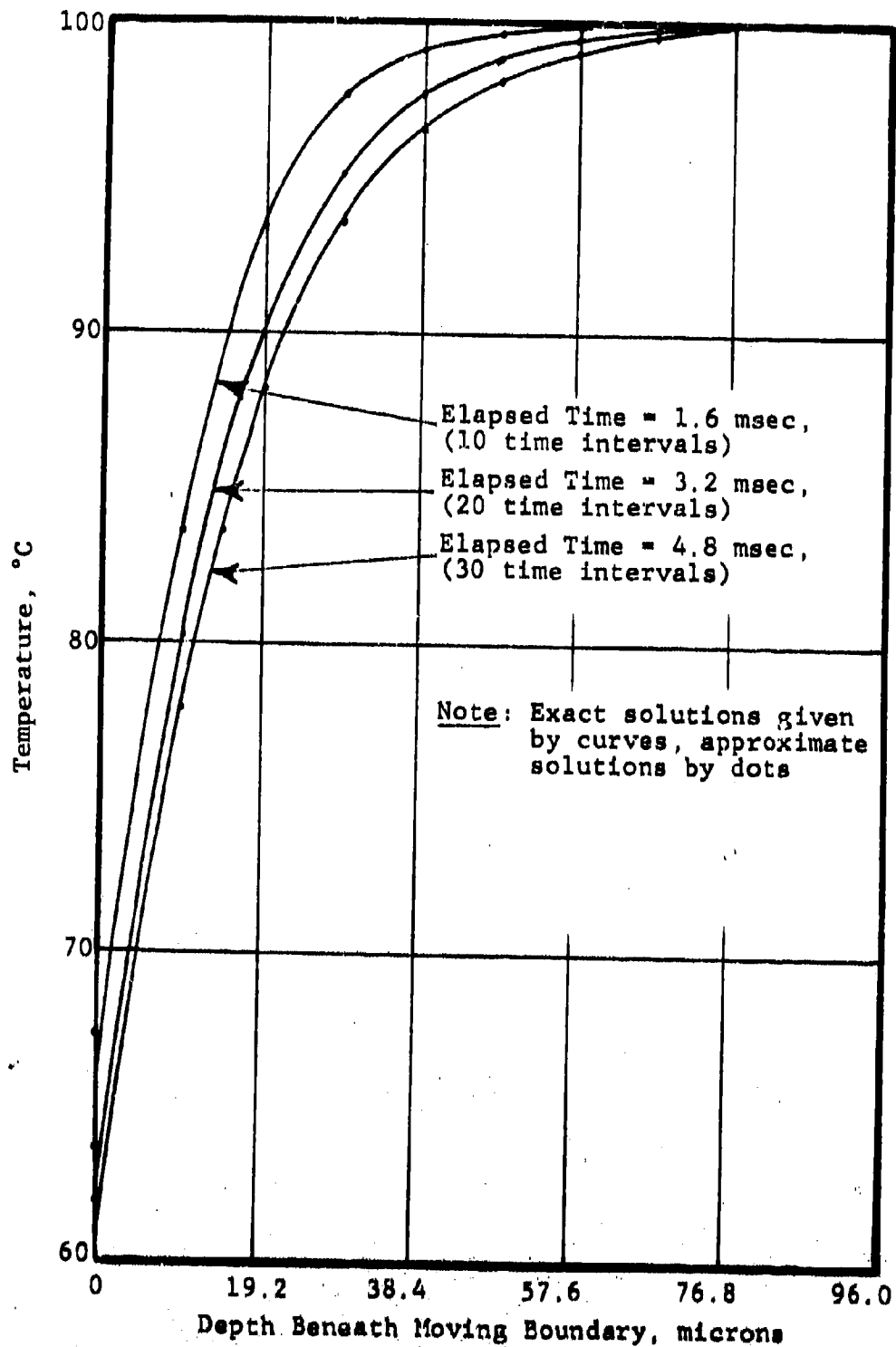


Figure 11 TEMPERATURES COMPUTED BY APPROXIMATE AND EXACT SOLUTIONS FOR A VELOCITY OF 1 CM/SEC

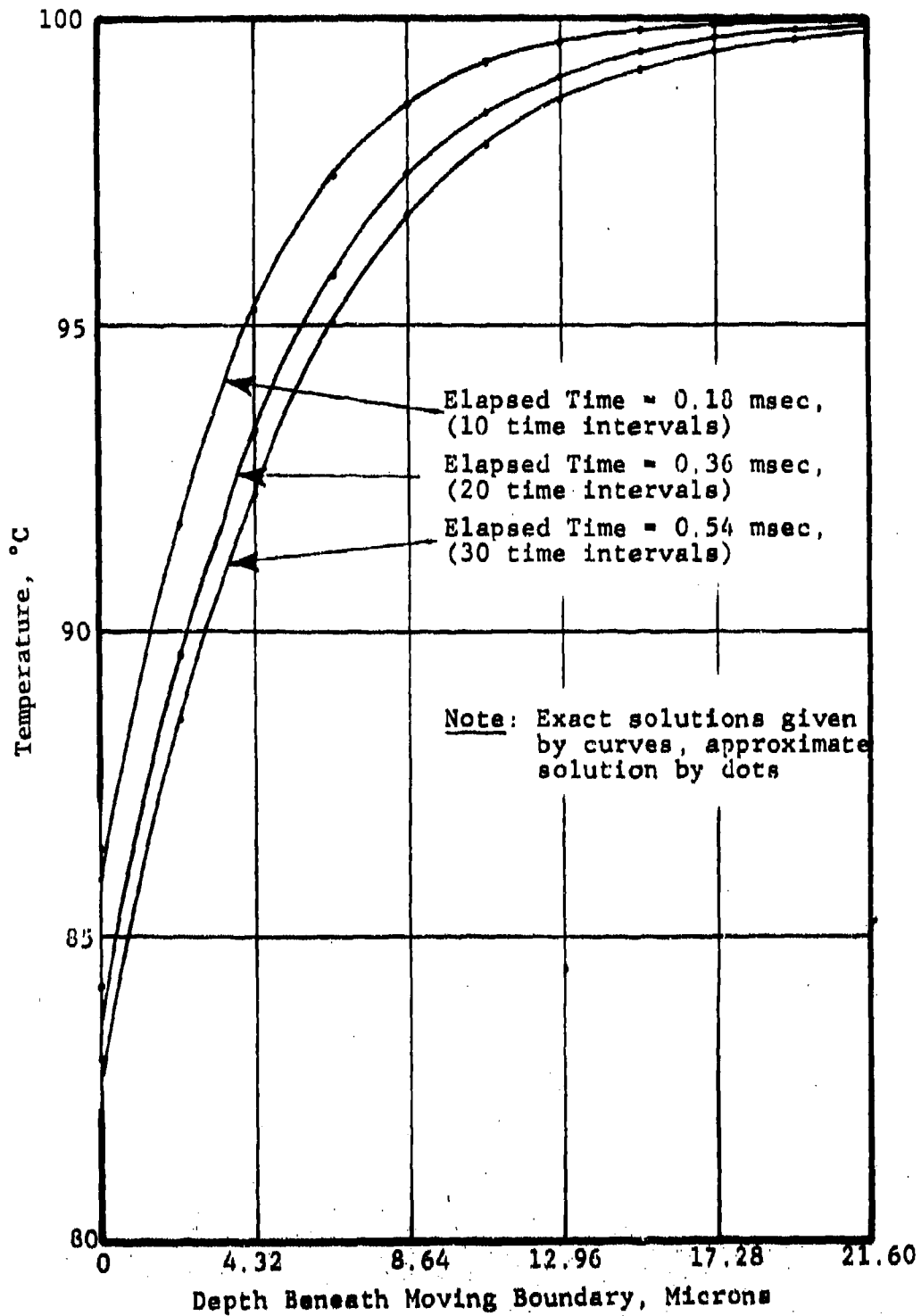


Figure 12 TEMPERATURES COMPUTED BY APPROXIMATE AND EXACT SOLUTIONS FOR A VELOCITY OF 3 CM/SEC

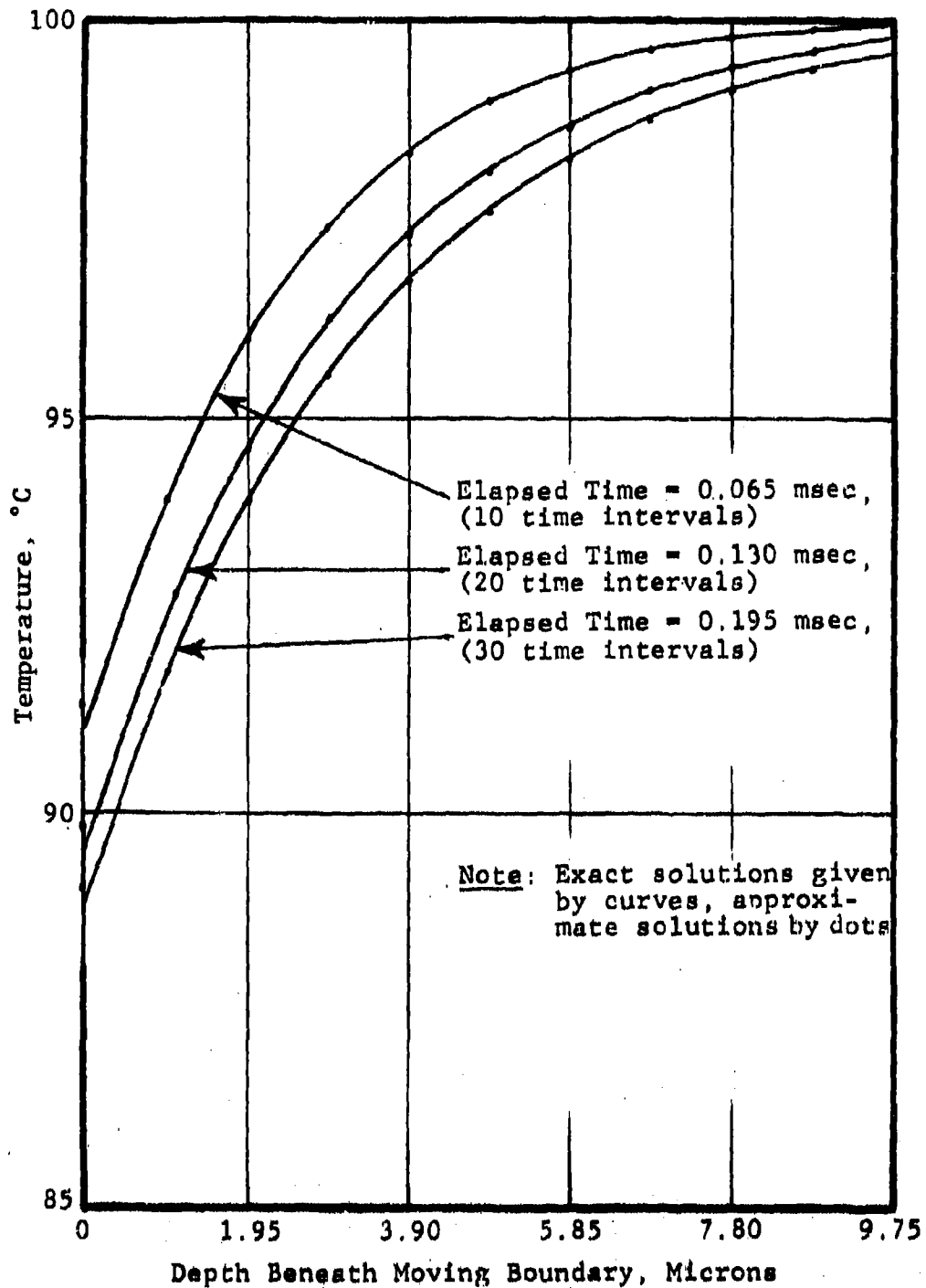


Figure 13 TEMPERATURES COMPUTED BY APPROXIMATE AND EXACT SOLUTIONS FOR A VELOCITY OF 5 CM/SEC

at the early times wherein only five time intervals are used. Thereafter the errors decrease progressively with time to values ranging from 1 to 2 percent.

Beneath the boundary the temperatures are in good agreement. In this regard errors associated with the loss of heat content are less than one percent for each of the three cases presented in Figs. 11, 12 and 13.

Tabular results associated with the three figures are presented in Appendix D. Included in this appendix is the consequence of varying the time intervals and depths at which the fluxes are applied within the boundary displacements.

Several observations may be gained by examining the tabular results. The first is that the errors decrease in a less than linear fashion with the time intervals. The second is that the errors are minimal when the fluxes are applied at depths corresponding to approximately three tenths of the displacements of the boundary. Finally, the errors are relatively insensitive to the velocity, and as with any numerical method can be held to any desired value by appropriate selection of the time intervals. Means for determining the time intervals are presented in Appendix D in terms of the velocity at which the propellants' surfaces regress; accuracy is maintained by decreasing the time intervals as the velocity increased.

#### Means for Predicting Regression Rates

There are two ways that propellants can regress into the gas stream, namely by the discharge of molten material and/or by the evolution of gas. To appreciate the significance of each phenomenon, provisions have been made in the codes to treat each of these ideal situations separately, and will be discussed in this section.

Rates at which gases evolve from propellants depend primarily upon the temperature distribution within the propellant, and to a

lesser extent upon the pressure to which the propellant is subjected. Here we shall neglect the effects of pressure apart from their effect in increasing the flux. Selection of the most appropriate means for predicting regression rates depends upon whether the mass of critically heated propellant remains constant or changes in an inverse fashion with the flux. For situations in which the mass of critically heated propellant remains essentially constant the following expression provides a valid approximation and is commonly used:

$$V = a \exp(-E/(T(0)+T_0)) \quad (9)$$

where  $a$  = constant

$E$  = activation energy divided by gas constant

$T(0)$  = temperature rise of surface of propellant

$T_0$  = initial absolute temperature of propellant

For situations in which the mass of critically heated propellant decreases in an inverse fashion with flux, it is more appropriate to integrate the Arrhenius relationship over depth  $x$  to arrive at the following expression.

$$V = Z \int_0^{\infty} \exp(-E/(T(x)+T_0)) dx \quad (10)$$

where  $Z$  = frequency constant

Means for approximating the above integral are described in Appendix A. In Appendix A we have taken advantage of the fact that most of the gas evolves from shallow depths compared to the depths of heated propellant. Temperature rises near the surface are assumed to decrease exponentially with depth as follows

$$T(x) = T(0) \exp(-Cx) \quad (11)$$

Using the above temperature profile in conjunction with the thermal gradient at the surface, the integral of Eq. 10 is approximated as follows:

$$V = KZ \exp(-E/(T(0)+T_0)) (T(0)+T_0)^2 / (qE) \quad (12)$$

where  $K$  = thermal conductivity of propellant

$q$  = effective thermal flux (incident plus internal)

The advantage of Eq. 12 over Eq. 10 is in eliminating the need to calculate temperatures below the surface.

For situations in which the surface regresses due to the discharge of molten propellant, the surface temperature is maintained at the melt temperature as long as melting occurs. Provisions for achieving this end are discussed in Appendix A.

In both of these highly idealized situations, displacements of the moving boundary are found by trial and error methods. These methods are discussed in Section 3 of Appendix A.

#### 2.3.4 Model Results for Arbitrary Thermal Fluxes

Here we shall consider the effects of sudden flux increases upon the rate of surface regression. Figure 14 presents the calculated results for HMX propellant, while Fig. 15 presents similar results for a propellant with a lower activation energy E.

In both cases, the propellant is considered to be initially exposed to a constant flux of  $500 \text{ cal/cm}^2\text{-sec}$  which is maintained until near steady velocities are achieved. This flux is similar in value to convective fluxes produced by hot high-velocity high-pressure gases in cracks. Then the flux is abruptly increased by an arbitrary factor of 5 and maintained at its new value for all future times. Values of the constants for HMX were acquired from Ref. 36 and are considered as independent of temperature.

It may be observed that the consequence of the sudden flux increase is a rapid acceleration of the velocity to high values followed by a gradual decrease to values approaching steady-state velocities. The overshoot is caused by the sensible heat within the propellant being greater than that required for steady burning at the higher flux. Velocities will continue to exceed their quasi-steady state counterparts as long as the flux continues to rise. If the flux remains constant, the excess sensible heat will be consumed by the burning and the velocity will decrease asymptotically to steady-state values as shown in Figs. 14 and 15. If the flux decreases appreciably, the velocities will drop below

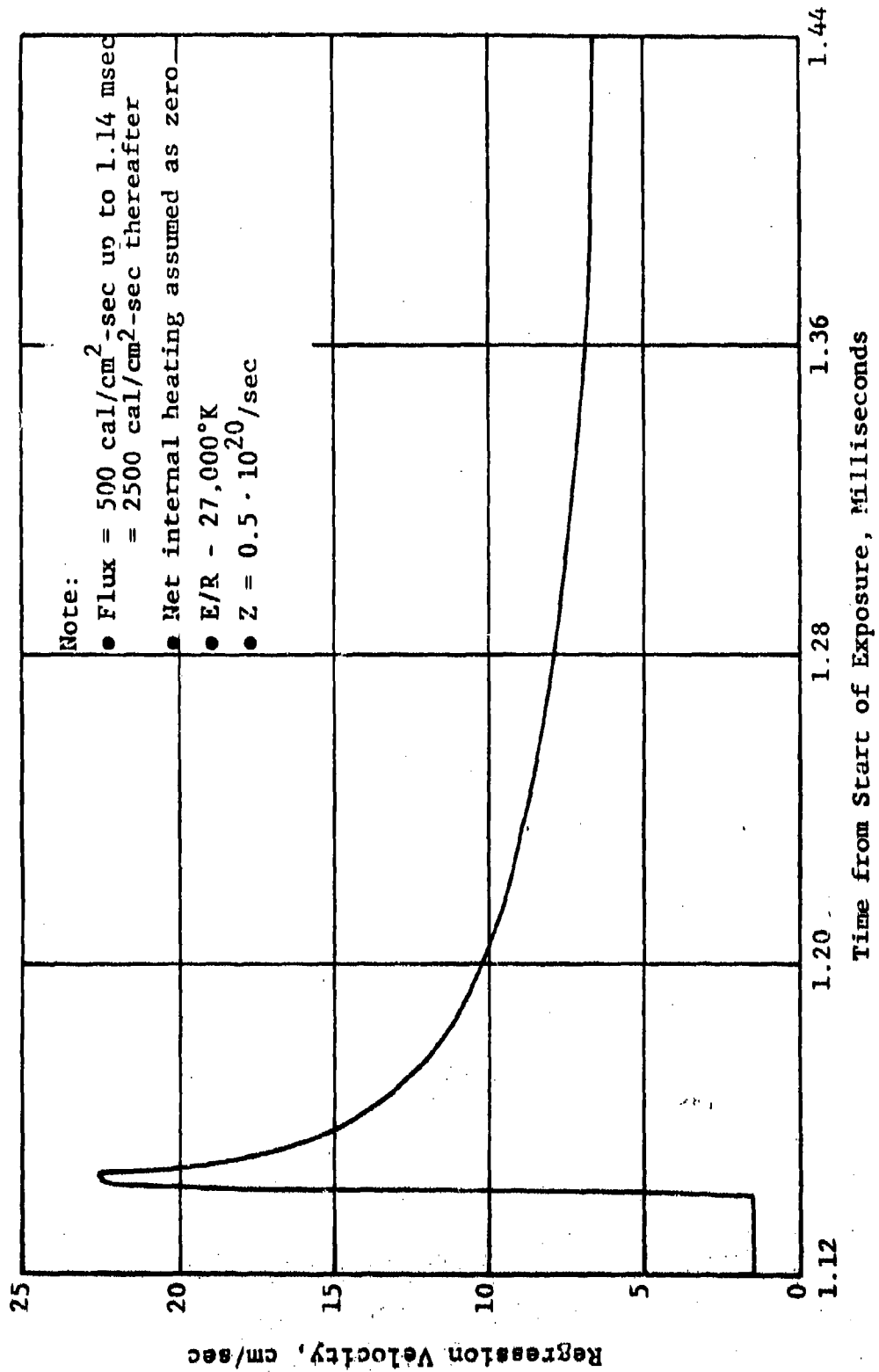


Figure 14 CALCULATED EFFECT OF ABRUPT RISE OF HEAT FLUX UPON REGRESSION VELOCITY OF IMX

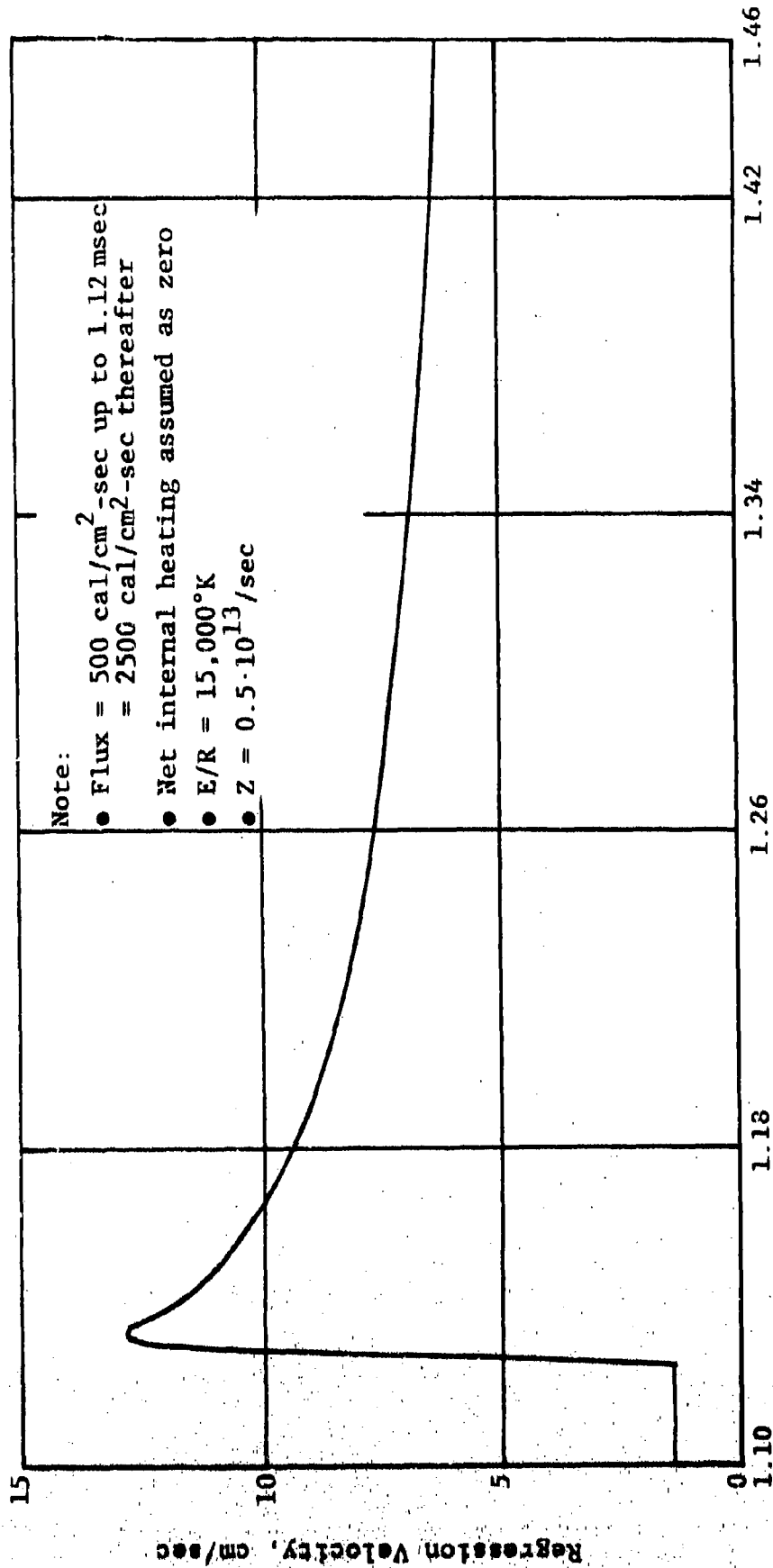


Figure 15 CALCULATED EFFECT OF ABRUPT RISE OF HEAT FLUX UPON REGRESSION VELOCITY OF PROPELLANT WITH E/R = 15,000°K

their quasi-steady-state values and could extinguish further burning. This, of course, is the reason for the recovery of the explosive fragments shown in Fig. 1.

It may be observed that the overshoots are most pronounced with the higher E/R value. For example, the peak velocity of Fig. 14 is about 3 times greater than their quasi-steady-state counterpart while Fig. 15 indicates a factor of about 2.

In addition to dampening any velocity increases, lower E/R values also delay the occurrence of the peak velocities. This could have important implications in the problem of crack burning since the delay times are of similar magnitude as the time involved in the final stages of crack collapse wherein high pressures are expected.

Each of the above effects is not at all surprising in that propellants with higher E/R values are more sensitive to temperature charges. The primary factor here is differences in the temperature rises necessary to achieve specific velocity changes. These temperature rises are less with propellants having higher E/R values.

Another possibly important factor in accentuating the velocities is internal heating. Exothermic heating over and above that needed for sublimation will accentuate each of the above effects -- namely more rapid and pronounced velocity increases. However, until more is known regarding the internal heating produced during extremely transient high-pressure burning, one cannot quantify this effect.

### 3. DYNAMIC MODEL OF CRACK BURNING

This model assesses the transient burning rates and pressures caused by the sudden exposure of a crack (within a monopropellant) to a cavity of hot gases held at a constant pressure and temperature. The initial pressure and temperature of the gas within this crack is considered much lower than that of the cavity in order to accentuate the burning and crack deformations, and in turn the possibilities for pronounced pressure buildup within the crack.

Major assumptions used to expedite development of the model were

- One-dimensional gas flow with friction
- Perfect gas
- Instantaneous reaction of evolved propellant
- Propellant behaves as a simple isotropic viscoelastic material
- Fully established turbulent gas flow
- One-dimensional heating of propellant surfaces
- Constant gas and propellant properties

#### 3.1 Computer Code

This code has been designed primarily as a research tool to assist in identifying the essential features of DDT. As a consequence it is subject to periodic revisions as key aspects of the problem are identified. For this reason we shall limit this discussion to the principal features of the code. Specific techniques used to treat various aspects of the problem are discussed elsewhere in this report. Functions performed by various portions of the code are described by Fig. 16.

The main program and each of the subroutines are used once during each time interval. These intervals are computed in the main program using criteria involving the

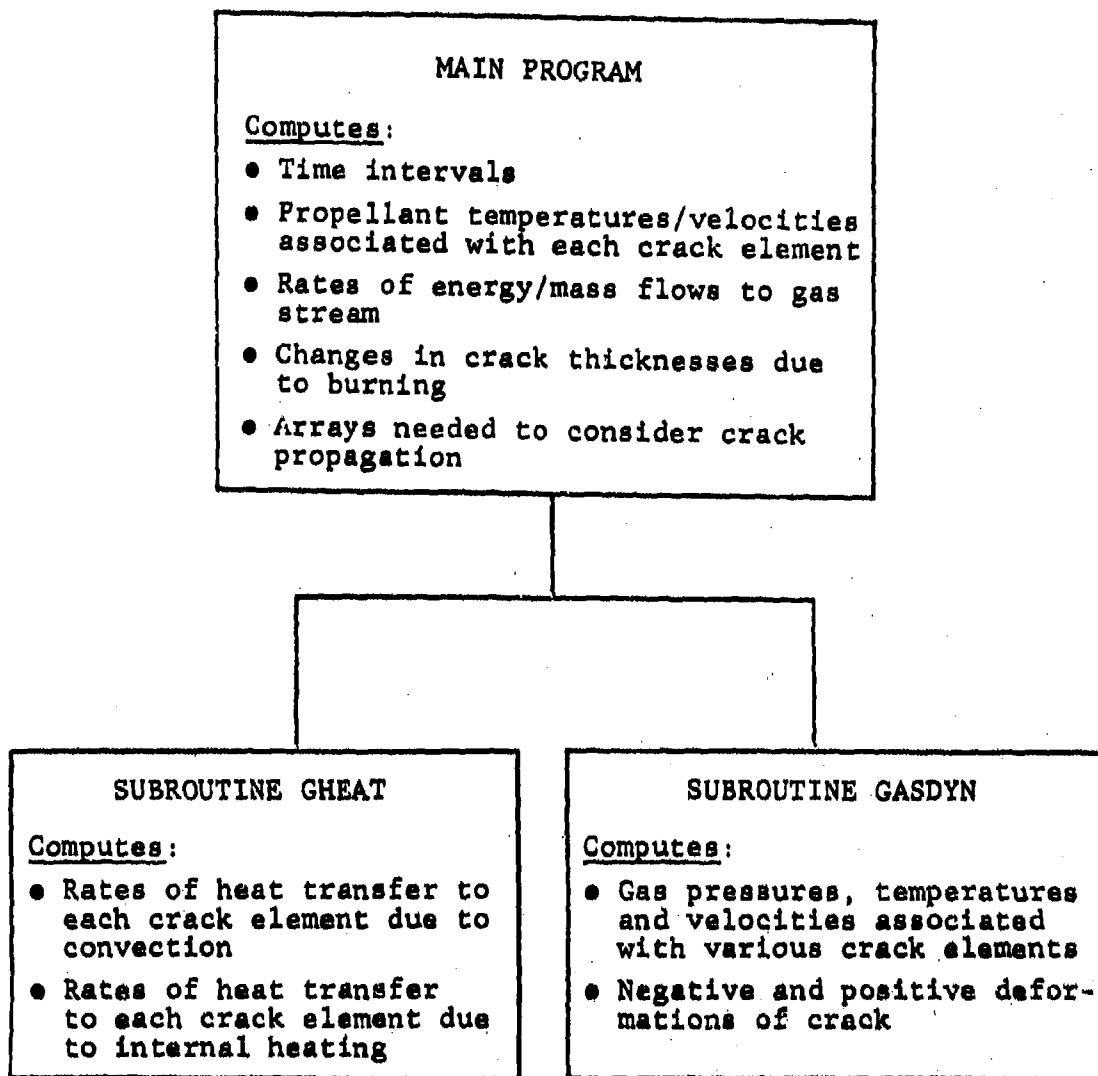


Figure 16 PRINCIPAL FEATURES OF DYNAMIC MODEL

- Propellant regression rates along with thermal fluxes (see Appendix A)
- Gas and sound velocities (see Appendix B)
- Crack thicknesses and deformation velocities (see Appendix C)

These criteria are applied to each of the crack elements to find the smallest time interval required. In this regard, the user has the option of using somewhat larger time intervals than needed by the gas dynamic calculations whenever the consequence upon the propellant is small. Time intervals decrease as the velocities associated with the gas, propellant, and crack deformations increase.

Following the selection of the time interval, subroutine Gasdyn is called to compute the gas pressures, velocities and temperatures associated with each crack element. This subroutine also calculates the mechanical deformations of the crack.

Subroutine Gheat then uses the predicted gas pressures, temperatures and velocities to compute the convective fluxes entering the propellant at each crack element. These fluxes are then added to the net internal heating to arrive at the total flux. Finally the main program is reentered to compute the propellant temperatures/velocities. Before commencing the next time interval, the rates of energy and mass discharge from the propellant are calculated along with changes in crack thickness due to propellant regression for subsequent use by subroutine Gasdyn.

As mentioned previously, provisions have been made in the code for investigating the consequence of various aspects of the problem. These include

- Variable crack shapes, lengths, thicknesses and end conditions
- Crack propagation (at present induced arbitrarily)
- Double or single propellant surfaces to distinguish between propellant crack from motor case debonds

- Choice of one of two idealized situations in which molten propellant
  - remains in place
  - is immediately swept into gas stream upon formation

### 3.2 Results from Dynamic Model

In this section we shall present some of the more pertinent findings obtained from dynamic model. In view of various simplifications and uncertainties in the data, the results are of a preliminary nature and are primarily intended to identify essential features of the problem requiring more detailed consideration and study. In each of the cases treated, the propellant surfaces are assumed to regress by the evolution of gas.

Tables 1 and 2 indicate the effects of cavity pressure, and crack thicknesses and end condition upon the spread of burning and upon the mechanical deformation of cracks. In each of these tables the downstream end of open cracks is considered connected to a constant-pressure reservoir held at ambient pressure. Burning is arbitrarily defined as occurring when the regression velocities exceed 0.1 cm/sec.

Tables 1 and 2 indicate that the effect of cavity pressure upon the spread of burning is much more than linear. Also it may be observed that high upstream pressures tend to open the upstream end of the crack and close the downstream end of the crack. The degree to which various portions of a crack open or close depends upon the gas pressures within the crack and the intensity of the reflected stress wave. In this regard, stiff motor cases in close proximity to the crack are most conducive to crack closure.

Over the range of parameters considered, Tables 1 and 2 indicate that crack thickness affects the spread of burning less than the cavity pressure. This may not be true at lower gas pressures and crack thicknesses. Also it may be observed that with long cracks of the order of feet in length that the downstream end condition has a negligible effect upon the initial spread of burning. In this regard experimental studies (14)

Table 1  
SPREAD OF BURNING FROM CAVITY INTO CRACKS  
AS FUNCTION OF CAVITY PRESSURE\*

Cavity Pressure, Bars	Depths of Burning as Function of Time, cm				
	0.3 ms	0.4 ms	0.5 ms	0.6 ms	0.7 ms
50	0 (.33-.30)	0 (.34-.29)	0.5 (.34-.29)	1.0 (.34-.28)	4.0 (.34-.27)
100	8.0 (.36-.30)	16.0 (.37-.29)	20.5 (.38-.28)	22.0 (.38-.26)	26.5 (.39-.22)
200	28.0 (.42-.20)	34.0 (.45-.28)	38.0 (.47-.26)	40.0 (.49-.22)	40.5 (.50-.18)

\* Cavity gas at 2300°K; uniform cracks 0.30 cm wide, 60 cm long, open end

\*\* Numbers in parenthesis refer to crack thicknesses in cm at front and rear of crack as influenced by gas pressures and reflected stress waves (case stiffness and distance of motor case assumed as 5,000 Bars/cm and 5. cm, respectively)

Table 2  
SPREAD OF BURNING FROM CAVITY INTO CRACKS  
AS FUNCTION OF INITIAL CRACK THICKNESS\*

Initial Crack Width, cm	Depths of Burning as Function of Time, cm				
	0.3 ms	0.4 ms	0.5 ms	0.6 ms	0.7 ms
0.05 (open)	7.0 (.11-.05)	8.5 (.12-.04)	9.5 (.14-.03)	10.5 (.16-.01)	11.5 (.17-0)
0.12 (open)	7.5 (.36-.30)	12.0 (.37-.29)	15.0 (.38-.28)	16.0 (.38-.26)	17.0 (.39-.22)
0.30 (open)	8.0 (.36-.30)	16.0 (.37-.29)	20.5 (.38-.28)	22.0 (.38-.26)	26.5 (.39-.22)
0.30 (closed)	8.0 (.36-.29)	16.0 (.37-.29)	20.5 (.38-.29)	21.5 (.38-.30)	25.5 (.38-.32)

\* Cavity gas at 200 Bars, 2300°K; uniform cracks, 60 cm long

\*\* Numbers in parenthesis refer to crack thicknesses in cm at front and rear of crack as influenced by gas pressures and reflected stress waves (case stiffness and distance of motor case assumed as 5,000 Bars/cm and 5. cm, respectively)

with short cracks of the order of inches in length show that the end condition has a very important effect upon the spread of burning under essentially uniform pressures.

Finally it should be observed that the downstream end of closed-ended cracks tend to contract less than cracks connected to a low-pressure reservoir. In none of the above cases did the gas pressures within the crack rise appreciably above the cavity pressure.

In order to produce pronounced pressure rises within the crack we chose a long crack with an inverted taper to yield more uniform crack thicknesses following contraction. An inverted taper was chosen in that cracks tend to open at the upstream end and close at the downstream end. The upstream end of the crack was considered connected to a cavity held at a pressure of 200 Bars while the downstream end was considered closed. To accentuate the reflected stress wave we chose a very stiff motor case of 10,000 Bars/cm located at a distance of 5 cm from the crack.

Crack deformations, and gas pressure and velocities are shown in Fig. 17. The crack deformations are scaled independently of the crack length. Extent of burning is indicated by the dashed lines using an arbitrary burn criterion of 0.1 cm/sec. Gas velocities and pressures within the crack are presented along the length of the crack. Pressure and velocity predictions are not presented at 0.73 ms due to unaccountable energy losses from the gas. It is believed that the computational error is due to order of magnitude variations in the crack thicknesses during the final stages of crack collapse. Throughout the run, mass was conserved. In spite of large energy losses very rapid and pronounced pressure rises were predicted within the crack at 0.73 ms. However, the magnitude of these pressures cannot be defined until the code is revised to treat pronounced variations in the crack thicknesses.

From Fig. 17 it may be seen that the gas pressures are generally low up to 0.50 ms except at the closed end of the crack.



The elevated pressure is caused by the reflected shock. Up to this time high velocity gas flow is the prime cause of pressure changes rather than burning. The reverse would be expected if the crack contracts sufficiently. Important considerations in this regard are the extent to which a crack is able to contract in view of its highly irregular surfaces, and the consequences of possible impact. In the example cited by Fig. 17, the minimum crack thickness was achieved at 0.73 ms and subsequently increased. However, in view of the computational error cited earlier, it was not possible to quantify how close the propellant surfaces came to impacting.

Depths of propellant evolved were quite small -- ranging from a few microns to a few tens of microns. The greatest loss occurred at the upstream end of the crack due to higher heat-transfer rates and longer burning times. At the region of minimum crack thickness at 0.73 ms, only 2 microns of propellant were evolved. This suggests that crack surfaces may not be appreciably altered by the burning prior to any impact. Leaving much of the more sensitive propellant components at the surface could have important effects upon the consequences of crack closure/impact. This subject will be returned to in the next section.

#### 4. SUMMARY, CONCLUSIONS AND FUTURE NEEDS

In this section we shall summarize conclusions derived from this study. Following this we shall present our views regarding future studies to resolve this most complex problem.

##### 4.1 Summary and Conclusions

Several phenomena have been identified as playing an important role in causing rapid pressure rises within cracks. The first is pressure-induced deformations of cracks.

During periods of gas filling, cracks will expand in a non-uniform fashion as high-pressure gas flows into the crack. Crack surfaces can displace outward at rates as high as 100 to 200 cm/sec. Since the period of gas filling is of the order of milliseconds (depending upon crack dimensions), cracks can expand by as much as tenths of a centimeter.

Cracks will continue to expand at least until arrival of stress waves. These stress waves could arise from other cracks and/or by reflection from the motor case. In this study consideration was given only to reflected stress waves. With multiple cracks, the problem becomes highly statistical. Quantification of the conditions (cracks, motor case, and propellant composition) necessary to produce rapid closure of cracks has yet to be accomplished.

Another possibly important factor in causing rapid pressure rises is that burning velocities can achieve values at least 2 to 3 times larger than their quasi-steady-state counterparts as a consequence of rapid increases of heating. In this regard, increased gas pressures, temperatures and velocities produced during the final stages of crack collapse could have important implications in accelerating gas burning.

At least two aspects of propellants can play an important role in accentuating the propellant burning rates. The first is their activation energy. The higher the activation energy,

the less the temperature rise needs to be to increase the velocity by a given amount. Thus propellants with higher activation energies will exhibit more rapid and pronounced velocity responses to changing thermal fluxes. In this regard HMX is particularly hazardous, in that its activation energy is almost twice that of conventional propellant ingredients.

The second factor is internal heating. During the course of this study we have found that positive net internal heating will cause greater overshoots of the velocities than those indicated previously for zero net internal heating (see Figs. 14 and 15). The problem here is the lack of information describing internal heating during highly dynamic burning. Using steady-state values, while questionable, is the best alternative at the present time.

During the final stages of crack collapse the problem becomes more and more conjectural involving large uncertainties in the

- Consequence of possible impact
- Gas flow
- Amounts of heat feedback from burning propellant
- Internal heating
- Reaction kinetics

At some point during crack collapse, analysis will not suffice and one must resort to experiments. Model predictions will still be needed, however, to establish the experimental conditions. In the next section we shall briefly discuss the type of experiments needed to assess the consequence of crack collapse.

#### 4.2 Future Needs

Several important provisions need to be incorporated into the code. These are

- Equation of state
- Variable-length crack elements to expedite calculations

- Means for approximating heat feedback from burning propellant
- Means for accomodating highly variable crack thicknesses in the gas dynamic calculations
- Crack propagation criterion
- Provisions for branching cracks
- Time-dependent conditions at open ends of cracks
- Detonation criterion

Of paramount importance is knowledge regarding the consequence of impacting burning surface at elevated pressures. As noted earlier, such knowledge is best acquired experimentally. These experiments should involve impacting burning propellant surfaces at various ambient pressures. In such experiments care needs to be exercised to achieve realistic closure speeds, as well as crack surfaces and burning conditions.

The ultimate objective of such experiments should be the identification of the threshold conditions (closure speeds, burning conditions and pressures) required to initiate detonation. Once these threshold conditions have been established, the code shall be in a position to explore various means by which the threshold conditions may be avoided through changes in high-energy propellants, operational pressures, and motor design.

## REFERENCES

1. Takata, A.N., W. Wulff, et al., Study of the Behavior of Systems Containing High Explosives When Subject to Fire, Part I, DASA Report No. 1833, July 1966.
2. Bernecker, R.R., D. Price, Sensitivity of Explosives to Transition from Deflagration to Detonation, NOLTR Report 74-186, Feb. 1975.
3. Bernecker, R.R. and D. Price, "Studies in the Transition from Deflagration to Detonation in Granular Explosive-III. Proposed Mechanisms for Transition and Comparison with Other Proposals in the Literature," Combustion and Flame 22, pp 161-170, 1974.
4. Kot, C.A., H.S. Napadensky, et al., A Numerical Study of Impact Phenomena in Explosives and Propellants, presented at the First International Conference on Computational Methods in Nonlinear Mechanics, Sept. 1974.
5. Napadensky, H., et al., "Evaluating the Sensitivity of Propellants," Bull. Third ICRPG/AIAA Solid Propellant Conference, 1968.
6. Napadensky, H., "Sensitivity of Explosive Systems to Detonation and Subdetonation Reactions," Annals N.Y. Academy of Science 152, Oct. 1968.
7. Mader, C.L., "Shock and Hot Spot Initiation of Homogeneous Explosives," The Physics of Fluids 6(3), Mar. 1963.
8. Takata, A.N., Vulnerability of Nuclear Weapons to Fire - Studies of Burning Explosives, DASA Report 1417, Dec. 1963.
9. Baer, A.D. and N.W. Ryan, Ignition and Combustion of Solid Propellants, AFOSR Report 69-0349 TR, 1969.
10. Baer, A.D. and N.W. Ryan, Ignition and Combustion of Solid Propellants, AFOSR Report 68-1858, 1968.
11. Siddique, K.M. and I.E. Smith, "Hot Particle Ignition of Double-Base Propellants," J. Spacecraft 12(11), Nov. 1975.
12. Krasnov, Y.K., V.M. Margulis, A.D. Margolin and P.F. Pokhel, "Rate of Penetration of Combustion into Pores of an Explosive Charge," Combustion, Explosion and Shock Waves 6(3), Mar. 1973.
13. McAlevy, R.F. and R.S. Magee, Flame Spreading at Elevated Pressures Over Surface of Igniting Solid Propellants and Propellant Ingredients in Oxygen/Inert Environments, Final Report by Stevens Institute of Technology, Oct. 1967.
14. Godai, T., "Flame Propagation into Crack of Solid-Propellant Grain," AIAA Journal 8(7), July 1970.
15. Bernecker, R.R. and D. Price, "Studies in the Transition to Detonation in Granular Explosives - I. Experimental Arrangement and Behavior of Explosives Which Fail to Exhibit Detonation," Combustion and Flame 22, pp 111-117, 1974.

REFERENCES (contd)

16. Price, D. and R.R. Bernecker, "Sensitivity of Porous Explosives to Transition from Deflagration to Detonation," Combustion and Flame 25, pp 91-100, 1975.
17. Roth, J.F. and G.P. Wachtell, "Heat Transfer and Chemical Kinetics in the Ignition of Solid Propellants," I & EC Fundamentals 1(1), Feb. 1962.
18. Gross, D. and A.B. Amster, "Thermal Explosives: Adiabatic Self-Heating of Explosives and Propellants," Eighth Symposium (Intl) on Combustion Erosive Burning: Solid Propellants, published by The Williams & Wilkins Co., Baltimore Maryland, 1962.
19. Kuo, K.K., R. Vichnevetsky and M. Summerfield, "Theory of Flame Front Propagation in Porous Propellant Charges Inter Continent," AIAA Journal 11(4), Apr. 1973.
20. Kitchens, C.W. Jr., Characteristic Theory Applied to Flame Spreading in Porous Propellants, BRL Report 1604, Aug. 1972.
21. Krier, H. and S. Rajan, "Flame Spreading and Combustion in Packed Beds of Propellant Grains," AIAA paper 75-240, Jan. 1975.
22. Krier, H., J.S. Tien, W.A. Serigano, and M. Summerfield, "Non-steady Burning Phenomena of Solid Propellants: Theory and Experiments," AIAA Journal 6(2), Feb. 1968.
23. Krier, H., "Solid Propellant Burning Rate During a Pressure Transient," Comb. Sci. Tech. 5, 1972.
24. Belyaev, M.F. and N.N. Bakhman, "Theory of Burning of Powders and Solid Rocket Propellants," Combustion, Explosion and Shock Waves 2(4), Winter 1966.
25. Novozhilov, B.V., "Interpolation Formula for the Burning Rate of Certain Composite Systems," Fizcka Goreniya i Vzryra 5(4), Fall 1969.
26. Jacobs, S.J., "Recent Advances in Condensed Media Detonations," ARS Journal, Feb. 1960.
27. Beckstead, M.W., R.L. Derr and C.F. Price, "The Combustion of Solid Monopropellants and Composite Propellants," Thirteenth Symposium (Intl) on Combustion, 1971.
28. Beckstead, M.W., R.L. Derr and C.F. Price, "A Model of Composite Solid-Propellant Combustion Based on Multiple Flames," AIAA Journal 8(12), Dec. 1970.
29. Taylor, J.W., "The Burning of Secondary Explosive Powders by a Convective Mechanism," Faraday Soc. Trans. 58(I), pp 561-568, 1962.
30. Nelson, C.W., Response of Three Types of Transient Combustion Models to Gun Pressurization, BRL Report, Internal Memo Report No. 447, Oct. 1975.

REFERENCES (concl)

31. Jacobs, H.R., W.L. Hufferd and M.L. Williams, Further Studies of the Critical Nature of Cracks in Solid Propellant Grains, Air Force Rocket Propulsion Laboratory Report AFRPL-TR-75-14, Jan. 1975.
32. Francis, E.C., C.H. Carlton and G.H. Lindsey, "Viscoelastic Fracture of Solid Propellants in Pressurization Loading Conditions," J. Spacecraft 11(10), Oct. 1974.
33. Baer, A.D. and N.W. Ryan, Ignition and Combustion of Solid Propellants, Univ. of Utah Report under Air Force Grant AFOSR 67-40a, Sept. 1968.
34. McAdams, W.H., Heat Transmission, published by McGraw-Hill Book Co., Inc., New York, N.Y., 1954.
35. Carslaw, H.S. and J.C. Jaeger, Conduction of Heat in Solids, 2nd ed., published by Oxford Press, 1959.
36. Properties of Explosives of Military Interest, ORDP 20-177, May 1960.
37. Goodman, T.R., "The Heat-Balance Integral and its Application to Problems Involving a Change of Phase," Transactions of the ASME, Feb. 1958.
38. Citron, S.J., "Heat Conduction in a Melting Slab," J. Aerospace Sciences, Mar. 1960.
39. Sanders, "Transient Heat Conduction in a Melting Finite Slab: An Exact Solution," ARS Journal, Nov. 1960.

## APPENDIX A

### MEANS FOR PREDICTING REGRESSION VELOCITIES

#### A.1 INTRODUCTION

During burning, propellants can evolve material into the gas stream by the discharge of molten material and gas. These effects are not independent of each other in that molten material from one of the propellant constituents can flow over other constituents and affect the rates at which they evolve. Here we shall discount such an effect and concentrate our attention upon each of the two ideal situations cited above. The actual situations undoubtedly lie somewhere in between.

#### A.2 CRITERIA FOR ASSESSING VELOCITIES

##### A.2.1 Gas Evolution

A common practice is to predict regression velocities  $V$  using the surface temperature  $T(O) + T_0$  as follows

$$V = a \exp - (E/(T(O)+T_0)) \quad (A-1)$$

where  $a$  = constant, cm/sec

$E$  = activation energy divided by gas constant

Implicit in this expression is that there is a constant mass of material at temperature  $T(O) + T_0$ . Here we refer to the presence of a thin hot melt/solid layer from which much of the gas originates. Certainly this assumption is reasonable for steady or near-steady burning over a limited range of velocities.

In order to use Eq. A-1 it is first necessary to predict the surface temperature  $T(O)$ . This is usually accomplished by assuming

- all heat transfer through any molten layer and underlying propellant is conductive
- all internal heating and latent-heat absorption occurs at the surface

While neither of these assumptions are appealing they are presently necessary in lieu of adequate information and understanding of the many complex processes taking place near the surface.

In the remainder of this appendix we shall present an alternative to Eq. A-1, predicated upon changes of the mass from which gas evolves during highly dynamic burning. Choice of most appropriate approach depends upon how the mass of critically heated propellant changes during dynamic heating and burning. With Composition B, we have found the foam mass during steady burning to increase slightly with pressure (1). On the other hand, PBX resulted in decreases in mass as the pressure was elevated. Unfortunately such steady-state experiments do not indicate how the mass will change under dynamic heating conditions.

For this case we shall assume that the melt is indispersed with solid particulates in such a fashion that one can treat the heat transfer as conductive. All thermal properties are assumed as constant. Integrating the Arrhenius relationship over some depth  $\delta$  containing most of the heat yields

$$V = Z \int_0^{\delta} \exp(-E/(T(x)+T_0)) dx \quad (A-2)$$

where  $V$  = rate of surface regression  
 $T(x)$  = temperature rise at depth  $x$   
 $Z$  = frequency factor  
 $E$  = activation energy divided by universal gas constant  
 $T_0$  = initial temperature, absolute

Because of the exponential term in Eq. A-2 the integration needs to be performed only over shallow depths of propellant having temperatures in the vicinity of the surface temperature. Proceeding upon this fact, the near-surface temperatures  $T(x)$  will be approximated using the following exponential relationship:

$$T(x) = T(0) \exp-Cx \quad (A-3)$$

where  $C$  is a constant which for steady-state burning equals the velocity  $V$  divided by the thermal diffusivity  $\alpha$ . To determine

the appropriate expression for C for unsteady burning we shall multiply Eq. A-3 by -K and differentiate with respect to x to arrive at an effective flux q of

$$q = -K \left. \frac{\partial T(x)}{\partial x} \right|_{x=0} = KT(0)C \quad (\text{A-4})$$

where K = thermal conductivity. Solving Eq. A-4 for C yields

$$C = \frac{q}{KT(0)} \quad (\text{A-5})$$

Equation A-2 will now be approximated by first replacing the variable x by the variable y given below.

$$y = T(0) \exp(-Cx) + T_0 \quad (\text{A-6})$$

The result is

$$v = \frac{Z}{C} \int_{y_1}^{y_2} \frac{\exp(-E/y)}{y-T_0} dy \quad (\text{A-7})$$

$$\begin{aligned} \text{where } y_2 &= T(0) + T_0 \\ y_1 &= T(\delta) + T_0 \end{aligned}$$

Expanding the integral of Eq. A-7 by parts yields

$$\begin{aligned} \int_{y_1}^{y_2} \frac{\exp(-E/y)}{y-T_0} dy &= \frac{\exp(-E/y) \cdot y^2}{E(y-T_0)} \Big|_{y_1}^{y_2} - 2 \int_{y_1}^{y_2} \frac{\exp(-E/y) \cdot y}{E(y-T_0)} dy + \\ &\int_{y_1}^{y_2} \frac{\exp(-E/y) y^2 dy}{E(y-T_0)^2} \end{aligned} \quad (\text{A-8})$$

Here the two integrals on the right-hand side of Eq. A-8 are small compared to the integral on the left-hand side and tend to cancel each other out. Neglecting these terms, and the negligibly small contributions from the lower limit  $y_1$ , yields

$$v = \frac{Z}{CE} \exp(-E/(T(0)+T_0)) \cdot (T(0)+T_0)^2 / T(0) \quad (\text{A-9})$$

Using the appropriate expression for C, this equation can be applied to either steady or unsteady burning. For unsteady burning, the velocity from Eqs. A-5 and A-9 is

$$v \approx \frac{KZ}{qE} \exp(-E/(T(O)+T_0)) \cdot (T(O)+T_0)^2 \quad (A-10)$$

This equation presumes that the critical mass decreases inversely with the heat flux. Choice of Eq. A-1 or Eq. A-1 depends upon whether or not this assumption is more valid than a constant mass. Here we have arbitrarily chosen to use Eq. A-1 for HMX. Future analyses needs to be conducted to establish the consequence of the two assumptions upon detonation. If found important, experimental studies should be conducted to establish which of the two approaches is more valid for each of the more sensitive propellant ingredients.

#### A.2.2 Melt Evolution

To treat this ideal situation, the temperature of the regressing surface must be maintained at its melt temperature. Incident fluxes  $q'$  are discounted by the rate of heat absorption needed to melt the propellant at the computed velocity. The result is represented by the effective flux  $q$ . Temperatures are calculated as described by Appendix D.

In the next section we shall discuss how the required displacements are calculated for each time interval.

### A.3 COMPUTATIONAL SCHEMES FOR DETERMINING DISPLACEMENTS $\Delta x_i$

Displacements  $\Delta x$  are determined for each time interval by a trial and error method using the criteria discussed in Section 2 of this appendix. Here the displacement or velocity are approximated by computing limits within which the correct value lies --  $\Delta x_i$  for the case of gas evolution, of  $V_i$  for the case of melt evolution. These limits are progressively narrowed following each trial. Successive estimates are set close to the geometric mean for the case of gas evolution, or equal to the arithmetic mean for the case of melt loss.

#### A.3.1 Displacements by Gas Evolution

For each trial the temperature at  $x_{i-1} + \Delta x_i$  is computed using Eqs. D-21 and D-22 followed by a determination of the

velocity  $V_i$  using Eq. A-10. The estimated  $\Delta x_i$  and the resultant value for  $\overline{\Delta x}_i = (V_{i-1} + V_i) \Delta t_i / 2$  are then used to narrow the  $\Delta x$  limits. If  $\overline{\Delta x}_i > \Delta x_i$ , the lower limit is set equal to  $\Delta x_i$  while the upper limit is set equal to  $0.5\Delta x_i + 0.6\overline{\Delta x}_i$ .

If  $\overline{\Delta x}_i < \Delta x_i$ , the upper limit is set equal to  $\Delta x_i$  and the lower limit is set equal to  $0.5\Delta x_i + 0.4\overline{\Delta x}_i$ .

The reason for setting the limits as described is due to the fact that temperature decreases with depth. The result is non-linear decreases in the estimates of the velocity with increases in depth such that

$$|\overline{\Delta x}_i - \Delta x| > |\Delta x_i - \Delta x| \quad (\text{A-12})$$

where  $\Delta x_i$  and  $\overline{\Delta x}_i$  bracket the correct value  $\Delta x$ .

If the limits agree to within 5 percent the computations are completed. Otherwise, a new trial  $\Delta x_i$  is taken close to the geometric mean of the two limits and the process repeated. Generally 2 to 7 trials are needed.

### A.3.2 Displacements by Melt Evolution

This situation is treated in a very similar fashion as discussed in Section 3.1. The principal differences are in using velocity limits, and in using arithmetic means to upgrade the velocity estimates.

For each trial velocity, the trial displacement is substituted into Eqs. D-21 and D-22 to determine the surface temperature. Then the velocity limits are narrowed according to the calculated temperature  $T_i$  at the trial depth  $\Delta x_i$ . For the first trial, the upper velocity limit  $V_h$  is set equal to the highest value possible, namely

$$V_h = \frac{q}{\rho C T_m} \quad (\text{A-13})$$

where  $q$  = effective flux allowing for melting (See Eq. 2)  
 $\rho$  = density

C = specific heat

$T_m$  = melt temperature above initial temperature

Initially the lower limit  $V_l$  is set equal to 0. A trial velocity  $V$  is then taken halfway between the two limits, and used to determine the temperature rise  $T_1$  corresponding to the resultant displacement  $V \cdot \Delta t$ . Here  $\Delta t$  represents the time interval previously selected.

Limits are then adjusted according to whether or not  $T_1$  is above or below  $T_m$ . Here we use the temperature gradient to estimate the displacement and velocity changes necessary to yield  $T_m$ . To prevent overcorrections, only half of the velocity changes are used. The result is the new limiting velocity  $\bar{V}$  presented below

$$\bar{V} = V + \frac{K(T_1 - T_m)}{2q\Delta t} \quad (A-14)$$

If  $T_1$  is less than  $T_m$ , the upper limit  $V_h$  is set equal to the minimum of its previous value and  $\bar{V}$ . If  $T_1$  exceeds  $T_m$ ,  $V_l$  is set equal to the maximum of its previous value and  $\bar{V}$ .

A new trial value is then computed for  $V$  based upon the arithmetic mean of  $V_l$  and  $V_h$ . Once these limits agree to within 5 percent the computations are completed. Generally 2 to 7 trials are necessary to approximate the velocity and associated displacement  $\Delta x$ .

APPENDIX B  
GAS DYNAMIC MODEL

B.1 INTRODUCTION

One essential aspect of the initiation and burning of propellants in cracks is the transfer of the gaseous reaction products (and the energy and momentum associated with this gas) along the crack. Thus the establishment of a gas dynamic model which includes a variety of flow features which may be significant is a basic requirement of this study. This gas dynamic model, when properly coupled with the heat transfer, ignition, and burn models will allow for the appropriate interaction of these physical events to occur and permit an investigator to examine the severity and sequence of the events which occur in this complex problem for a variety of parameter values or model variations or assumptions. In this manner an insight into the occurrence of the accidental detonation of high energy propellants can be developed as well as providing a rational basis for the design of experiments with which to verify or evaluate the importance of some parameters or effects. This appendix presents the development of the gas dynamic model and its associated numerical representation for computer application.

The gas dynamic model which already includes a variety of features and effects is still considered to be a preliminary version subject to modifications. These modifications will be indicated by initial results and/or the limited treatment of some aspects of the initial model. The gas dynamic model is based upon an Eulerian representation of the flow region and is limited to a one-dimensional treatment. The selection of the Eulerian representation permits a simple identification with propellant locations along the crack and allows for the mixing of freshly burned reaction gas with gas from other gas movements. It is also convenient for the large movements experienced by some of the gas. The one-dimensional treatment is appropriate

because of the extreme length of the crack when compared to its thickness. It is recognized that flow gradients will exist across the thickness of the crack, thus the value of the variables used in the one-dimensional treatment are average cross-sectional values. The width of the crack is assumed to be much wider than the thickness and relatively uniform. Thus the most significant flow gradients and movements will occur in the direction along the length of the crack.

The current model treats a crack of some specified thickness variation at a reference time (defined as zero time). The gas in this crack at this time is of the same composition as the reaction products and exists in a rest state (no flow) at some low pressure and temperature (say the ambient temperature of the propellant). The crack is connected, at the upstream end, to the primary rocket motor chamber which is filled with gaseous reaction products which are at a high temperature and a high pressure. The chamber state is treated as a constant state with respect to time because of the relatively short duration of the events occurring within the crack. This simple treatment can be readily modified to accommodate some other specified chamber state variation. The crack is connected instantaneously to the chamber and thus a rapid inflow of hot gas occurs in the crack. This is the start of the process which may lead to the unwanted detonation of the high energy propellant. It would represent a situation in which an internal crack propagates until it intercepts the primary chamber. A number of other starting conditions could be formulated, however it is believed that the above stimuli is somewhat representative and should lead to conditions of interest in identifying the mechanisms and interactions which may lead to rapid propellant burning within the crack.

The downstream end of the crack can be represented by either a closed end or a connection to a low pressure chamber. In the latter case only gas outflow is permitted and the pressure in the low pressure chamber is held constant at the level of the initial

pressure within the crack. This situation represents a possible connection to a relatively large debonded region which is momentarily isolated from the primary chamber. In this case the crack length is constant. If the closed end crack condition is selected it is possible to permit the length of the crack to grow in some arbitrarily selected manner. This crack growth feature is not based, as it ultimately should be, upon some physically plausible crack propagation mechanism. The incorporation of such a criteria together with the possibility of the branching of a single crack to form a complex network of cracks represents some of the ultimate goals for the improvement of the overall physical model.

## B.2 BASIC EQUATIONS

The equations of fluid dynamics are written with respect to the Eulerian frame of reference in which the independent variables are the distance,  $x$ , along the crack and the time,  $t$ . These equations represent the conservation of mass, momentum, and energy. The present gas dynamic model includes the effects of inertia, wall friction, mechanical wall response, and mass and energy addition. Heat transfer effects are incorporated into the energy addition term. Furthermore the incorporation of mechanical wall response effects appear at this stage as wall movement and flow area variations along the crack. The mechanical response of the propellant to the imposed pressure environment is treated in Appendix C.

The conservation laws can be developed by considering a control surface enclosing an element of volume of length,  $dx$ . This control surface is illustrated in Figure B.1. The conservation laws state that the time rate of change of the entity considered, within the control volume must equal the net flux of this entity through the control surface, plus any related boundary contributions such as mass or energy addition, work done at the boundary, or boundary forces. The area of the flow channel,  $A$ , is one of dependent variables to be considered. However, in

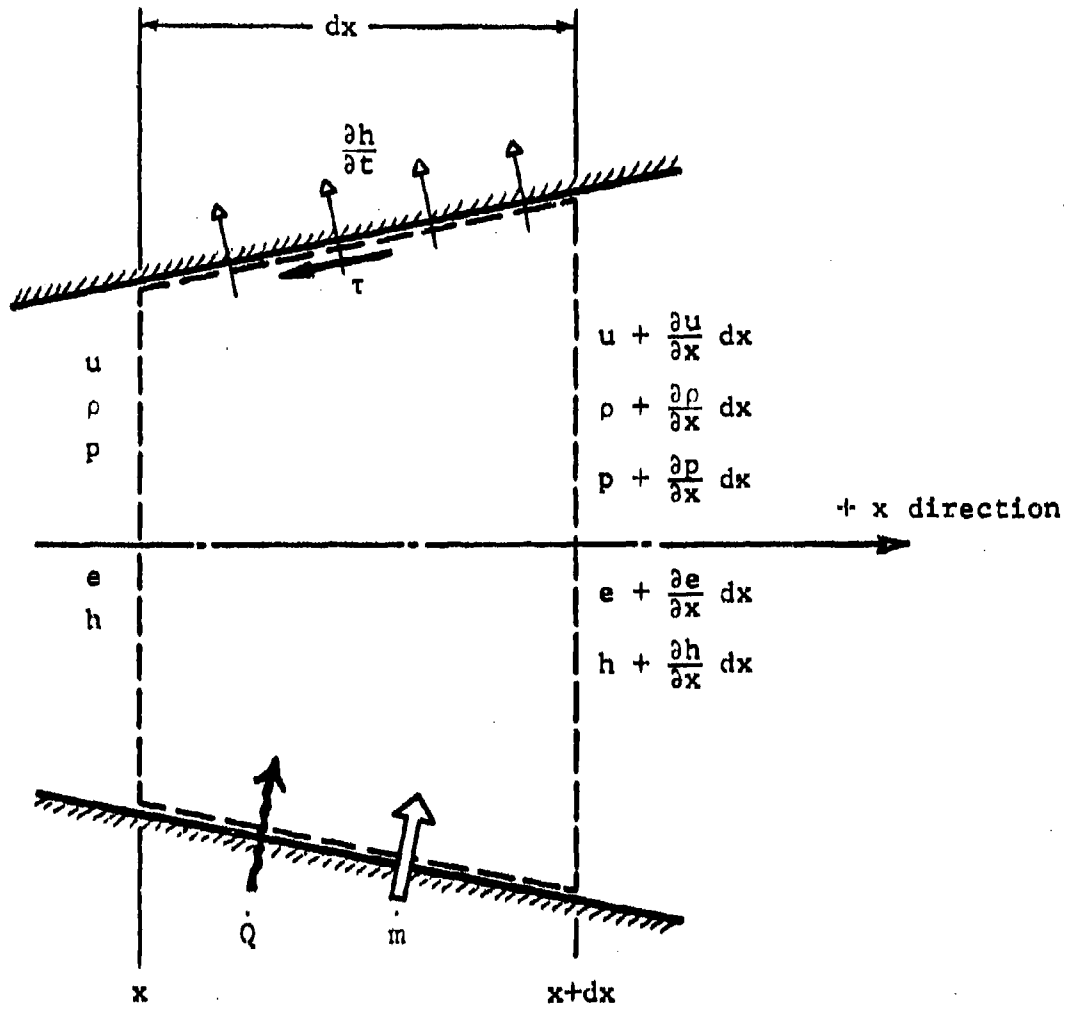


Figure B-1 Control Surface For Flow Channel

view of the fact that the crack is very wide compared to its thickness or height, the width of the flow channel can be set equal to unity and a corresponding variable, the crack height,  $h$ , can be used. Thus

$$A = 1 \cdot h \quad (B-1)$$

It should be noted that although this variable has the dimensions of length, a dimensional check of the following equations will imply that it should have the dimensions of length squared. This is the case when it represents the area of the flow channel.

The three conservation equations are:

Mass

$$\frac{\partial \rho}{\partial t} + \rho \frac{\partial u}{\partial x} + u \frac{\partial \rho}{\partial x} = \frac{\dot{m}}{h} - \frac{\rho u}{h} \frac{\partial h}{\partial x} - \frac{\rho}{h} \frac{\partial h}{\partial t} \quad (B-2)$$

where  $\rho$  = gas density

$u$  = gas velocity

$\dot{m}$  = mass addition per unit length per unit time

The wall motion (velocity) is given by  $(\partial h / \partial t)$  (see Figure B-1)

Momentum

$$\frac{\partial u}{\partial t} + u \frac{\partial u}{\partial x} + \frac{1}{\rho} \frac{\partial p}{\partial x} = - \frac{2\tau}{\rho h} - \frac{u\dot{m}}{\rho h} \quad (B-3)$$

where  $\tau$  = wall shearing stress. The wall shearing stress can be expressed in terms of the conventional pipe friction coefficient,  $f$ , defined by

$$f = \frac{\tau}{\frac{1}{2}\rho u^2} \quad (B-4)$$

Furthermore this stress acts in a direction opposite to the fluid motion. The momentum equation can then be reformulated as:

$$\frac{\partial u}{\partial t} + u \frac{\partial u}{\partial x} + \frac{1}{\rho} \frac{\partial p}{\partial x} = - f \frac{u|u|}{h} - \frac{u\dot{m}}{\rho h} \quad (B-5)$$

The coefficient  $f$  is assumed to be constant at a nominal value because its value and dependence are uncertain for this complex flow environment.

### Energy

$$\frac{\partial e_T}{\partial t} + u \frac{\partial e_T}{\partial x} + \frac{1}{\rho} \frac{\partial}{\partial x}(\rho u) = \frac{\dot{Q}}{\rho h} - \frac{\rho u}{\rho h} \frac{\partial h}{\partial x} - \frac{p}{\rho h} \frac{\partial h}{\partial t} - \frac{e_T \dot{m}}{\rho h} \quad (\text{B-6})$$

where  $\dot{Q}$  = energy addition per unit length per unit time

$e_T$  = specific total energy

The specific total energy is given by

$$e_T = e + \frac{1}{2} u^2 \quad (\text{B-7})$$

where  $e$  = specific internal energy.

Equations (B-2), (B-5) and (B-6) have been arranged so that the terms which define the contributions of the special effects are grouped on the right hand side of the equal sign. When the sum of the terms of the right hand side are set equal to zero the conventional gas dynamic equations for the nonsteady flow in a constant area channel are obtained. These reduced equations will be used to establish the numerical method.

### B.3 EQUATION OF STATE

The equation of state which has been selected initially for the propellant reaction products is that of a perfect gas. This equation of state is considered to be adequate for the initial phases of the investigation, but eventually a better formulation must be established.

The perfect gas representation is the following:

$$p = \rho R T \quad (\text{B-8})$$

where  $R$  = gas constant

$T$  = absolute temperature of the gas.

Furthermore, the specific heats at constant pressure and at constant volume are both constant. The internal energy is given as

$$e = \frac{p}{(\gamma-1)} \quad (\text{B-9})$$

where  $\gamma$  = ratio of specific heats.

The sound velocity of the gas,  $c$ , is given as

$$c = \sqrt{\frac{\gamma P}{\rho}} \quad (\text{B-10})$$

The values of the gas constant, the two specific heats and the ratio of specific heats are subject to some uncertainty. The following values have been selected for the gas constant and the ratio of specific heats for the reaction products

$$R = 3228. \quad (\text{cm}^2/\text{C})$$

$$\gamma = 1.2$$

#### B.4 FLOW CONFIGURATIONS AND BOUNDARY CONDITIONS

The solutions of the above field equations are subject to the initial conditions within the crack and to boundary conditions at both the upstream and downstream end of the flow channel. The initial conditions are those of a gas at rest ( $u(x) \equiv 0$ ) and at some pressure  $p_0$ , and temperature,  $T_0$ . The initial height,  $h_0(x)$  of the channel is also specified, however no initial wall motion is permitted (i.e.  $(\partial h_0/\partial t) \equiv 0$ ). The propellant mass in the vicinity of the crack is thus in mechanical equilibrium with the initial pressure field within the crack.

Two basic crack configurations are treated. These are illustrated in Figure B-2. They consist of a high pressure cavity connected to the upstream end ( $x=0$ ) of a crack of length,  $L_c$ , together with one of two downstream end conditions. One configuration has a simple closed end while the other configuration consists of a connection to a low pressure cavity. The high pressure cavity contains a gas at a pressure  $p_c$  and temperature  $T_c$ , both of which are held constant with respect to time. The gas pressure within the low pressure cavity is held constant at the level of the initial gas pressure within the crack (i.e.  $p_0$ ) and only outflow is permitted.

The boundary conditions at the high pressure cavity end will depend upon whether the gas flow is into (inflow) or out of the crack (outflow). These boundary conditions are illustrated in the Hodograph plane of Figure B-3. The cavity State,  $S_c$ , (a rest

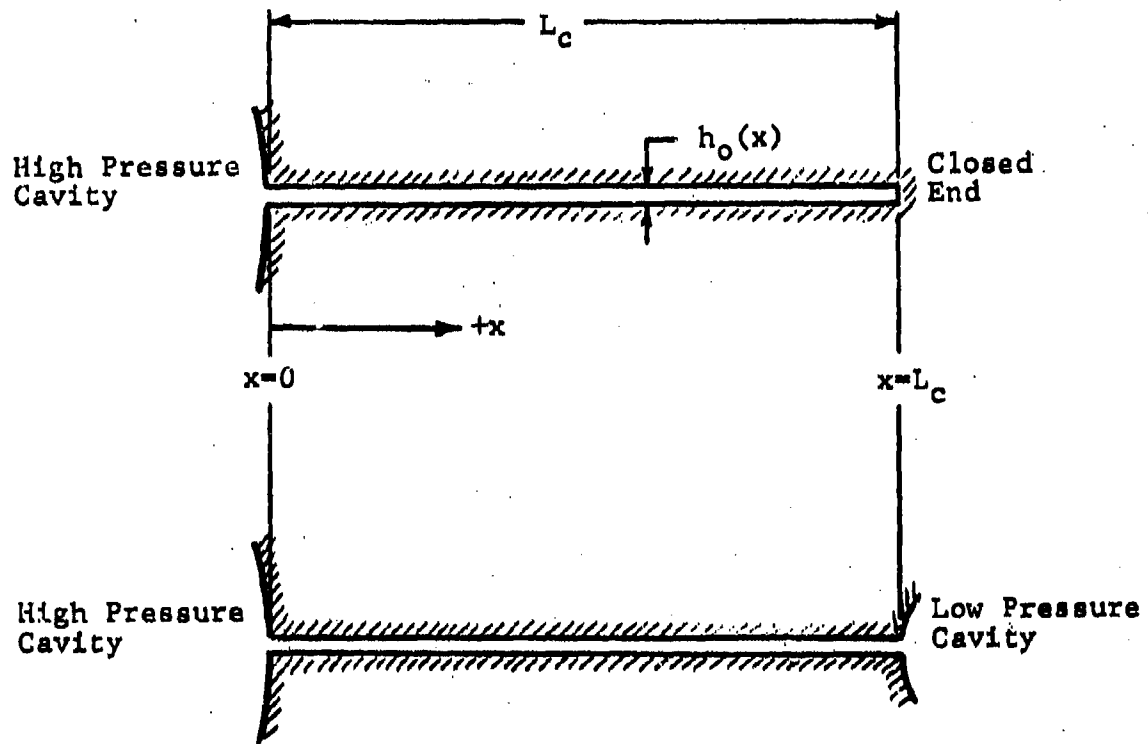


Figure B-2 Basic Crack Configurations

state) is the appropriate reference state. When the pressure is low relative to the cavity pressure at the downstream end of the crack inflow may occur. If inflow does occur, the cavity gas will flow into the crack after first expanding isentropically (at constant energy) in the vicinity of the inlet. This expansion process will accelerate the gas and lower both the pressure and the sound velocity. The flow Mach number,  $M$ , ( $M \equiv u/c$ ) will increase until it reaches a state which is in equilibrium with the internal flow at the boundary provided it does not exceed a value of unity. At that critical point no further expansion can occur since, in effect, no further information regarding any additional expansion can be communicated back to the cavity. Any additional expansion, if it can occur, will occur as a non-steady expansion within the crack. The field equation will provide for the solution of this additional expansion. Thus the permissible boundary conditions at the downstream end of the crack under inflow conditions will be those states associated with the energy line bounded by the cavity State,  $S_c$ , at one end and the sonic inflow State  $S_{s1}$  at the other end. The energy line is defined by

$$c_c^2 = c^2 + \left(\frac{\gamma-1}{2}\right) u^2 \quad (\text{B-11})$$

If subsonic outflow occurs the pressure at the upstream end of the crack will be equal to the cavity pressure,  $p_c$  (see Figure B-3). However, if the flow becomes sonic or supersonic then the pressure can change to any value such that the boundary state within the crack lies in the supersonic outflow region bounded by the sonic outflow line. This region is illustrated in Figure B-3.

The same boundary conditions apply at the low pressure cavity end of the crack when this configuration is used, however the present model does not permit inflow to occur. Some model modifications in this area may ultimately be made however, they will be influenced by the physical model associated with this low pressure cavity, such as for example a cavity filling process with a subsequent buildup of pressure and temperature within the finite volume cavity.

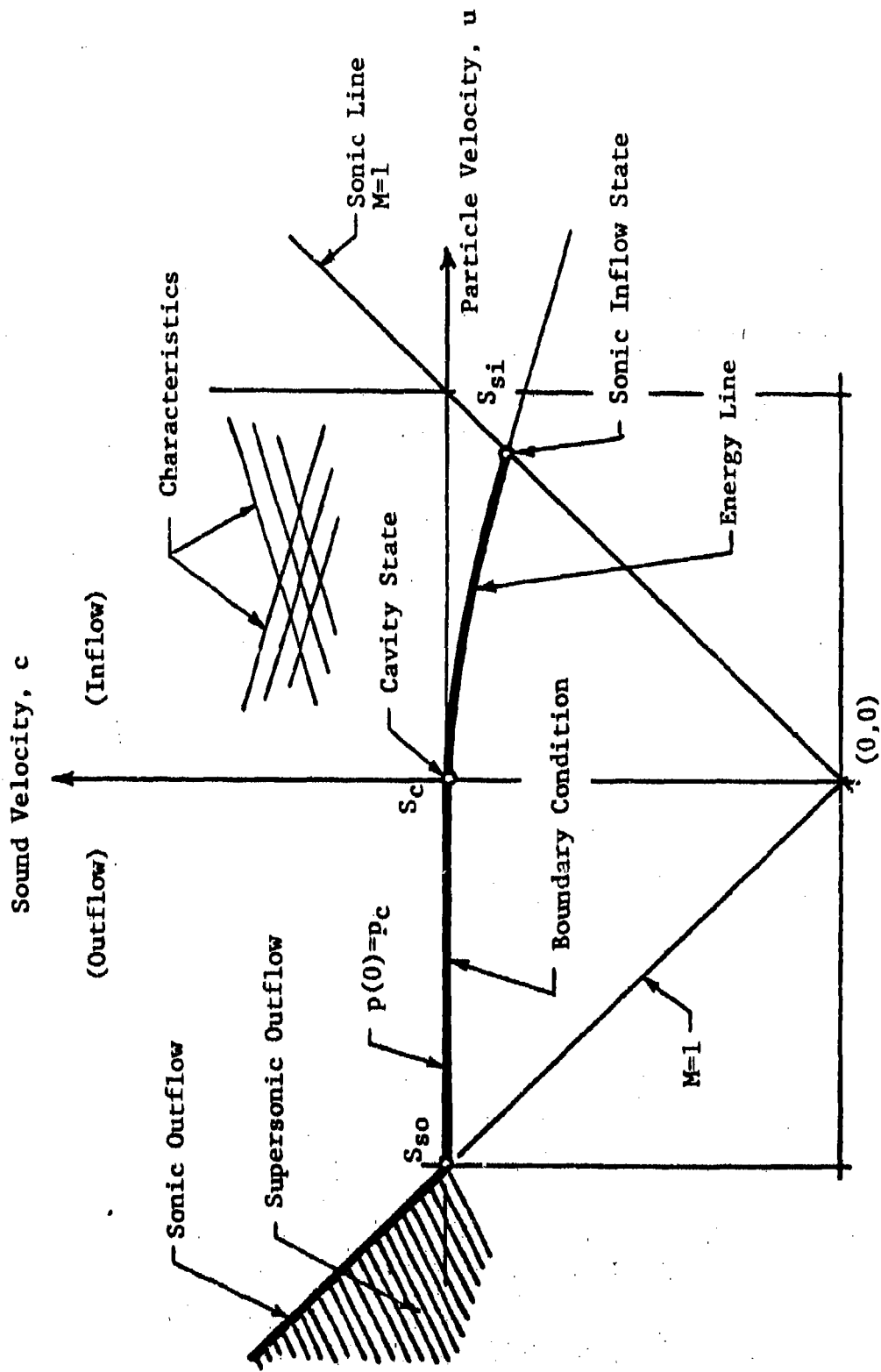


Figure B-3 Hodograph Plane. - Boundary Conditions At Cavity End

The boundary condition for the closed end is a simple one of no flow (i.e.  $u(L_c) = 0$ ). The current model does permit the crack length to be extended arbitrarily whenever this configuration is used. Whenever the crack is extended, the new portion is filled with a rest gas at the initial pressure and temperature ( $p_0, T_0$ ) and the closed end boundary condition is applied to the new closed end location. This crack extension is, in effect, an instantaneous crack extension.

### B.5 NUMERICAL PROCEDURE

The numerical solution technique employed in the gas dynamic model of the present study is, in its reduced form, a rather conventional Eulerian method of the FLIC (fluid in cell) type. This method was originally developed at the Los Alamos Scientific Laboratory.

The numerical solution of the foregoing equations proceeds from the initial conditions specified in a forward stepping time wise manner subject to the numerical solution of the field equations, auxiliary timewise inputs, and the appropriate boundary conditions. An artificial viscous pressure term,  $q$ , is added to the thermodynamic pressure during the computations when the flow is subsonic and the compression rate is positive. This contributes to the suppression of flow discontinuities and to the computational stability in regions of subsonic flow.

#### B.5.1 The Computing Mesh

A one-dimensional mesh of uniform length  $\Delta x$ , cells is established. Each cell is identified by an indice,  $i$ , corresponding to its center. Thus the boundaries of the  $i$ th cell are at the location  $i\pm\frac{1}{2}\Delta x$ . Increasing  $i$  corresponds to increasing  $x$ . The selection of uniform cell length is an initial convenience. If subsequent results indicate that one portion of the crack requires substantially greater resolution in the space variable,  $x$ , than do other portions then variable length cells can be introduced with little additional complications.

The values of the dependent variables are associated with the cell centers with the exception of the pseudoviscous terms which are computed at the cell boundaries. Assuming that all properties are known for each cell at some time  $t^n$ , the computational procedure is to determine the state in each cell at a later time  $t^{n+1} = t^n + \Delta t$ . The time step  $\Delta t$  is restricted in magnitude by conditions required for stability of the computations. The resulting space time grid network is illustrated in Figure B-4.

### B.5.2 Stability Formulation

There are several stability type conditions that other investigators have found applicable with this type numerical technique. One such restriction is that  $(u_{\max} \Delta t) / \Delta x < 1$ . If fluid particles were explicitly treated in the computation, this criterion would prevent a particle from crossing a complete cell during one time step. In the pure Eulerian scheme the interpretation is made that the transport terms are calculated more accurately with corresponding improved averaging of the numerical fluctuations. A second restriction is the familiar Courant condition,  $c\Delta t / \Delta x < 1$ , which limits the propagation of fluctuations in the subsonic flow regions. Another source of instability is the computation of negative internal energies in the cell due primarily to the treatment of boundary conditions, but also from inherent numerical fluctuations. For a fluid obeying the ideal gas relation, the criterion that prevents negative internal energies is that  $4(\gamma-1) u_{\max} \Delta t / \Delta x < 1$ . These stability criteria can be written as

$$\Delta t < \text{Min} \left( \frac{\Delta x}{u_1} \right), \text{ over } i \quad (\text{B-12})$$

$$\Delta t < \text{Min} \left( \frac{\Delta x}{c_1} \right), \text{ over } i \quad (\text{B-13})$$

$$\Delta t < .625 \text{ Min} \left( \frac{\Delta x}{u_1} \right), \text{ over } i \quad (\text{B-14})$$

In the last equation a value of 1.4 for  $\gamma$  was used. A simple stability criteria which satisfies all of the foregoing requirements and which is used in the calculations is

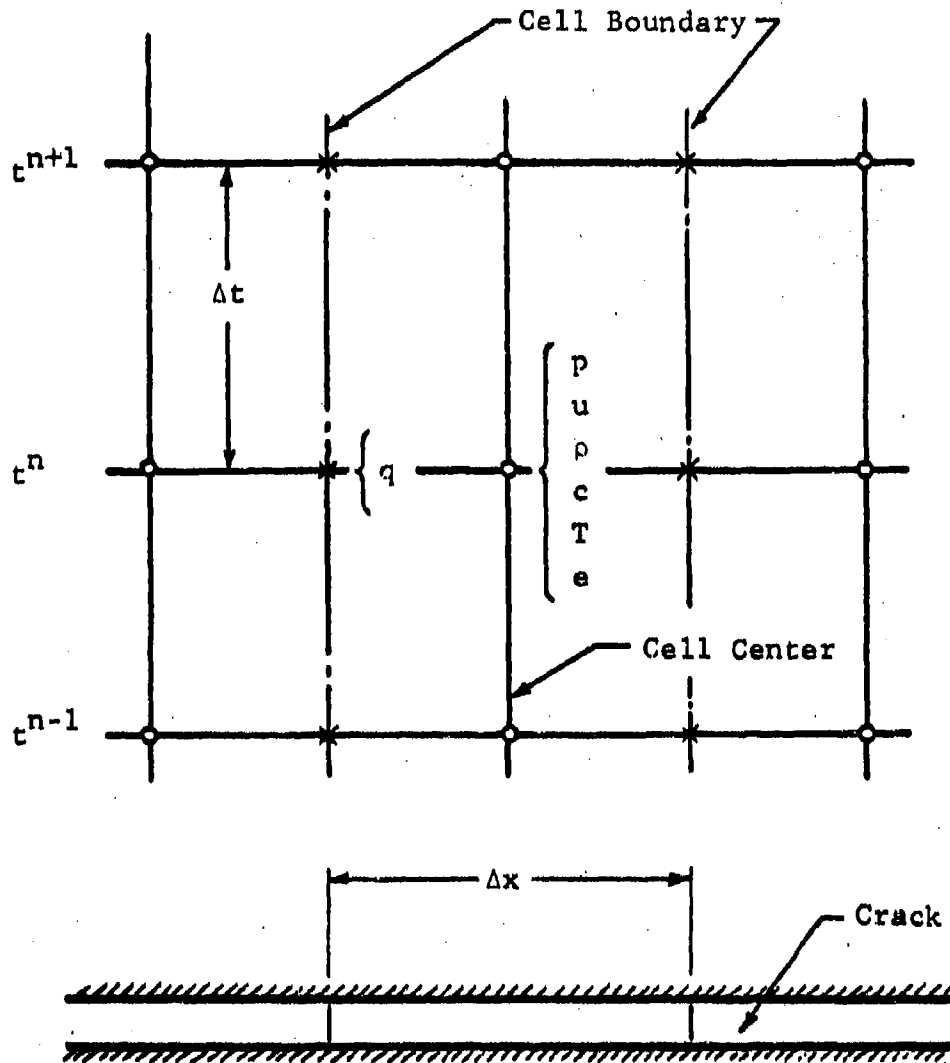


Figure B-4 One Dimensional Eulerian Space Time Mesh

$$\Delta t = \frac{1}{2} \text{Min} \left( \frac{\Delta x}{\text{Max}(u_i, c_i)} \right), \text{ over } i \quad (\text{B-15})$$

where the factor  $\frac{1}{2}$  is chosen to reflect the typical severity with which the inequalities (B-12) to (B-14) are generally applied. The introduction of special effects may have an impact upon the stability of the calculations, therefore additional time step criteria may have to be introduced.

### B.5.3 Artificial Viscosity Term

Artificial viscous pressure terms are computed at time  $t^n$  at those cell boundaries across which a negative velocity component gradient exists, provided that the local Mach number does not exceed a prescribed value defined by a constant,  $A_g$ . The terms are proportional to the velocity component differences between adjoining cells at the boundary where it is applied. Specifically,

$$q_{i+\frac{1}{2}} = B_{\rho_{i+\frac{1}{2}}} C_{i+\frac{1}{2}} (u_i - u_{i+1}) \quad (\text{B-16})$$

provided  $u_i - u_{i+1} > 0$

and  $A_g u_{i+\frac{1}{2}}^2 - C_{i+\frac{1}{2}}^2 < 0$

If either of the indicated flow conditions is not satisfied, the viscosity term is set equal to zero. The values of  $A_g$  and  $B$  used in the calculations were 100 and 0.5 respectively. The subsonic limit correspond to a Mach number of 0.1.

### B.5.4 Intermediate Values of the Flow Variables

At this stage of the development of the numerical method only the reduced form of the field equations will be treated. These equations are rewritten in the following form.

$$\frac{\partial \rho}{\partial t} + \frac{\partial}{\partial x} (\rho u) = 0 \quad (\text{B-17})$$

$$\frac{\partial u}{\partial t} + u \frac{\partial u}{\partial x} = - \frac{1}{\rho} \frac{\partial p}{\partial x} = - \frac{\partial \tilde{u}}{\partial t} \quad (\text{B-18})$$

and

$$\frac{\partial e_T}{\partial t} + \frac{\partial e_T}{\partial x} = - \frac{1}{\rho} \frac{\partial}{\partial x} (\rho u) = \frac{\partial \tilde{e}_T}{\partial t} \quad (\text{B-19})$$

where intermediate values of the velocity and the internal energy (denoted by the circumflex  $\tilde{\nu}$ ) are computed from their local rates of change neglecting the transport terms in the field equations. The gradient and divergence terms in the momentum and energy equations are calculated from numerical approximations to the equivalent surface integrals of pressure and velocity over the cell boundaries. The resulting difference equations are

$$\tilde{u}_i^n = u_i^n - \frac{\Delta t}{\rho_i^n \Delta x} \left[ (p+q)_{i+\frac{1}{2}}^n - (p+q)_{i-\frac{1}{2}}^n \right] \quad (\text{B-20})$$

and

$$\begin{aligned} \tilde{e}_i^n = e_i^n - \frac{\Delta t}{\rho_i^n \Delta x} \left[ \bar{u}_{i+\frac{1}{2}}^n (p_{i+\frac{1}{2}}^n + q_{i+\frac{1}{2}}^n) - \bar{u}_{i-\frac{1}{2}}^n (p_i^n + q_{i-\frac{1}{2}}^n) \right. \\ \left. - \bar{u}_i^n (q_{i+\frac{1}{2}}^n - q_{i-\frac{1}{2}}^n) \right] \quad (\text{B-21}) \end{aligned}$$

where the macrons used in Equation (B-21) represent the average  $(u^n + \tilde{u}^n)/2$  at the indicated subscript. These forms provide significant advantages in the development of numerical solution algorithms.

An intermediate value of the total energy  $\tilde{e}_T$  is computed from its definition, Equation (B-7), using the intermediate values of internal energy and velocity just calculated.

#### B.5.5 New Values of the Flow Variables

Final values of the flow variables at the new time  $t^{n+1}$  are calculated next for the cell centers by including the transport effects. The procedure, in principle, is to associate with the intermediate flow field a transport of mass, momentum and total energy, defined in terms of their intermediate values, across the cell boundaries. The technique of donor cell differencing is used in which the transport of these quantities is

calculated from the donor cell, i.e., the cell from which the fluid is flowing. This technique prevents cells from developing negative densities due to numerical fluctuations and provides good stability properties in the far subsonic regions of the flow.

The mass flow terms are calculated from the numerical approximation of the surface integral equivalent to the divergent term appearing in Equation (B-2), resulting in

$$\Delta M_{i+\frac{1}{2}}^n = (\rho_{i+\frac{1}{2}}^n)^{D,n} \bar{u}_{i+\frac{1}{2}}^n \Delta t \quad (B-22)$$

The superscript D is used to indicate that the density is assigned the value according to the donor cell requirement, which may be written as:

$$(\rho_{i+\frac{1}{2}}^n)^D = \begin{cases} \rho_i^n, & \bar{u}_{i+\frac{1}{2}}^n > 0 \\ \rho_{i+1}^n, & \bar{u}_{i+\frac{1}{2}}^n < 0 \end{cases} \quad (B-23)$$

It is now appropriate to rewrite the momentum and energy equations, Equations (B-17) to (B-19) as

$$\frac{\partial u}{\partial t} = \frac{\partial \bar{u}}{\partial t} - u \frac{\partial u}{\partial x} \quad (B-24)$$

and

$$\frac{\partial e_T}{\partial t} = \frac{\partial \bar{e}_T}{\partial t} - u \frac{\partial e_T}{\partial x} \quad (B-25)$$

where the reduced nonconvective equation, (Equations (B-17) to (B-19)) that are used to define the intermediate flow variables that have been used. The transport terms appearing in Equations (B-24) and (B-25) are evaluated from numerical approximate to their equivalent surface integral representations. Next, applying first order finite-differences to all temporal derivatives, the following general difference formulation of the reduced field Equations (B-17), (B-24) and (B-25) is obtained.

$$\rho_i^{n+1} F_i^{n+1} = \left\{ \rho_i \tilde{F}_i + \frac{1}{h\Delta x} \left[ \tilde{F}_{i-\frac{1}{2}}^D \Delta M_{i-\frac{1}{2}} - \tilde{F}_{i+\frac{1}{2}}^D \Delta M_{i+\frac{1}{2}} \right] \right\}^n \quad (\text{B-26})$$

where the variable F is used to represent in turn the various flow variables according to

$$F_i = \{1, u_i, (e_T)_i\} \quad (\text{B-27})$$

The identity value of F can be interpreted as a mass flow which transports only itself, thereby conserving mass and allowing Equation (B-26) to be used in the calculations of the new cell density  $\rho_i^{n+1}$ . The donor cell requirement on F is given by

$$(\tilde{F}_{i+\frac{1}{2}})^D = \begin{cases} \tilde{F}_i^n, \tilde{u}_{i+\frac{1}{2}}^n > 0 \\ \tilde{F}_{i+1}^n, \tilde{u}_{i+\frac{1}{2}}^n < 0 \end{cases} \quad (\text{B-28})$$

Substituting the mass flow equation (B-22) into Equation (B-26) yields the following calculational form for which extremely efficient numerical solution algorithms may be developed:

$$\rho_i^{n+1} F_i^{n+1} = \left\{ \rho_i \tilde{F}_i + \frac{\Delta t}{\Delta x} \left[ \rho_{i-\frac{1}{2}}^D \tilde{F}_{i-\frac{1}{2}}^D \tilde{u}_{i-\frac{1}{2}} - \rho_{i+\frac{1}{2}}^D \tilde{F}_{i+\frac{1}{2}}^D \tilde{u}_{i+\frac{1}{2}} \right] \right\} \quad (\text{B-29})$$

Once Equation (B-29) has been evaluated for the density, velocity and total energy, the new values of internal energy, pressure, sound velocity and temperature are readily calculated from Equations (B-7), (B-9), (B-10), and (B-8), respectively.

#### B.5.6 Treatment of the Special Terms

The previous description of the numerical procedure dealt with the reduced form of the basic equations (Equation (B-2), (B-5) and (B-6)). The special terms of these equations can be incorporated into the numerical procedure in a relatively simple manner. First consider the friction term of the momentum equation. This term contributes to the local rate of change and can therefore be incorporated into the calculation of  $\tilde{u}$ . Thus Equation (B-19) can be expanded as

$$\frac{\partial \tilde{u}}{\partial t} = - \frac{1}{\rho} \frac{\partial p}{\partial x} - \frac{fu|u|}{h} \quad (\text{B-30})$$

and changes Equation (B-20) to

$$\tilde{u}^n = u_i^n - \frac{\Delta t}{\rho_i^n \Delta x} \left[ (p+q)_{i+\frac{1}{2}}^n - (p+q)_{i-\frac{1}{2}}^n \right] - \Delta t \cdot \frac{fu_i^n |u_i^n|}{h_i^n} \quad (\text{B-31})$$

The mass and energy equations can be rewritten in the form.

$$\frac{\partial \rho}{\partial t} + \frac{1}{h} \frac{\partial}{\partial x} (\rho u h) = \frac{\dot{m}}{h} - \frac{p\dot{W}}{h} \quad (\text{B-32})$$

where  $\dot{W} = \partial h / \partial t =$  wall velocity and

$$\frac{\partial e_T}{\partial t} + u \frac{\partial e_T}{\partial x} + \frac{1}{\rho h} \frac{\partial}{\partial x} (\rho u h) = \frac{\dot{Q}}{\rho h} - \frac{p\dot{W}}{\rho h} - \frac{e_T \dot{m}}{\rho h} \quad (\text{B-33})$$

The intermediate value of the internal energy is now computed from:

$$\frac{\partial \tilde{e}_T}{\partial t} = - \frac{1}{\rho h} \frac{\partial}{\partial x} (\rho u h) - \frac{p\dot{W}}{\rho h} \quad (\text{B-34})$$

Therefore Equation (B-21) becomes

$$\begin{aligned} \tilde{e}_i^n = e_i^n - \frac{1}{\rho_i^n h_i^n} \left\{ \frac{\Delta t}{\Delta x} \left[ \tilde{u}_{i+\frac{1}{2}}^n h_{i+\frac{1}{2}}^n (p_{i+\frac{1}{2}}^n + q_{i+\frac{1}{2}}^n) \right. \right. \\ \left. \left. - \tilde{u}_{i-\frac{1}{2}}^n h_{i-\frac{1}{2}}^n (p_{i-\frac{1}{2}}^n + q_{i-\frac{1}{2}}^n) - \tilde{u}_i^n h_i^n (q_{i+\frac{1}{2}}^n - q_{i-\frac{1}{2}}^n) \right] \right. \\ \left. + \Delta t \rho_i^n \tilde{w}_i^n \right\} \quad (\text{B-35}) \end{aligned}$$

The final values of the flow variable at the new time  $t^{n+1}$  are then calculated from considerations of the following expanded equations for momentum and energy

$$\frac{\partial u}{\partial t} = \frac{\partial \tilde{u}}{\partial t} - u \frac{\partial u}{\partial x} - \frac{u \dot{m}}{\rho h} \quad (\text{B-36})$$

$$\frac{\partial e_T}{\partial t} + \frac{\partial \tilde{e}_T}{\partial t} - u \frac{\partial e_T}{\partial x} + \frac{\dot{Q}}{\rho h} - \frac{e_T \dot{m}}{\rho h} \quad (\text{B-37})$$

and Equation (B-32).

The general solution equation, Equation (B-29) is no longer applicable because of the various special terms. Rather three, somewhat similar relations are needed. These are the following.

$$\rho_i^{n+1} = \rho_i + \frac{1}{h_i} \left\{ \frac{\Delta t}{\Delta x} \left[ \rho_{i-\frac{1}{2}}^D h_{i-\frac{1}{2}} \tilde{u}_{i-\frac{1}{2}} - \rho_{i+\frac{1}{2}}^D h_{i+\frac{1}{2}} \tilde{u}_{i+\frac{1}{2}} \right] - \Delta t (\rho_i \dot{W}_i - \dot{m}_i) \right\} \quad (B-38)$$

$$\rho_i^{n+1} u_i^{n+1} = \rho_i \tilde{u}_i + \frac{\Delta t}{\Delta x} \left\{ \rho_{i-\frac{1}{2}}^D \tilde{F}_{i-\frac{1}{2}}^D \tilde{u}_{i-\frac{1}{2}} - \rho_{i+\frac{1}{2}}^D \tilde{F}_{i+\frac{1}{2}}^D \tilde{u}_{i+\frac{1}{2}} \right\} - \frac{\Delta t \tilde{u}_i \dot{m}_i}{h_i} \quad (B-39)$$

where  $\tilde{F}_{i+\frac{1}{2}}^D$  is defined by Equations (B-27) and (B-28).  
and

$$\rho_i^{n+1} (e_T)_i^{n+1} = \rho_i (\tilde{e}_T)_i + \frac{\Delta t}{\Delta x} \left\{ \rho_{i-\frac{1}{2}}^D \tilde{F}_{i-\frac{1}{2}}^D \tilde{u}_{i-\frac{1}{2}} - \rho_{i+\frac{1}{2}}^D \tilde{F}_{i+\frac{1}{2}}^D \tilde{u}_{i+\frac{1}{2}} \right\} + \frac{\Delta t}{h_i} \left[ \dot{Q}_i - (\tilde{e}_T)_i \dot{m}_i \right] \quad (B-40)$$

### B.5.7 Boundary Conditions

The boundary conditions imposed upon the two ends of the flow channel are accommodated by the use of one dummy cell at each end. The first upstream cell of the flow channel is designated by  $i=2$  and the associated dummy cell is designated by  $i=1$ . If  $i_n$  cells are used to represent the flow channel then the last real cell is designated by  $i_b = i_n + 1$ . The downstream dummy cell is designated  $i_c = i_b + 1$ . Thus a total of  $i_c$  cells are used.

The cell  $i=1$  represents the boundary cell for the high pressure cavity and some values of the variable in this cell will depend upon whether inflow or outflow conditions exist. This condition is determined by examining the value of  $u_2$  at any time  $t^n$ . For outflow  $p_1 = p_c$  provided the flow is subsonic, otherwise  $p_1 = p_2$ . This latter relation provides better numerical uncoupling from the cavity under sonic and supersonic outflow conditions.

For inflow  $p_1$  is determined from the energy equation in the following form

$$p_1 = p_c \left[ 1 - \frac{(\gamma-1)}{2} \cdot \frac{u_1^2}{c_c^2} \right]^{\frac{\gamma}{\gamma-1}} \quad (B-41)$$

where  $u_1 = u_2$  provided that its value does not exceed the sonic value,  $u_m$ . This critical value is

$$u_m = c_c \sqrt{\frac{2}{\gamma+1}} \quad (B-42)$$

The cavity sound velocity,  $c_c$ , is determined from Equations (B-8) and (B-10). The velocities  $\hat{u}$  and  $\bar{u}$  in cell 1 for both inflow and outflow are set equal to their corresponding values of cell 2, viz.

$$\begin{aligned} \hat{u}_1 &= \hat{u}_2 \\ \bar{u}_1 &= \bar{u}_2 \end{aligned} \quad (B-43)$$

provided that they do not exceed the algebraic value of  $u_m$ . This limiting requirement can only be experienced during inflow. The density  $\rho_1$  and total energy  $(e_T)_1$  are required for inflow. They are given by the following relations.

$$\rho_1 = \rho_c \left( \frac{p_1}{p_c} \right)^{\frac{1}{\gamma}} \quad (B-44)$$

and

$$(e_T)_1 = \frac{RT_c}{(\gamma-1)} \quad (B-45)$$

The boundary conditions at the downstream end are dependent upon the type of end condition being used. For the closed end configuration the particle velocity at the end of the channel must vanish. This is accomplished by setting the intermediate values of the velocities  $\hat{u}$  and  $\bar{u}$  in cell  $i_c$  equal to the negative of the values of their corresponding values in cell  $i_b$ , viz.

$$\begin{aligned}\tilde{u}_{ic} &= -\tilde{u}_{ib} \\ \bar{u}_{ic} &= -\bar{u}_{ib}\end{aligned}\tag{B-46}$$

In addition the required state variables of cell  $i_c$  are set equal to the corresponding values of cell  $i_b$  to, in effect, create a plane of symmetry, specifically

$$\begin{aligned}P_{ic} &= P_{ib} \\ \rho_{ic} &= \rho_{ib} \\ (e_T)_{ic} &= (e_T)_{ib}\end{aligned}\tag{B-47}$$

The downstream boundary conditions for the low pressure cavity are considerably simpler than those for the high pressure cavity because only outflow is permitted to occur. The following values are needed.

$$\begin{aligned}P_{ic} &= p_0 \quad \text{if } M_{ib} < 0, \text{ otherwise } P_{ic} = P_{ib} \\ \tilde{u}_{ic} &= \tilde{u}_{ib} \\ \bar{u}_{ic} &= \bar{u}_{ib}\end{aligned}\tag{B-48}$$

Where  $p_0$  is the initial pressure of the gas within the crack.

#### B.5.8 Calculation Method

The basic calculation procedure is to evaluate Equations (B-16), (B-31), (B-35), (B-38), (B-39), (B-40), (B-9), (B-7), (B-10), and (B-8) and the appropriate auxiliary equations for each cell of the computing mesh (cells  $i=2$  to  $i_b$ ) during each time step. The numerical results computed at the end of any time step, together with a new set of boundary conditions, then serve as the initial conditions for the next time step, and in this manner the numerical solution is advanced in time.

## B.6 CODE VERIFICATION

A computer program was developed to implement the preceding gas dynamic model. This computer program exists (1) in the form of a main program with which to examine some aspects of the gas dynamic phenomena and to serve as a vehicle for further development, and (2) in the form of a subroutine of the overall propellant detonation computer model. These codes were programmed in FORTRAN IV user-oriented source language and have been successfully executed on a UNIVAC 1108, a large scientific computer.

The gas dynamic code has been exercised to evaluate its adequacy for the subject problem area. Current results indicate that reasonable resolution can be obtained for a class of simple flow problems if approximately 20 or more cells are used to define the crack length. Comparisons have been made with a number of analytic solutions for both transient and steady state (late time) flows and indicate that the present form is adequate except for the treatment of the variable area and thus moving wall features. It is not clear at the present time whether the difficulty is due to the limited number of cells used to define a large change in area, a time step requirement, or to some other cause. The source of the error must be examined in more detail and the gas dynamic code will then be modified accordingly. This problem is not considered to be a limiting problem.

## APPENDIX C

### MECHANICAL RESPONSE MODELS

#### C.1 INTRODUCTION

The flow of high pressure gases into cracks within and adjacent to the propellant mass and any subsequent burning of these propellant surfaces will create a time varying pressure environment with the cracks. The surrounding propellant mass, which was originally in mechanical equilibrium with a low pressure distribution within the crack will respond to these new mechanical loads. It is the purpose of this appendix to describe several mechanical response models which have been used in conjunction with the gas dynamic model described in Appendix B. One response model treats the early phases of the mechanical response when stress waves radiate from the crack and the crack is in a growth phase. The second model tests, in a simple fashion, the interaction of these radiating waves with the confining shell structure and their subsequent interaction with the crack. Under these conditions the crack growth will generally be arrested and may ultimately lead to partial or complete crack collapse.

#### C.2 MECHANICAL PROPERTIES OF THE PROPELLANT

The propellant response to the transient pressure loads within a crack will be that associated with the generation and propagations of stress waves in the propellant mass. The mechanical properties of most propellant materials are quite complex in that they are generally nonlinear, rate sensitive, and hysteretic in nature. Any simple mechanical response model cannot deal effectively with these types of complex behavior characteristics; however their impact upon the subject problem is not considered to be important. Rather it should be sufficient to model in some simple way the gross compressibility characteristics of the material. Thus the material will be viewed initially as a simple linear isotropic elastic material which does not yield or fail in any manner under the imposed stresses.

An elastic material will support two basic types of stress waves, i.e., dilatation and shear waves. These waves will propagate at the following speeds.

Dilatation Wave Speed,  $c_d$

$$c_d = \sqrt{\frac{E}{\rho}} \sqrt{\frac{(1-\tau)}{(1-2\tau)(1+\tau)}} \quad (C-1)$$

Shear Wave Speed,  $c_s$

$$c_s = \sqrt{\frac{E}{\rho}} \sqrt{\frac{1}{2(1+\tau)}} \quad (C-2)$$

where  $E$  = Young's modulus  
 $\tau$  = Poisson's ratio  
 $\rho$  = density

The ratio of these two wave speeds is dependent only upon Poisson's ratio, vis:

$$\frac{c_s}{c_p} = \sqrt{\frac{1-2\tau}{2(1-\tau)}} \quad (C-3)$$

The influence of Poisson's ratio is not great until it exceeds a value of about .45 and then it primarily affects the dilatation wave speed. The effective wave speed  $c^* = \sqrt{E/\rho}$  is the most significant parameter. Since Poisson's ratio may be in the broad range of from 0.2 to 0.4 the dilatation wave speed will be approximately 1.2  $C^*$  while and the shear wave speed will be approximately 0.6  $C^*$ . Thus the wave speed ratio will be approximately 0.5. The density of the propellants are well known and a nominal value of 1.5 g/cm<sup>3</sup> is used in the mechanical response models. A nominal value of 250 cm/ms was selected for the effective wave speed. This corresponds to a value of approximately 10<sup>6</sup> psi for Young's modulus and yields dilatation and shear wave speeds of 300 cm/ms (approximately 10,000 fps) and 150 cm/ms respectively.

### C.3 INITIAL RESPONSE MODEL

During the entry phase of the gas flow into the crack a shock wave is generated which propagates at a speed (depending upon a number of parameters) of approximately 150 cm/ms. The pressure distribution behind this shock wave is relatively uniform. Weak disturbances (i.e., sound waves) propagate at the local sound speed relative to the gas. The sound speed is generally in the approximate range of from 50 to 100 cm/ms while the particle velocity is in the range of from -50 to 100 cm/ms. Thus these disturbances will propagate, on the average, at an absolute velocity of about 100 cm/ms. These considerations lead us to the following approximate inequality,

$$|(\underline{u}+c)| < U \approx c_g < c_d \quad (C-4)$$

where  $U$  = shock velocity in the gas  
 $\underline{u}$  = particle velocity of the gas  
 $c$  = sound velocity of the gas

Thus the wave system illustrated in Figure 8 of the main text should exist initially. While this wave system is quite complex many of the waves should be weak and need not be considered. This is especially true for the outrunning waves. The primary motion of the propellant mass will be in a direction normal to the crack, causing the crack height to increase locally. For this reason, a very simple, one dimension wave propagation (plane strain) model has been selected with which to define the response of the propellant adjacent to the crack. The momentum equation for this case is of the form

$$\Delta \tau = (\rho c_d) \Delta \mu \quad (C-5)$$

where  $\Delta \tau$  = change in stress at the crack boundary  
 $\Delta \mu$  = change in velocity at the crack boundary

The change in the stress at a given location along the crack is identical to the change in the corresponding gas pressure. Thus the wall velocity  $\dot{W}$  used in the gas dynamic model is given for the  $i$ th cell as

$$\dot{W}_i = (\rho c_d)(P_i - P_o) \quad (C-6)$$

where  $\rho c_d$  = shock impedance ( $\approx 450$  bars-ms/cm)

$P_i$  = gas pressure

$P_o$  = initial gas pressure

This expression was modified to include some contribution from the adjacent cells ( $i-1$ , and  $i+1$ ). In this manner some influence of the spreading nature of the propagation within the propellant mass was included, at least in a crude manner.

#### C.4 INFLUENCE OF REMOTE BOUNDARIES

The stress wave which radiates away from the crack will eventually react with the remote boundaries of the propellant mass, reflect and return, in some modified form, to the crack. These reflected waves will also influence the response crack walls. This type of wave system is illustrated in Figure 9(a) of the main text. The nature of reflected wave system will be very complex and varied. For this reason a number of idealized reflection models will have to be established to define the configurations and conditions of interest.

As an initial attempt to treat the influence of the remote boundaries of the propellant mass one idealized model was established. This model is illustrated in Figure 9(b). It is designed to introduce the ultimate confining influence of a cased mass of propellant. A radiative stress field,  $\Delta p_r$ , which is the integrated or averaged value of the current local stress field along the entire crack is defined and assumed to propagate, under the conditions of plane strain, into the propellant mass. These stress waves interact with the remote boundary after a delay time corresponding to a boundary/crack separation distance,  $L_e$ . The case is treated as a spring supported mass characterized by its inertia (weight per unit area) and stiffness (breathing mode of the case). The reflected wave system,  $\Delta p_g$  is evaluated from this case boundary interaction and applied uniformly along the crack after the appropriate

delay period. This reflected wave system then interacts locally with the crack boundary such that the wall velocity changes according to the following momentum consideration

$$\Delta W_i = -2\Delta p_s / (\rho c_s) \quad (C-7)$$

APPENDIX D  
TECHNIQUE FOR PREDICTING PROPELLANT TEMPERATURES

D.1 INTRODUCTION

In this appendix we shall discuss the techniques used to compute transient temperature rises within regressing propellants produced by known time-dependent thermal fluxes. Topics covered in order of presentation are

- prediction of transient temperature rises
- selection of time steps
- means used to expedite computations
- validation of the technique by comparison with an exact solution

Means for predicting the transient velocities of the regressing boundary are discussed in Appendix A.

In essence the method involves a series of constant thermal fluxes applied at various locations of a regressing boundary within a semi-infinite body during selected time intervals. These fluxes include incident fluxes along with appropriate combinations of conductive fluxes produced at other depths and times by the incident fluxes. The net result is a series of independent heat conduction problems which are then solved and summed to arrive at the temperature rises within the remaining propellant.

## D.2 PROPELLANT TEMPERATURES

Prediction of temperatures beneath accelerating boundaries have been handled by a variety of techniques (37-39). Of all the methods examined, finite-difference techniques are the most versatile and appropriate. Unfortunately, finite-difference techniques require considerable computer storage and execution times due to the large number of spacial and temporal elements needed to accommodate rapid changes of velocities and temperatures. This is true with implicit, explicit or implicit-explicit methods -- all of which require very long computational times to treat highly dynamic problems.

As a result a novel technique was developed by modifying a closed-form solution of transient heat conduction within a semi-infinite body with a stationary boundary exposed to a constant flux. Here a fixed coordinate system is used within which the boundary is allowed to regress in a discrete fashion during selected time intervals. During each time interval, the incident flux is held constant corresponding to a step-wise approximation of the time-dependent flux  $q(t)$  at the propellant boundary. By determining the rates of heat conduction occurring at various depths and times, one arrives at a series of simple heat conduction problems from which the temperatures rises within the moving propellant are closely approximated.

To illustrate the process the reader is referred to Fig. D-1. In this figure the boundary is considered to commence to move starting at  $t_{j-1}$  and to arrive at  $x_j$  at the end of the time interval  $\Delta t_j$ . Incident fluxes and mean depths are represented by  $q_i$  and  $\bar{x}_i$ .

Once the boundary is displaced, fluxes  $\bar{q}_i$  lower than  $q_i$  are used to negate undesirable conductive fluxes arising in the computational scheme from prior incident fluxes.

$i$	Heat Fluxes	Boundary Locations	Time Intervals	Elapsed Time at End of $\Delta t_i$
1	$\bar{q}_1 = q_1$ 	$\bar{x}_1 = 0$  stationary	$\Delta t_1$	$t_1$
2	$\bar{q}_2 = q_2$ 	$\bar{x}_2 = 0$  stationary	$\Delta t_2$	$t_2$
$\vdots$	$\vdots$	$\vdots$	$\vdots$	$\vdots$
$j-1$	$\bar{q}_{j-1} = q_{j-1}$ 	$\bar{x}_{j-1} = 0$  stationary	$\Delta t_{j-1}$	$t_{j-1}$
$j$	$\bar{q}_j < q_j$ 	$\bar{x}_j > 0$  moving	$\Delta t_j$	$t_j$
$j+1$	$\bar{q}_{j+1} < q_{j+1}$ 	$\bar{x}_{j+1} > 0$  moving	$\Delta t_{j+1}$	$t_{j+1}$
$\vdots$	$\vdots$	$\vdots$	$\vdots$	$\vdots$
$n$	$\bar{q}_n < q_n$ 	$\bar{x}_n > 0$ 	$\Delta t_n$	$t_n$

Figure D-1 NOMENCLATURE USED TO PREDICT TEMPERATURE RISES

The technique starts with the heat conduction equations for temperature rises  $T(x,t)$  produced within a semi-infinite body exposed to a constant flux  $q_1$  applied at some depth  $\bar{x}_1$  for times  $t > t_{i-1}$ . These equations are presented below.

$$\alpha \frac{\partial^2 T}{\partial x^2} = \frac{\partial T}{\partial t}, \quad x > \bar{x}_1, \quad t > t_{i-1} \quad (D-1)$$

$$-K \frac{\partial T}{\partial x} = q_1, \quad x = \bar{x}_1, \quad t > t_{i-1} \quad (D-2)$$

$$T(x,t) = 0, \quad x \geq \bar{x}_1, \quad t \leq t_{i-1} \quad (D-3)$$

$$T(\infty, t) = 0, \quad t \geq t_{i-1} \quad (D-4)$$

where  $\alpha, K$  are the thermal diffusivity and conductivity of the propellant.

Assumption of a semi-infinite body is a valid one since heat penetration is relatively shallow compared to propellant depths. Solution of the above problem with  $\bar{x}_1 = t_{i-1} = 0$  is given in Ref. 36. By simple transformation of this solution one arrives at the following solution of the above equations.

$$T(x,t) = C' q_1 \sqrt{t-t_{i-1}} \operatorname{ierfc} \frac{x-\bar{x}_1}{2 \sqrt{\alpha(t-t_{i-1})}} \quad (D-5)$$

$$\text{for } x \geq \bar{x}_1, \quad t \geq t_{i-1}$$

where  $C' = 2/\sqrt{K\rho C}$  and  $K, \rho, C$  represent the thermal conductivity, density and specific heat of the propellant, respectively.

#### D.2.1 Stationary Boundaries

For this case  $\bar{x}_1$  is zero. In view of the boundary condition of Eq. D-2, it is possible to compute the temperature rises produced by each  $q_1$  at  $\bar{x}_1 = 0$  separately, and sum the resultant temperatures. To demonstrate this fact we shall replace Eq. D-2 with the following boundary conditions associated with each of a series of fluxes  $q_1$  applied in a sequential manner.

$$-K \frac{\partial T_i}{\partial x} = \begin{cases} q_i & \bar{x}_i = 0, \quad t_{i-1} < t \leq t_i \\ 0 & \bar{x}_i = 0, \quad \text{other } t \end{cases} \quad (D-6)$$

Applying Duhamel's principal to Eq. D-5 to accommodate the boundary conditions of Eq. D-6 for any single  $q_i$  yields

$$\begin{aligned} T_i(x, t) &= C' q_i \sqrt{t-t_{i-1}} \operatorname{ierfc} \frac{x}{2 \sqrt{\alpha(t-t_{i-1})}}, \quad \text{for } t_{i-1} < t < t_i \\ &= C' q_i \left( \sqrt{t-t_{i-1}} \operatorname{ierfc} \frac{x}{2 \sqrt{\alpha(t-t_{i-1})}} - \sqrt{t-t_i} \operatorname{ierfc} \frac{x}{2 \sqrt{\alpha(t-t_i)}} \right) \\ &\quad \text{for } t > t_i \end{aligned} \quad (D-7)$$

Assuming the temperature rises produced by each  $q_i$  are additive, then the temperature rises  $T(x, t)$  produced by the first  $k$  fluxes  $q_i$ , where  $k \leq i-1$ , is

$$\begin{aligned} T(x, t) &= \sum_{i=1}^k T_i(x, t) \quad (D-8) \\ &= C' \sum_{i=1}^{k-1} q_i \left( \sqrt{t-t_{i-1}} \operatorname{ierfc} \frac{x}{2 \sqrt{\alpha(t-t_{i-1})}} - \sqrt{t-t_i} \operatorname{ierfc} \frac{x}{2 \sqrt{\alpha(t-t_i)}} \right) \\ &\quad + C' q_k \sqrt{t-t_{k-1}} \operatorname{ierfc} \frac{x}{2 \sqrt{\alpha(t-t_{k-1})}}, \quad \text{for } t_{k-1} < t < t_k \end{aligned}$$

To prove that Eq. D-8 satisfies the boundary conditions of Eq. D-6, let us multiply Eq. D-8 by  $-K$  and differentiate with respect to  $x$  to arrive at the flux given below.

$$\sum_{i=1}^{k-1} q_i \left( \operatorname{erfc} \frac{x}{2 \sqrt{\alpha(t-t_{i-1})}} - \operatorname{erfc} \frac{x}{2 \sqrt{\alpha(t-t_i)}} \right) + q_k \operatorname{erfc} \frac{x}{2 \sqrt{\alpha(t-t_{k-1})}} \quad (D-9)$$

For the first time interval  $k=1$ . And since  $t_0=0$ , Eq. D-9 reduces to

$$q_1 \operatorname{erfc} \frac{x}{2\sqrt{\alpha t}}, \quad 0 < t < t_1 \quad (\text{D-10})$$

At  $x=0$ , it is clear that the flux is  $q_1$ . During the second time interval wherein  $k=2$ , Eq. D-9 reduces to

$$q_1 \left( \operatorname{erfc} \frac{x}{2\sqrt{\alpha t}} - \operatorname{erfc} \frac{x}{2\sqrt{\alpha(t-t_1)}} \right) + q_2 \operatorname{erfc} \frac{x}{2\sqrt{\alpha(t-t_1)}} \quad (\text{D-11})$$

for  $t_1 < t < t_2$

At  $x=0$ , the flux is  $q_2$  during the above time interval.

By continuing the process for the first  $j-1$  time intervals, the boundary conditions cited by Eq. D-6 can be shown to be satisfied for each of the fluxes  $q_i$ . And since Eq. D-8 satisfies Eqs. D-1, D-3, and D-4 on a term by term basis, it correctly describes the temperature rises produced by the first  $j-1$  fluxes  $q_i$ .

#### D.2.2 Moving Boundaries

Once the boundary starts to move, one must commence to discount the most recent fluxes produced at the displaced boundary by prior  $q_i$ . To illustrate the procedure, we shall first treat the problem following the initial displacement of the boundary to  $x_j$ . Then we shall generalize the results for multiple displacements.

For the initial displacement we shall assume a solution of Eqs. D-1, D-3, D-4 and D-6 of identical form as Eq. D-8, namely

$$T(x, t) = C' \sum_{i=1}^{j-1} \bar{q}_i \left( \sqrt{t-t_{i-1}} \operatorname{ierfc} \frac{x-\bar{x}_i}{2\sqrt{\alpha(t-t_{i-1})}} - \sqrt{t-t_i} \operatorname{ierfc} \frac{x-\bar{x}_i}{2\sqrt{\alpha(t-t_i)}} \right) + C' \sqrt{t-t_{j-1}} \bar{q}_j \operatorname{ierfc} \frac{x-\bar{x}_j}{2\sqrt{\alpha(t-t_{j-1})}}, \quad x > \bar{x}_j, \quad t_{j-1} < t < t_j \quad (\text{D-12})$$

where  $\bar{x}_i$  represents the effective depth at which the  $\bar{q}_i$  are applied and is given by

$$\bar{x}_i = x_{i-1} + C_2 \cdot \Delta x_i \quad (D-13)$$

Within the summation sign of Eq. D-12, each of the  $\bar{x}_i$  are zero and  $\bar{q}_i = q_i$  (see Fig. D-1). For prior times, Eq. D-12 reduces to Eq. D-8.

Here the fluxes  $q_i$  are applied at given depths within the displacements  $x_i$  to which they are associated. This means that the constant  $C_2$  has a positive value less than 1. The consequence of using various  $C_2$  values is presented in Section 5 of this appendix. In this regard it was found that a  $C_2$  value of about 0.3 yields the most accurate approximations of the temperature profiles and heat content within the receding material.

Equation D-12 obviously satisfies Eqs. D-1, D-3 and D-4. To satisfy the boundary condition of Eq. D-6 associated with the most recent time interval  $\Delta t_j$ , we shall first multiply Eq. D-12 by  $-K$  and then differentiate the result with respect to  $x$ . Setting  $t = t_j$  and  $x = \bar{x}_j$  yields the following approximation for the flux  $q_j$ :

$$q_j = \sum_{i=1}^{j-1} \bar{q}_i \left( \operatorname{erfc} \frac{\bar{x}_j - \bar{x}_i}{2\sqrt{\alpha}(t_j - t_{i-1})} - \operatorname{erfc} \frac{\bar{x}_j - \bar{x}_i}{2\sqrt{\alpha}(t_j - t_i)} \right) + \bar{q}_j \quad (D-14)$$

Here the approximate expression within the summation sign represents relatively small undesirable conductive fluxes arising in the computational scheme from prior  $q_i$  at  $\bar{x}_j$  during  $\Delta t_j$ . Recognizing that the undesirable fluxes depend upon time, a more exact correction can be achieved by integrating the fluxes over the most recent time interval  $t_j - t_{j-1} = \Delta t_j$ . This can be accomplished by replacing each of the  $i$ th terms within the summation sign of Eq. D-14 with

$$\bar{q}_i \left[ \int_0^{\Delta t_j} \operatorname{erfc} \frac{\bar{x}_j - \bar{x}_i}{2\sqrt{\alpha}(t_{j-1} - t_{i-1} + \tau)} d\tau - \int_0^{\Delta t_j} \operatorname{erfc} \frac{\bar{x}_j - \bar{x}_i}{2\sqrt{\alpha}(t_{j-1} - t_i + \tau)} d\tau \right] \quad (D-15)$$

Letting  $\beta$  equal the argument of either erfc function of Eq. D-15 and performing the integrations by parts yields

$$\bar{q}_i \frac{C_3^2}{\Delta t_j} \left[ \gamma(\beta) \left| \frac{C_3}{\sqrt{t_{j-1}-t_{i-1}}} \right. - \gamma(\beta) \left| \frac{C_3}{\sqrt{t_{j-1}-t_i}} \right. \right] \quad (D-16)$$

$$\text{where } C_3 = \frac{\bar{x}_j - \bar{x}_i}{2\sqrt{\alpha}} \quad (D-17)$$

$$\gamma(\beta) = -\text{erfc } \beta \left( \frac{1}{\beta^2} + 2 \right) + \frac{2}{\beta\sqrt{\pi}} \exp -\beta^2 + 2 \quad (D-18)$$

Replacing the terms within the summation sign of Eq. D-14 by the expression given by Eq. D-16 and solving for  $\bar{q}_j$  yields

$$\bar{q}_j = q_j - \sum_{x=1}^{j-1} \bar{q}_i \frac{(\bar{x}_j - \bar{x}_i)^2}{4\alpha(t_j - t_{j-1})} \left[ \gamma(\beta) \left| \frac{C_3}{\sqrt{t_{j-1}-t_{i-1}}} \right. - \gamma(\beta) \left| \frac{C_3}{\sqrt{t_{j-1}-t_i}} \right. \right] \quad (D-19)$$

To speed computer execution time the function  $\gamma(\beta)$  may be approximated by the following series

$$\gamma(\beta) = \begin{cases} \frac{-1.0013}{\beta^2} + \frac{2.2703}{\beta} - .0577 + .8789\beta - .1465\beta^2, & \beta < 1.5 \\ 2, & \beta > 1.5 \end{cases} \quad (D-20)$$

Here sufficient terms have been taken in the series expansion so that the above approximation agrees to within one percent of that presented by Eq. D-18. Errors introduced into the computed temperature changes by the above approximation for  $\gamma(\beta)$  are less than one percent.

Substituting the expression for  $\bar{q}_j$  given by Eq. D-19 into Eq. D-12 yields the temperature rises following the initial displacement  $\Delta x_j$  of the boundary. By continuing the procedure one arrives at the method for multiple displacements given in the next section.

### D.2.3 Summary

In general, the temperature rises are given by

$$T(x, t_n) = C' \sum_{i=1}^{n-1} \bar{q}_i \left( \sqrt{t_n - t_{i-1}} \operatorname{ierfc} \frac{x - \bar{x}_i}{2\sqrt{\alpha(t_n - t_{i-1})}} \right. \quad (D-21)$$

$$\left. - \sqrt{t_n - t_i} \operatorname{ierfc} \frac{x - \bar{x}_i}{2\sqrt{\alpha(t_n - t_i)}} \right) + C' \bar{q}_n \sqrt{t_n - t_{n-1}} \operatorname{ierfc} \frac{x - \bar{x}_n}{2\sqrt{\alpha(t_n - t_{n-1})}}$$

for  $x \geq \bar{x}_n$ . The term  $\bar{q}_n$  is given by the following recursion formula:

$$\bar{q}_n = q_n - \sum_{i=1}^{n-1} \bar{q}_i \frac{(\bar{x}_n - \bar{x}_i)^2}{4\alpha(t_n - t_{n-1})} \left[ \gamma(\beta) \left| \frac{\frac{\bar{x}_n - \bar{x}_i}{2\sqrt{\alpha(t_{n-1} - t_{i-1})}}}{\frac{\bar{x}_n - \bar{x}_i}{2\sqrt{\alpha(t_n - t_{i-1})}}} \right. \right. \quad (D-22)$$

$$\left. \left. - \gamma(\beta) \left[ \frac{\frac{\bar{x}_n - \bar{x}_i}{2\sqrt{\alpha(t_{n-1} - t_i)}}}{\frac{\bar{x}_n - \bar{x}_i}{2\sqrt{\alpha(t_n - t_i)}}} \right] \right]$$

### D.3 SELECTION OF TIME INTERVALS

An important benefit of this method is its capability of using relatively large time intervals compared to finite-difference methods. There are no problems of instability. The principal restriction on the time intervals is that they must be kept sufficiently small to accurately describe the incident thermal fluxes and prevent flux variations across the displacements  $\Delta x_i$  from becoming excessively large.

During the initial heating period before the boundary commences to move, the time intervals are selected solely on the basis of yielding a reasonable step-wise approximation of the time-dependent changes in the flux. Once the boundary commences to move, the time intervals are computed as follows:

$$\Delta t_i = \alpha (C_1 q_{i-1} / (V_{i-1} q_i))^2 \quad (D-23)$$

where  $\alpha$  = thermal diffusivity in  $\text{cm}^2/\text{sec}$   
 $q_i$  = thermal flux in  $\text{cal}/\text{cm}^2\text{-sec}$  during the time interval  $\Delta t_i$  in sec  
 $C_1$  = constant usually equal to 0.3 or less  
 $V_{i-1}$  = previous velocity in  $\text{cm}/\text{sec}$

This expression limits the most recent arguments of the  $\text{ierfc}$  and  $\text{erfc}$  functions to values of about  $C_1/2$ . Accuracy will increase as the constant  $C_1$  is decreased since such will lower the  $\Delta x_i$  and  $\Delta t_i$  values. Fluxes are included in Eq. D-23 along with the previous velocity  $V_{i-1}$  for linearly approximating the new velocity  $V_i$ . In situations in which the dependence is not close to linear, it is advisable to alter this dependence accordingly. The consequence of using various  $C_1$  values is presented in Section 5 of this appendix.

#### D.4 MINIMIZING COMPUTATION TIMES

In that the computational times are proportional to the square of the number of time intervals used, it is important to minimize the number of time intervals used consistent with accurate predictions. In this section we shall discuss means for minimizing the number of time intervals.

##### D.4.1 Elimination of Early Time Intervals

Two means were examined in this regard. The most obvious possibility is to eliminate early  $q_1$  when they cease to be important. Unfortunately this is not particularly fruitful in that only rarely do the effects of the early  $q_1$  become insignificant. A more practical technique is to consolidate groups of the early fluxes into single effective fluxes applied over some depth during some time interval. This approach has yielded good results provided the incident fluxes occur at the same depth. However the problem of consolidating fluxes applied at different depths remains to be completed (see Section 6 of this Appendix).

##### D.4.2 Temporary Skipping of Temperature Calculations

Another means used to minimize computational times is based upon the fact that the burning can become highly variable over the crack elements. In such situations, much smaller time steps are needed at the crack locations involving rapid regression rates than at other locations. In that a single time interval is used for all crack elements, there are instances wherein the changes of the temperatures or regression rates of some of the crack elements becomes insignificant. This occurs when extremely small time intervals are applied to crack elements involving little or no regression.

Whenever such situations arise, the temperature/velocity computations at crack locations involving little or no regression are temporarily suspended. The criterion used to make this decision is that the time interval required to produce important changes at the crack location exceed the time interval being used by a factor of at least 10. Time intervals temporarily skipped are

stored for future use. Temperature/velocity computations are resumed when the number of skipped time intervals exceeds a specified value -- generally three.

#### D.5 ACCURACY

In order to check the accuracy of the method we have applied it to a moving-boundary problem having the analytical solution described by Eq. 8. This problem involves a constant-velocity boundary that loses heat convectively to a constant-temperature environment. Initially the body is considered to have a temperature 100°C above its environment. Convective heat fluxes are computed using a heat-transfer coefficient of 0.5 cal/cm<sup>2</sup>-sec-°C. Transient fluxes required by the approximate method were determined by using the temperatures at the midpoints of the time intervals provided by the analytical solution described by Eq. 8.

Decreases of temperature obtained by the two solutions are given in Tables D1, D2 and D3 for velocities of 1, 3 and 5 cm/sec, respectively. These temperature decreases are equal to the difference between the initial temperature of 100°C minus the computed temperatures within the body, and are presented since they afford the most appropriate measure of the accuracy of the method. Time intervals were constant for each of the three cases treated and were determined using Eq. D-23 with  $C_1$  set equal to 0.3.

From the above tables it may be observed that the agreement with the exact temperature changes is good at all depths, and times for each of the velocities considered. Percentage errors associated with these results are shown in Tables D4, D5 and D6. On a percentage basis errors are generally largest at depths incurring small temperature changes of less than 1 C. This is due to taking small differences between approximations of the erfc and ierfc functions. Included, in the latter tables in the consequence of using  $C_1$  values larger than 0.3. From Eq. D-23 it may be observed that the  $C_1$  value of 0.6 corresponds to time intervals four times larger than those associated with a  $C_1$  value

Table D-1

TEMPERATURE COMPARISONS FOR A VELOCITY  
OF 1 CM/SEC WITH  $C_1 = C_2 = 0.3^*$

Elapsed Time, msec	Total No. of Time Intervals Used	Temperature Decreases in °C at Given Depths in Microns -- Top Rows Represent Approximate Values, Bottom Rows Represent Exact Values										
		0	9.6	19.2	28.8	38.4	48.0	57.6	67.2	76.8	86.4	
.8	5	27.92	10.68	3.14	.73	.13	.02	0	0	0	0	0
		28.82	10.48	3.06	.70	.13	.02	0	0	0	0	0
1.6	10	32.58	15.56	6.51	2.42	.80	.23	.07	.01	0	0	0
		33.56	15.40	6.40	2.38	.79	.23	.06	.01	0	0	0
2.4	15	34.94	18.19	8.59	3.84	1.56	.59	.20	.07	.02	.01	.01
		35.90	18.06	8.53	3.78	1.54	.58	.20	.06	.02	.01	.01
3.2	20	36.40	19.79	10.04	4.93	2.24	.97	.39	.16	.06	.02	.02
		37.29	19.66	9.93	4.80	2.19	.94	.38	.15	.05	.02	.02
4.0	25	37.44	20.86	11.05	5.74	2.79	1.29	.57	.23	.11	.04	.04
		38.22	20.76	10.98	5.55	2.71	1.27	.57	.24	.10	.04	.04
4.8	30	38.22	21.60	11.67	6.29	3.23	1.55	.73	.34	.17	.07	.07
		38.87	21.58	11.65	6.13	3.12	1.54	.73	.33	.15	.06	.06

\* Constants  $C_1$  and  $C_2$  used in Eqs. D-13 and D-23, respectively.

Table D-2

TEMPERATURE COMPARISONS FOR A VELOCITY  
OF 3 CM/SEC WITH  $C_1 = C_2 = 0.3^*$

Elapsed Time, msec	Total No. of Time Intervals Used	Temperature Decreases in °C at Given Depths in Microns -- Top Rows Represent Approximate Values, Bottom Rows Represent Exact Values											
		0	2.16	4.32	6.48	8.64	10.80	12.96	15.12	17.28	19.44		
.09	5	11.20	5.97	2.61	1.18	.45	.15	.05	.01	0	0		
		11.62	5.98	2.76	1.15	.44	.15	.05	.01	0	0		
.18	10	13.69	8.37	4.81	2.60	1.34	.65	.30	.13	.05	.02		
		14.11	8.34	4.73	2.56	1.32	.64	.30	.13	.06	.02		
.27	15	15.04	9.69	6.04	3.56	2.02	1.15	.61	.32	.16	.08		
		15.49	9.68	5.94	3.51	2.03	1.13	.61	.32	.16	.08		
.36	20	15.91	10.58	6.79	4.25	2.53	1.55	.90	.50	.28	.15		
		16.32	10.58	6.72	4.18	2.56	1.52	.88	.50	.28	.15		
.45	25	16.55	11.19	7.38	4.73	2.99	1.86	1.15	.67	.39	.23		
		16.88	11.16	7.28	4.68	2.95	1.83	1.12	.67	.40	.23		
.54	30	17.03	11.60	7.73	5.07	3.22	2.12	1.36	.83	.49	.29		
		17.30	11.58	7.67	5.03	3.25	2.08	1.31	.81	.50	.30		

\* Constants  $C_1$  and  $C_2$  used in Eqs. D-13 and D-23, respectively.

Table D-3

TEMPERATURE COMPARISONS FOR A VELOCITY  
OF 5 CM/SEC WITH  $C_1 = C_2 = 0.3^*$

Elapsed Time, msec	Total No. of Time Intervals Used	Temperature Decreases in °C at Given Depths in Microns -- Top Rows Represent Approximate Values, Bottom Rows Represent Exact Values										
		0	.98	1.95	2.93	3.90	4.88	5.85	6.83	7.80	8.78	
.033	5	7.00	4.41	2.58	1.41	.73	.35	.16	.07	.03	.01	
		7.29	4.42	2.55	1.39	.71	.35	.16	.07	.02	.01	
.065	10	8.66	6.02	4.02	2.57	1.63	.98	.59	.34	.19	.10	
		8.92	6.05	3.96	2.57	1.60	.97	.58	.33	.18	.10	
.098	15	9.57	6.93	4.86	3.28	2.24	1.50	.96	.61	.38	.24	
		9.87	6.97	4.83	3.28	2.20	1.46	.95	.61	.38	.23	
.130	20	10.19	7.53	5.42	3.80	2.70	1.88	1.28	.86	.56	.37	
		10.44	7.53	5.38	3.80	2.65	1.83	1.25	.84	.56	.36	
.163	25	10.63	7.95	5.81	4.16	3.01	2.16	1.52	1.06	.73	.49	
		10.83	7.94	5.77	4.16	2.97	2.11	1.47	1.02	.70	.48	
.195	30	10.96	8.26	6.10	4.42	3.24	2.35	1.69	1.22	.86	.60	
		11.14	8.24	6.05	4.41	3.20	2.31	1.66	1.18	.83	.58	

\* Constants  $C_1$  and  $C_2$  used in Eqs. D-13 and D-23, respectively.

ERRORS IN COMPUTED DECREASES OF TEMPERATURE  
AND HEAT CONTENT OF EXISTING MATERIAL USING A VELOCITY OF 1 CM/SEC

Table D-4

$C_1^*$	Elapsed Time, msec	Total No. of Time Intervals Used	Mean Errors of Temperature Decreases in Percent for Various $C_2$ † Values		Errors in Lost Heat Content in Percent for Various $C_2$ Values			
			0.2	0.3**	0.2	0.3**		
0.3**	.8	5	2.5	3.9	7.1	-2.1	-.5	2.8
	1.6	10	3.0	4.2	7.1	-1.5	-.4	2.0
	2.4	15	2.9	3.7	6.5	-1.5	-.4	1.8
	3.2	20	3.1	4.4	6.9	-.9	.1	2.0
	4.0	25	3.4	3.9	5.5	-.8	.1	2.0
	4.8	30	3.0	3.4	5.4	-.8	.1	1.9
0.6	3.2	5	3.7	7.1	17.4	-4.4	-.3	8.0
	6.4	10	3.8	4.7	12.4	-4.1	-.5	6.8
0.9	7.2	5	6.6	7.2	24.5	-10.7	-3.5	12.3

\* Constant that established the size of the time intervals, see Eq. D-23

† Constant that establishes the depths at which the fluxes  $q_i$  are applied within each displacement  $\Delta x_i$ , depths =  $C_2 \Delta x_i$

\*\* Recommended values for  $C_1$  and  $C_2$

Table D-4  
 ERRORS IN COMPUTED DECREASES OF TEMPERATURE  
 AND HEAT CONTENT OF EXISTING MATERIAL USING A VELOCITY OF 1 CM/SEC

$C_1^*$	Elapsed Time, msec	Total No. of Time Intervals Used	Mean Errors of Temperature Decreases in Percent for Various $C_2^\dagger$ Values	Errors in Lost Heat Content in Percent for Various $C_2$ Values
			0.2    0.3**    0.5	0.2    0.3**    0.5
0.3**	.8	5	2.5    3.9    7.1	-2.1    -.5    2.8
	1.6	10	3.0    4.2    7.1	-1.5    -.4    2.0
	2.4	15	2.9    3.7    6.5	-1.5    -.4    1.8
	3.2	20	3.1    4.4    6.9	-.9    .1    2.0
	4.0	25	3.4    3.9    5.5	-.8    .1    2.0
	4.8	30	3.0    3.4    5.4	-.8    .1    1.9
0.6	3.2	5	3.7    7.1    17.4	-4.4    -.3    8.0
	6.4	10	3.8    4.7    12.4	-4.1    -.5    6.8
0.9	7.2	5	6.6    7.2    24.5	-10.7    -3.5    12.3

\* Constant that established the size of the time intervals, see Eq. D-23

† Constant that establishes the depths at which the fluxes  $\bar{q}_i$  are applied within each displacement  $\Delta x_i$ , depths =  $C_2 \Delta x_i$

\*\* Recommended values for  $C_1$  and  $C_2$

Table D-5  
**ERRORS IN COMPUTED DECREASES OF TEMPERATURE  
 AND HEAT CONTENT OF EXISTING MATERIAL USING A VELOCITY OF 3 CM/SEC**

$C_1^*$	Elapsed Time, msec	Total No. of Time Intervals Used	Mean Errors of Temperature Decreases in Percent for Various $C_2^{\dagger}$ Values	Errors in Lost Heat Content in Percent for Various $C_2$ Values
			0.2    0.3**    0.5	0.2    0.3**    0.5
0.3**	.09	5	2.8    3.9    8.2	-2.5    -.8    2.8
	.18	10	2.5    3.0    5.9	-1.4    -.1    2.5
	.27	15	1.6    1.5    3.3	-1.3    -.1    2.2
	.36	20	1.3    1.1    3.2	-1.2    -.1    2.1
	.45	25	1.5    1.4    2.7	-1.0    .1    2.2
	.54	30	1.8    1.7    2.6	-.9    .1    2.1
0.6	.36	5	3.1    3.5    12.8	-4.8    -.6    8.2
	.72	10	2.9    2.4    9.8	-3.9    .3    7.4
0.9	.81	5	7.5    5.0    19.9	-10.6    -3.5    12.6

\* Constant that establishes the size of the time intervals, see Eq. D-23

† Constant that establishes the depths at which the fluxes  $\bar{q}_1$  are applied within each displacement  $\Delta x_1$ , depths =  $C_2 \Delta x_1$

\*\* Recommended values for  $C_1$  and  $C_2$

Table D-6  
 ERRORS IN COMPUTED DECREASES OF TEMPERATURE  
 AND HEAT CONTENT OF EXISTING MATERIAL USING A VELOCITY OF 5 CM/SEC

$C_1^*$	Elapsed Time, msec	Total No. of Time Intervals Used	Mean Errors of Temperature Decreases in Percent for Various $C_2^\dagger$ Values	Errors in Lost Heat Content in Percent for Various $C_2$ Values
			0.2    0.3**    0.5	0.2    0.3**    0.5
0.3**	.033	5	2.8    3.8    7.9	-2.2    -.4    3.0
	.065	10	1.2    1.7    4.4	-1.5    -.2    2.5
	.098	15	1.3    1.2    3.4	-1.4    -.3    2.1
	.130	20	1.0    1.5    3.6	-.9    .2    2.4
	.163	25	1.4    2.0    4.0	-.6    .5    2.7
	.195	30	1.2    1.9    3.8	-.5    .5    2.6
0.6	.130	5	3.2    3.5    11.4	-5.0    -.7    8.0
	.260	10	2.7    2.6    9.2	-3.8    -.1    7.5
0.9	.293	5	8.3    4.9    18.0	-11.0    -3.6    12.4

\* Constant that establishes the size of the time intervals, see Eq. D-23

† Constant that establishes the depths at which the fluxes  $\bar{q}_i$  are applied within each displacement  $\Delta x_i$ , depths =  $C_2 \Delta x_i$

\*\* Recommended values for  $C_1$  and  $C_2$

of 0.3 while the  $C_1$  value of 0.9 increases the time intervals by a factor of nine. As one would expect, increased  $C_1$  values usually increase the errors. Also it should be observed that the effect of varying  $C_2$  is most pronounced with the larger  $C_1$  values. This is not at all surprising in that lower  $C_1$  values yield smaller displacements  $\Delta x_1$ . The result is a lessening of the thermal resistance across the displacements, and hence of the importance of where the source fluxes  $\bar{q}_1$  are located within  $\Delta x_1$ .

In view of the above results, it is advisable to use  $C_1$  values of 0.3 or less depending upon the accuracy desired. Here one should be particularly cognizant of trade-offs between accuracy and computer execution times in that the execution times associated with a given period of time are roughly proportional to  $1/C_1^4$ . Means for speeding the execution times are discussed in the next section.

## D.6 SUMMARY

In summary, the time-dependent flux is approximated by a series of constant fluxes  $q_1$  applied during various time intervals  $\Delta t_1$ . In order to use solutions for a stationary semi-infinite body, it is necessary to account for two facts. The first is that there should be no fluxes conducted across the displaced boundary from previous fluxes. The second is that in-depth heating caused by prior fluxes must be maintained. To achieve these objectives, an additional flux is introduced to cancel the undesirable heat conducted across a given depth from earlier fluxes during the most recent time interval. This depth corresponds to where the next constant flux is to be applied and will be discussed in the next paragraph. The result is a flux  $\bar{q}_1$  lower than  $q_1$  by the mean conductive flux arising from prior  $\bar{q}_1$ .

Next it is necessary to approximate the heat conducted across the depth at which the boundary ultimately arrives at the end of the time interval. This is accomplished by selecting sufficiently small time intervals of  $C_1$  values so that the thermal resistance across displacement  $\Delta x_1$  is small. By doing so the variations of the conductive fluxes across the displacements are also kept small. Fluxes  $\bar{q}_1$  are then located at an effective depth within the small displacements according to the value assigned the constant  $C_2$ .

Finally Duhamel's principle is used to account for the fact that each of the fluxes  $\bar{q}_1$  exist only over given time intervals  $\Delta t_1$ . By this technique one arrives at a series of constant fluxes  $\bar{q}_1$  applied at various depths  $\bar{x}_1$  and time intervals  $\Delta t_1$  with which to determine the temperature changes of the regressing propellant.

The advantage of this method over finite-difference techniques is threefold. The first is that temperature predictions require less stored information than needed by finite-difference methods. This is important in treating numerous crack elements. Secondly, the method provides reasonably accurate predictions of the temperatures

using relatively large time intervals. Finally, the method does not require periodic refinements of the spacial grid to accommodate pronounced changes in the thermal gradients with depth as the burning accelerates.

The most undesirable feature of the method is that the computer execution times increase approximately linearly with the number of time intervals involved in each set of computations. Means have been formulated for limiting the number of time intervals by first determining the amount of heat conducted across the most recent depth  $\bar{x}_1$  during each time interval. Then the time-dependent heat conduction is approximated by a series of constant fluxes over one or more time intervals. During early times, wherein the fluxes are least important, the time intervals are consolidated yielding a courser approximation of the flux at the early times. Preliminary computer runs suggest it is possible to limit the number of time intervals being used to about 30 without introducing errors of more than one percent in the temperature rises. However, criteria for approximating the fluxes at early times in terms of various dynamic burn conditions has yet to be established.

SECURITY CLASSIFICATION OF THIS PAGE (When Data Entered)

(19) REPORT DOCUMENTATION PAGE		READ INSTRUCTIONS BEFORE COMPLETING FORM
1. REPORT NUMBER AFOSR - TR - 76 - 1068	2. GOVT ACCESSION NO.	3. RECIPIENT'S CATALOG NUMBER
4. TITLE (and Subtitle) INITIATION MECHANISMS OF SOLID ROCKET PROPELLANT DETONATION	5. TYPE OF REPORT & PERIOD COVERED INTERIM REPORT Jan 75 - June 1976	
6. AUTHOR(s) A. N. TAKATA A. H. NIEDERMANN	7. AUTHORING ORGANIZATION NAME(S) & ADDRESS(ES) IIT RESEARCH INSTITUTE 10 WEST 35th STREET CHICAGO, ILL 60616	8. PERFORMING ORGANIZATION NAME(S) & ADDRESS(ES) IIT RESEARCH INSTITUTE 10 WEST 35th STREET CHICAGO, ILL 60616
9. CONTROLLING OFFICE NAME AND ADDRESS AIR FORCE OFFICE OF SCIENTIFIC RESEARCH/NA BLDG 410 BOLLING AIR FORCE BASE, D C 20332	10. PROGRAM ELEMENT, PROJECT, TASK AREA & WORK UNIT NUMBERS AF-9711	11. REPORT NUMBER 9711Q1
12. MONITORING AGENCY NAME & ADDRESS (if different from Controlling Office)	13. SECURITY CLASS. (of this report) UNCLASSIFIED	14. SECURITY CLASS. (of this report) UNCLASSIFIED
15. DISTRIBUTION STATEMENT (of this Report) Approved for public release; distribution unlimited.		
16. DISTRIBUTION STATEMENT (of the abstract entered in Block 20, if different from Report)		
17. SUPPLEMENTARY NOTES		
18. KEY WORDS (Continue on reverse side if necessary and identify by block number) DEFLAGRATION TO DETONATION (DDT) ROCKET MOTOR DETONATION NUMERICAL METHODS PROPELLANTS		
19. ABSTRACT (Continue on reverse side if necessary and identify by block number) This study involves the development of a computerized model with which to identify the causes of solid propellant rocket motor detonations during firing. The model treats the problem of suddenly exposing propellant cracks (or flaws or debonds) to chamber gases at higher pressures and temperatures than gases initially in the crack. Simplified analyses are used to compute the transient pressures produced by the gas flows, burning and crack deformations (positive and negative). These predictions are made in terms of a variety of parameters associated with the crack, chamber, motor case and propellant. Two phenomena		

appear important in producing pronounced pressure rises. These are: (1) partial or complete crack collapse due to stress waves reflected from the motor case and (2) rapid acceleration of the burning during the final stages of crack collapse. The latter is due to the relatively large quantities of heat acquired by the propellant during the relatively long periods of gas filling. Quantification of these effects remains to be accomplished.

**UNCLASSIFIED**